ABSTRACT

DESIGN OF NOVEL DRUG DELIVERY SYSTEM AND OPTIMAL DOSAGE REGIMENS

by
Kwang Seok Kim

Three representative drug delivery systems were analyzed to emphasize the roles of mathematical models and computer-aided simulations in pharmaceutical research. In the first project, a protocol was developed so that the optimal regimen, consisting of the intravenous boluses and subsequent infusion of theophylline, could be obtained once information on the pharmacokinetics became available. The method was based on a two-compartment model of the human body. A module was created and posted on a website for free access. The second project dealt with the transdermal heat-assisted delivery of corticosterone. Heat conduction and drug diffusion through the patch and the skin were expressed in the mathematical model. Four design parameters were estimated. This model was validated using clinical data from the administration of fentanyl. Cortisone concentrations through the patch and skin layers were predicted. The results were used to rank the relative impacts of the design parameters on the corticosterone delivery and to make proper suggestions for fabricating the products. Finally, the simultaneous application of an electric current and soluble microneedles were proposed for the first time. Preliminary experimental studies suggested that the electric field enhanced the flux by increasing drug diffusion and, thereby, the dissolution of the microneedles. One-, two- and three-dimensional simulations were conducted. In addition, protocols were proposed to help with the analysis of laboratory data.

DESIGN OF NOVEL DRUG DELIVERY SYSTEM AND OPTIMAL DOSAGE REGIMENS

by
Kwang Seok Kim

A Dissertation
Submitted to the Faculty of
New Jersey Institute of Technology
in Partial Fulfillment of the Requirements for the Degree of
Doctor of Philosophy in Chemical Engineering

Otto H. York Department of
Chemical, Biological and Pharmaceutical Engineering

August 2010

APPROVAL PAGE

DESIGN OF NOVEL DRUG DELIVERY SYSTEM AND OPTIMAL DOSAGE REGIMENS

Kwang Seok Kim

Dr. Laurent Simon, Dissertation Advisor Date
Associate Professor of Chemical, Biological and Pharmaceutical Engineering, NJIT

Dr. Piero M. Armenante, Committee Member Date
Distinguished Professor of Chemical, Biological and Pharmaceutical Engineering, NJIT

Dr. Norman Loney, Committee Member Date
Professor of Chemical, Biological and Pharmaceutical Engineering, NJIT

Dr. Kun S. Hyun, Committee Member Date
Research Professor of Chemical, Biological and Pharmaceutical Engineering, NJIT

Dr. Bozena Michniak-Kohn, Committee Member Date
Professor of Pharmaceutics, Rutgers University, New Brunswick, NJ

BIOGRAPHICAL SKETCH

Author: Kwang Seok Kim

Degree: Doctor of Philosophy

Date: August 2010

Undergraduate and Graduate Education:

- Doctor of Philosophy in Chemical Engineering,
  New Jersey Institute of Technology, Newark, New Jersey, 2010
- Master of Science in Chemical Engineering,
  University of Seoul, Seoul, South Korea, 2006
- Bachelor of Science in Chemical Engineering,
  University of Seoul, Seoul, South Korea, 2004

Major: Chemical Engineering

Publications and Presentations:

K.S. Kim and L. Simon, Evidence of a dissolution-diffusion mechanism in the release of 5-fluorouracil from microspheres, Int. J. Eng. Sci., in review.

K.S. Kim and L. Simon, Transport mechanisms in oral transmucosal drug delivery: implications for pain management, Math. Biosci., in review.

L. Simon, K.S. Kim and K. Kanneganti, Effects of epidermal turnover on the dynamics of percutaneous drug absorption, Math. Biosci., in review.

L. Simon, K. Kanneganti and K.S. Kim, Drug transport and pharmacokinetics for chemical engineer, Chem. Eng. Edu., in press.

K.S. Kim and L. Simon, Modeling and design of transdermal drug delivery patches containing an external heating device, Comput. Chem. Eng., in review.

K.S. Kim and L. Simon, Optimal intravenous bolus-infusion drug dosage regimen based on two-compartment pharmacokinetic models, Comput. Chem. Eng. 33 (2009) 1212-1219.

K.S. Kim KS and H. Kim, Hydraulic-jump behavior of a thin film flowing down an inclined plane under an electrostatic field, Korean J. Chem. Eng. 25 (2008) 1-9.

K.S. Kim and L. Simon, Design of a heat-aided transdermal drug delivery, ISPE New Jersey Chapter Meeting & Student Poster Competition, NJIT, Newark, NJ, Apr. 28, 2009.

K.S. Kim and L. Simon, Two-compartment modeling and computer programs to find the optimal intravenous drug dosage regimens, The Dana Knox Student Research Showcase, NJIT, Newark, NJ, Apr. 8, 2009.

K.S. Kim and L. Simon, Two-compartment modeling and computer programs to find optimal intravenous drug dosage regimens, AIChE Annual meeting, Philadelphia, PA, Nov. 16-21, 2008, Ref. No.: 572be.

K.S. Kim, S.Y. Park and H. Kim, Solutions of integral boundary layer approaches to solitary waves on a falling film under an electrostatic field, AIChE Annual meeting, Philadelphia, PA, Nov. 16-21, 2008, Ref. No.: 186aj.

For My Wife, Ms. Chae,
Without Her Enthusiasm, This Dissertation Would Never Be Finished

And

For My Parents, Ji Chon Kim and Seon Ui Hong, My Brother, Young Ho Kim,
Who Have Given Me Ceaseless Love

ACKNOWLEDGMENT

Above all, I would like to thank Dr. Laurent Simon who has offered me continued help in the past three years as a dissertation advisor. When I arrived in the United States on January, 2007, I worked with him as his research assistant. Six months later, I decided to join Dr. Simon's group. Now, I think that I made a very good choice. By that time, I was not familiar with pharmaceutical engineering. Without his great efforts to ensure a smooth transition into the filed, I would not be able to complete the doctoral dissertation.

I also want to thank Dr. Piero M. Armenante for not hesitating to provide critical comments on my dissertation. In addition, I attended a class he taught on pharmacokinetics, which helped me tremendously with the dissertation.

Dr. Norman Loney is the person I contacted when I applied for the doctoral program at NJIT. He was always willing to encourage me to work on mathematical modeling and computer simulations. Recently, he gave me a book that is useful in programming and sent me an email on an educational opportunity in the filed that, unfortunately, I could not afford to attend. I know he always thinks of me. Thank you very much.

Dr. Gun S. Hyun is one of the committee members. He gave me a lot of valuable comments to improve my dissertation. He is a Korean, and I knew him through one of my Korean friend at NJIT. He gave me and my friends the opportunity to review current bio- and nano-technologies in drug delivery systems via an Independent Study course.

Dr. Bozena Michniak-Kohn in Rutgers University accepted to join the dissertation committee. Since my research has been mostly on the use of mathematics, she has offered me the opportunity to consider the practical aspects of the technologies.

Dr. (soon-to-be) Jin Uk Ha is the friend I want to thank. He has been with me at NJIT during the past three and half years. He picked me up at the JFK airport when I arrived in the United States. He has offered me valuable advices on life at NJIT and in the United States. He also introduced me to Dr. Hyun, one of the committee members. I wish

him and his family all the best in Korea.

Dr. Hyo Kim is my Master thesis advisor. I really want to thank him. He made it possible for me to dream about pursuing a doctoral degree in the United States.

My wife, Ms. Hee Jung Chae, married me in 2008. Without her brave-hearted sacrifice, I would not be able to finish my doctorate work. I will always be indebted to her and would like to thank her from the bottom of my heart.

My son, Ryan H. Kim, is a genius. Event though he is only one year old, he has typed a lot of sentences in my dissertation.

My parents, Ji Chon Kim and Seon UI Hong, and my brother, Young Ho Kim, have waited for my Ph.D. for a long time. So far, they have always given me something. But I gave them nothing. Thank you very much for your endless love.

TABLE OF CONTENTS

TABLE OF CONTENTS
(Continued)

Chapter **Page**

TABLE OF CONTENTS
(Continued)

Chapter **Page**

LIST OF TABLES

Table **Page**

LIST OF FIGURES

LIST OF FIGURES
(Continued)

Figure **Page**

LIST OF FIGURES
(Continued)

Figure **Page**

LIST OF FIGURES
(Continued)

Figure **Page**

CHAPTER 1

INTRODUCTION

1.1 Objectives

This work focuses on the development of mathematical models and the application of control protocols to gain a better understanding of drug delivery platforms. The use of analytical tools in the design controlled-release devices allows drug manufacturers, pharmaceutical scientists and medical professionals to evaluate molecular transport through various biological barriers. In addition, they may be able to monitor drug concentration profiles in the plasma and link a desired release profile to the formulation composition. The modeling and design approach is based on the application of mass, energy and momentum balances to elucidate pertinent transport mechanisms. Computer simulations serve as virtual non-invasive sensors which provide continuous and non-invasive measurements when physical devices are unsuitable, unavailable or difficult to install. For example, in the transdermal delivery of a pain killer, the drug level in the serum or present in the patch are easily measured off-line. However, no sensor has been developed to capture the spatial distribution of drugs through the thin dermal layers. In this case, such a profile can be deduced from mathematical models and measured quantities (e.g., blood plasma drug concentration) which agree well with other measurable quantities [1]. The development of a state estimator, made possible by a fundamental knowledge of the system and computer simulations, may allow researchers to identify the effects of changes in individual or lumped design variable(s) on the comprehensive therapy [2, 3].

In light of these advantages, each of three following chapters in this dissertation is focused on the derivation and applications of models describing pharmacokinetics and their implications for new delivery platforms. In Chapter 2, the optimization protocol for the best regimens, including two different intravenous dosage forms, is developed. Bolus

dosage of a drug allows the instantaneous increase in the serum concentration, but patients need to endure unpleasant pains from hypodermal needles as they take medications [4]. On the other hand, infusion provides constant-rate administration of a drug with only a one-time administration. However, patients may have to wait a long time until the serum concentration reaches the minimum therapeutic level so that the medication goes into effect [5]. The proposed protocol implements both dosage forms in a treatment schedule and finds the best regimens, i.e., bolus dose sizes and times at which boluses are injected or infusion starts.

In Chapter 3, the process design of a transdermal corticosterone delivery patch enhanced by an external heating source is considered. A corticosterone is a steroid hormone which takes part in regulation of behaviors, life boundaries and even appetite of mammals including human [6]. Since a human body needs only small amounts of such hormones, the transdermal route may be a good candidate to a long-time corticosterone treatment. However, the only drawback of the transdermal patch is a delayed therapeutic effect due to the slow passage of drug through skin [7]. To overcome this, temperatures of patch and skin are slightly elevated by covering the patch with a heating pad [8, 9]. Higher temperature allows drug material to penetrate membranes of the patch and the skin easily, and thus, faster release of corticosterone, i.e., earlier therapeutic effect, can be achieved. Chapter 3 is devoted to the identification of main design factors of such drug delivery protocol for the safe and effective purposes.

Finally, in Chapter 4, parallel use of electric field in a self-dissolving microneedle patch is proposed. The stratum corneum is an outermost layer of skin which acts as a formidable barrier to transdermal drug delivery [7]. An array of microneedles makes small holes on the stratum corneum through which drug is released [10]. There is no pain due to a micro-sized needle, and fast penetration of drug can be achieved. An advanced application implements a water-soluble material mixed with drug in the fabrication of microneedles so that, once the needle is put under the stratum corneum, it starts to be degraded releasing

enclosed drug into epidermis/dermis layers [11]. For even faster and controllable release, the use of an electric field is proposed in this dissertation. An attempt to include an iontophoresis in the self-dissolving microneedle technique was already made [12]. In that platform, an electric current was applied at the skin surface after the patch had been worn and removed [12]. In the newly proposed system, however, the electrode has the similar shape as the microneedle. An array on a patch contains self-dissolving microneedles and electrodes located in alternate sequences. Once a patch is worn, the circuit is closed, and thus, space charges carry medications in the parallel directions to the skin in addition to passive diffusion. This eliminates drug around the needles faster and results in quicker dissolution of the needles. Since this platform has not been considered before, the proposed concept is first tested through preliminary studies. Then, the mathematical model is set up for one-, two- and three-dimensional simulations. The results are used to make guidelines for further experiments and products.

Concluding remarks about the roles of mathematical modeling and simulations in drug delivery technology are offered in Chapter 5. The solutions of partial differential equations shown in Chapters 2, 3 and 4 may be able to be solved more conveniently using commercial softwares. However, the current budgetary situations of most small pharmaceutical companies do not allow them to purchase such expensive softwares, and they do not have expertise on computer programming to use the tools. In light of this dilemma, all programs used to solve the problems in this dissertation are written in the Mathematica® (Wolfram Research, Inc.) environment for the purpose of free public access. Once a Mathematica® code for solving a problem is prepared, it will be posted online in the form of an interactive dialogue powered by webMathematica® so that an anonymous user can put his/her data from experiments or pertinent information into given spaces on the webpage and obtain the results of simulations by clicking a submit button. In that computing paradigm, knowledge of engineering, mathematics or programming language is not required.

1.2 Motivations

The primary goals of this dissertation are to advance the state of knowledge in drug delivery and collaborate with Big Pharma as well as small pharmaceutical companies around the world. Studies on the global health care conditions are conducted in 2006 by the World Health Organization (WHO). According to the statistics, health care expenses are not leading indicators of life expectancy; people around the world suffer from a range of diseases during a significant fraction of their lives in spite of large investments in health care. Developed countries spent a larger portion of their GDP on health care than the developing and the undeveloped countries did (Figure 1.1). The only exception to this trend is New Zealand. Although the United States spends the highest percentage of its GDP on improving health condition of its population, most Americans do not live healthier lives than people from the other countries. Figure 1.2 represents the Life Expectation at Birth (LEB) and the Healthy Life Expectation at Birth (HLEB) for the countries listed in Figure 1.1.

The LEBs of the United States were 75 years for males and 80 years for females in 2006. These numbers are smaller than those in Canada, the United Kingdom, Japan and New Zealand which spend a lower share of their GDP on health. In addition, the country with the highest LEB (i.e., Japan) spends nearly eight percent of its GDP on health (fifth in expenditures as % of GDP). It is also evident, from these findings, that people, by and large, suffer from various forms of illness for a total of 10 years during their life spans.

The quality of modern health services has improved from that of hundreds years ago. The invention of digital computers and many imaging instruments helps healthcare providers to cumulate medical knowledge, diagnose quickly and accurately the diseases from which their patients suffer, and conduct surgical operations safely. In addition, the developments in biosciences such as biology, microbiology and pharmaceutics result in the daily discoveries of new and life-saving active pharmaceutical ingredients (APIs). Nevertheless, most people in the developed and developing countries must still fight against a variety of serious health problems. There may be a host of recognized and unrecognized

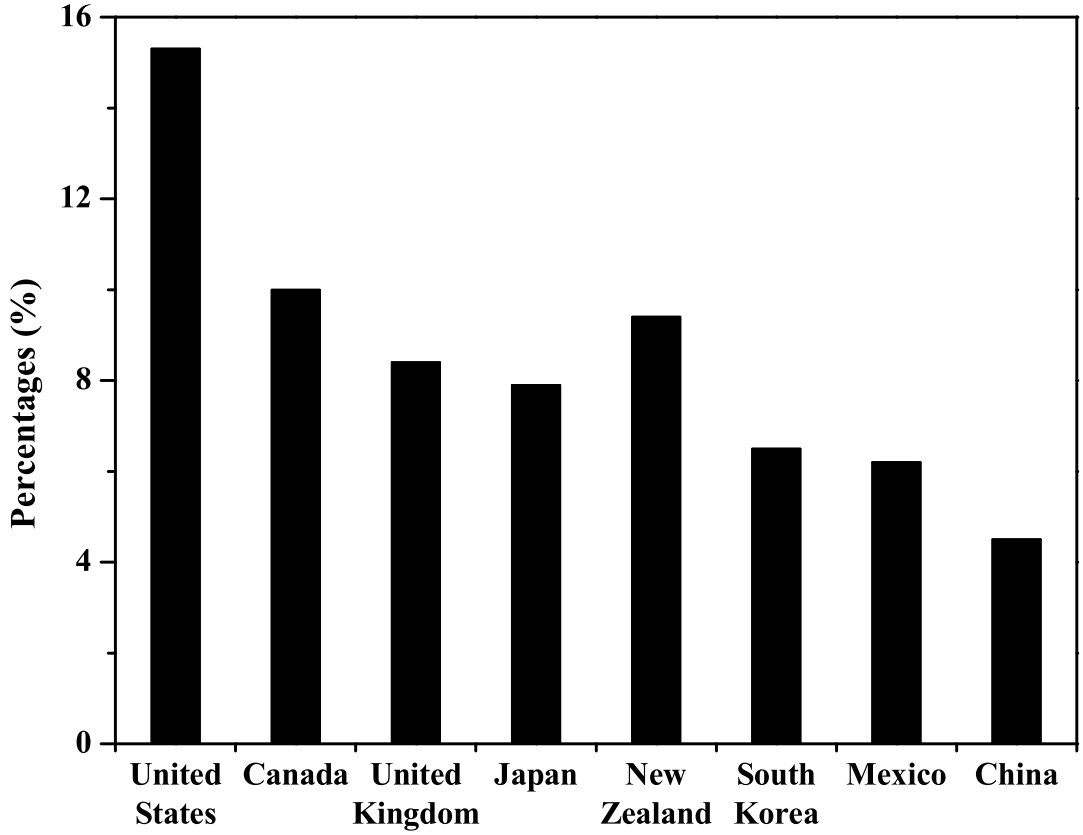

Figure 1.1 The portions of Gross Domestic Products spent on health care in some countries.

reasons that could explain such a situation. For example, the doughnut hole gap is widely referred to as a major problem in existing healthcare systems of some developed countries. From a chemical and pharmaceutical engineering standpoint, the best solution to narrow such gap is to manufacture the pharmaceutical products at lowest costs so that more and more patients in need can afford medicines. It may also be the best way to minimize the use of expensive APIs most of which are currently protected under patent. In other word, new drug delivery system should be designed to maximize the efficacy and bioavailability of APIs.

In the United States, the government has recently decided to reform its healthcare system in order to minimize the doughnut hole gap. As a result, the demands of pharmaceutical products will be dramatically increased. In addition, most blockbuster APIs are

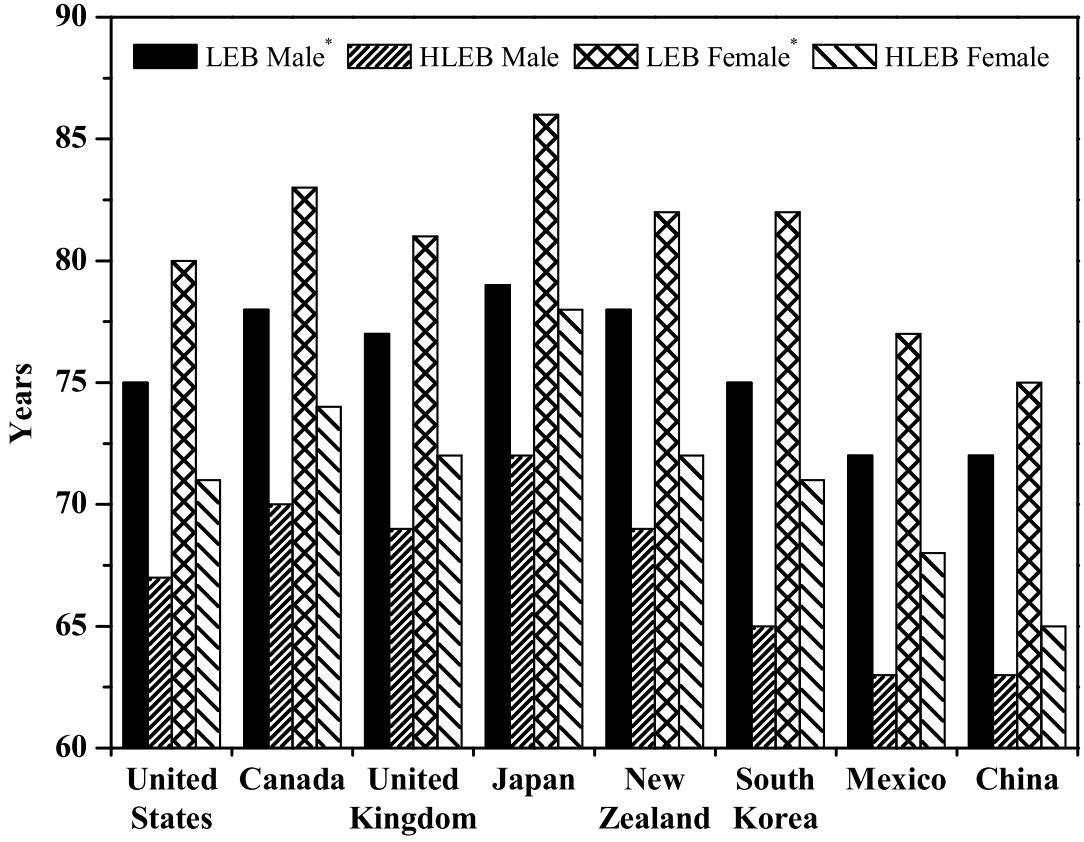

Figure 1.2 Life expectations at birth and healthy life expectations at birth in some countries.

going to be off-patent in a near future. Then, a large amount of cheap generic drugs will be flooded into the pharmaceutical markets. The effects of those phenomena are expected not to be limited to the market expansion of the United States. Indeed, many international big and small pharmaceutical companies are responding to the trends. They understand that the development of new dosage forms and formulations are the most competent alternatives of off-patent APIs against generic drugs because the discoveries of new APIs take longer times than the development of new delivery systems. For example, oral transmucosal fentanyl citrate delivery through an orally dissolving film (ODF) is developed by NAL Pharma Ltd. This product will compete with Actiq® (Cephalon Inc.) which also releases fentanyl citrate from lozenge through oral mucosa. Compared to traditional tablets, both products deliver the API much faster, with higher bioavailability ($\sim$ 0.32 orally; $\sim$ 0.52 transmucos-

ally) and more conveniently, i.e., they do not require water when administering.

1.3 Roles of Mathematical Models in Drug Delivery System

Pharmacokinetics and pharmacodynamics (PK/PD) are important areas of pharmaceutical engineering [13]. The pharmacokinetics is the study that reveals the mechanisms and the speed of drug transport from the device to systemic circulation, while pharmacodynamics helps to identify the extent of therapeutic effect as a function of the serum concentration [14]. Although the mathematical modeling is used in both studies in drug delivery, this dissertation deals with the pharmacokinetics.

When a new drug delivery device is invented, a series of clinical experiments are conducted to estimate the various pharmacokinetic parameters: maximum serum concentration, time to reach the maximum concentration and area under curve of concentration vs. time [15]. The dosage regimen is determined based on those parameters. Clinical experiments require very special cautions: the scientists should not violate numerous rules for human rights of subjects, the placebo effect of drug should be controlled as well as the inter-individual variability of pharmacokinetic parameters [16]. Consequently, the costs of the clinical studies are limitlessly high, and pharmaceutical companies have to cope with such budgetary loads. The burden is much more increased and the development time is getting even longer when companies seek to produce a new device for customized drug delivery based only on laboratory data gathered from patients. In addition, the tremendous number of clinical tests should be performed under carefully controlled protocols. For example, the pharmacokinetic studies performed so far have averaged the results over all subjects. In the development of the customized devices, subjects who have similar pharmacokinetics should be grouped for averaging, and then the clinical tests are conducted for each group.

A good mathematical model can help researchers reduce costs and production time by adding in silico experiments to their database (i.e., filling the gaps between laboratory experiments) and extrapolating to unexplored cases. The detailed procedure is as follows.

The mathematical models are composed primarily of the differential equations describing mass conservation in a domain to be analyzed (Chapters 2, 3 and 4). Depending on the delivery platform, additional equations representing the conservations of energy (Chapter 3) and/or momentum (Chapter 4) may be involved. The solutions of these governing equations, with appropriate boundary conditions and available parameter values, provide the concentration profiles within the domain. This result is used to estimate the absorption rate of drug into the systemic circulation. It can be further implemented to predict serum concentration change from which the maximum concentration, time to reach the maximum concentration and the area under curve are calculated. The existences of the analytical solutions depend on the governing equations or the model reduction capabilities of process engineers. In early times, an asymptotic solution to a specific problem was preferably pursued due to the limited computer resources. Nowadays, on the contrary, nonlinear partial differential equations, resulting from the combined effects of drug delivery mechanisms on the release profile, are often solved by numerical methods. Recent advances in digital computing technology have allowed the efficient solution of such complex problems.

CHAPTER 2

OPTIMAL DRUG DOSAGE REGIMEN

In Chapter 2, the optimization of intravenous drug dosage regimens was investigated based on a two-compartment pharmacokinetic model. Two dosage forms were considered for the intravenous administration of the modeled drug, theophylline: intravenous bolus and infusion. The advantage of bolus dosage form is that it increases plasma drug concentration promptly, whereas steady intake of drug is achieved by infusion. In clinical therapy, drug is administered as intravenous bolus injections followed by continuous infusion to minimize the time required for the pharmaceutical agent to produce a desired therapeutic effect. This work aims at providing patients with the quickest and safest therapy by properly calculating the administering amount and time of each dosage.

2.1 Problem Statements

An intravenous (i.v.) infusion treatment has been applied to maintain plasma drug concentration within a prescribed range in a long-term therapy. However, in the beginning of a treatment, patients may experience discomfort or pain before the drug, supplied to blood stream, reaches and remains at a therapeutic concentration. In cases where immediate pain management is necessary, this dead time is not desirable and it should be curtailed. This challenge has long been addressed by researchers. Mitenko and Ogilvie [17] conducted clinical experiments in which subjects were administered 61.2 mg of theophylline per minute in a well-controlled environment. Blood samples were collected at specific times and analyzed. The data were fit to a two-compartment model in order to estimate pharmacokinetic parameters, such as first-order drug elimination and inter-compartmental distribution rate constants. Wagner [18] conducted computer simulations with two-compartment model using two different infusion-rate administration protocols. The parameters obtained

from [17] were used.

A bolus form of administration usually releases drug instantaneously leading to a fast increase in a plasma drug concentration whereas a continuous infusion supplies drug to body at a steady rate. Therefore, in the latter case, a sustained drug level can be achieved by mitigating the effects of metabolism and elimination. Depending on the application, bolus injections may not provide the best option because frequent dosages are often required for an effective treatment. Infusion administrations also suffer from a major drawback in that it takes a long time for the drug to be within a therapeutic range. Therefore, a combined protocol, consisting of multiple boluses prior to infusion, was proposed in [17] to achieve both fast and efficacious results. In this hybrid system, it is important to keep the blood concentration within a therapeutic range because, if the concentration is less than the minimum level, the benefits of the drug will not be observed. Above a minimum toxic concentration, serious side effects may occur. In order to guarantee safety and effectiveness of the treatment, clinicians must select appropriate bolus injection schedules, dosage sizes and infusion rates very carefully. The general optimization methodology developed by Wheeler and Sheiner [19] helps researchers determine dosage regimens that agree with the criteria described above. The influence of the infusion rate, with and without initial i.v. boluses, on the plasma drug concentrations was investigated in a simulation study [19]. The results helped to assess the effectiveness of several regimens by comparing the minimum deviations from a desired blood concentration (i.e., mean-square error). According to their findings, an increase in the number of i.v. boluses led to an increase in the performance, as measured by the mean-square error between desired and estimated drug concentrations. The study suggests that a patient should be given a large number of i.v. boluses, which is impractical due to compliance issues. Besides, their strategy did not take into consideration the times at which bolus injections are administered. Also, a finite-difference method was employed to solve the governing differential equations. More efficient numerical computational methods are available.

In this study, orthogonal collocation on finite elements (OCFE) techniques and regression algorithms were applied to find the most effective and safe administration method based on a least mean-square error. Both the dosage times and sizes were considered in this investigation. Note that the orthogonal collocation method is known to give more accurate and effective computations than a finite-difference discretization [20, 21]. Since the end-user may be clinicians and healthcare providers, with limited knowledge of mathematical physiology and computer programming, programs were developed and packaged as user-friendly add-ons that took multiple inputs (pharmacokinetic parameters and dosage regimen) and then produced a single output (i.e., an-square error).

A two-compartment pharmacokinetic model is used to elucidate the delivery mechanism of drug into body, see Figure 2.1. The human body is modeled as two compartments: blood as Compartment I (sometimes it is called as serum or quickly perfused tissues) and peripheral tissues as Compartment II (or slowly perfused tissues). The masses are expressed as y_1 for Compartment I and y_2 for Compartment II. The medicament is exchanged between the two vessels following first-order kinetics; k_1 and k_2 represent forward and backward rate constants, respectively. Drug elimination is assumed to take place only in Compartment I since this process occurs at a much smaller scale in peripheral tissues (e.g., fats). Renal clearance in the bladder, metabolic degradation by microbiology and chemical reaction with other species are examples of potential drug removal processes [22]. The clearance kinetics, $E(t)$, associated with the different modes shows high nonlinearity with respect to the plasma drug mass, e.g., Michaelis-Menten kinetics for metabolic degradation. In this case, an analytical approach may not be possible and numerical solution is a viable option. If the elimination kinetics is given as a linear function of mass, e.g., only renal clearance occurs, analytical approaches are available. This study examines both cases. The size of bolus dosage is denoted as M_b; R_i is the constant infusion rate.

The use of two compartments provides more accurate predictions of drug transport in the body than one-compartment models. In general, a high number of compartments

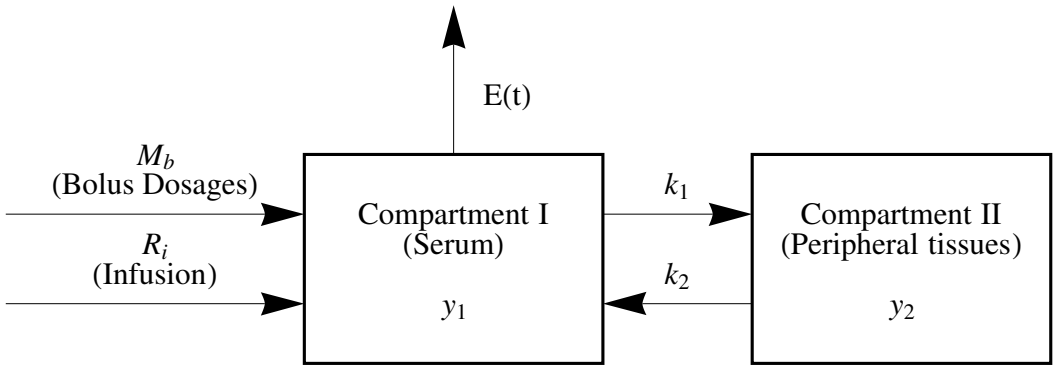

Figure 2.1 Two-compartment pharmacokinetic model with a hybrid dosage form (bolus plus infusion).

would capture nonlinear trends better than a small number of compartments because the solution of N-compartment model shows N-manifolds, i.e., N eigenvalues, which agrees with experimental results. Levitt and Levittąŕs clinical experiments demonstrate the multi-modal behavior of declining concentration of ethanol after cessation of a long-time steady-rate infusion. On the other hand, a large number of compartments causes an increase in the number of parameters to be recovered and, consequently, enhances the problem complexity. Most clinical research employs up to two compartments for the estimation of the parameters.

2.2 Mathematical Formulations

The governing equations for the model in Figure 2.1 are based on mass balance analysis around both compartments:

$$\frac{dy_1}{dt} = -k_1 y_1 + k_2 y_2 + R_i(t) - E(t) \tag{2.1}$$

and

$$\frac{dy_2}{dt} = k_1 y_1 - k_2 y_2 \tag{2.2}$$

When N boluses are administered, followed by a constant-rate infusion, the therapeutic period is divided into N subperiods. Before treatment begins, both compartments are drug-free. The first bolus is injected at $t = 0$; the initial mass corresponding to the first subperiod is the initial dosage size. The initial mass of the j-th subperiod is calculated by adding the j-th dosage size to the final masses of the (j-1)-th subperiod. Since i.v. boluses are directly injected in Compartment I, a jump is observed in the drug mass in Compartment I at the interface of adjacent subperiods. This behavior is not noticed in Compartment II. The infusion rate $R_i(t)$ is

$$R_i(t) = \begin{cases} 0 & t < t_N \\ R_{i0} & t \geq t_N \end{cases} \tag{2.3}$$

where t_N is the initial time of the last (N-th) subperiod, and R_{i0} is a constant infusion rate. The steady-state masses, $y_{1,ss}$ and $y_{2,ss}$, are determined by solving the equations obtained by setting all time derivatives in Equations (2.1) and (2.2) equal to zero. For instance, the following equation must hold at steady state:

$$E(t) = R_i(t) \tag{2.4}$$

According to the nonlinearity of the elimination rate $E(t)$, Equations (2.1) and (2.2) are solved differently. In this research, two case studies were investigated.

2.2.1 Elimination Rate Proportional to Mass in Compartment I

In the case where the elimination kinetics is expressed as

$$E(t) = k_E y_1 \tag{2.5}$$

Equation (2.1) is reduced to a linear first-order ODE such that

$$\frac{dy_1}{dt} = -(k_1 - k_E) y_1 + k_2 y_2 + R_i(t) \tag{2.6}$$

The general solutions of Equations (2.2) and (2.6) are

$$\begin{aligned} y_1(t) = \frac{R_i(t)}{k_E} - \frac{1}{2\delta}\left(\gamma y_{1,0} + \varepsilon \frac{R_i(t)}{k_E} - 2k_2 y_{2,0}\right) e^{-\frac{1}{2}\beta t} \\ + \frac{1}{2\delta}\left(\phi y_{1,0} + \eta \frac{R_i(t)}{k_E} - 2k_2 y_{2,0}\right) e^{-\frac{1}{2}\alpha t} \end{aligned}, \tag{2.7}$$

and

$$\begin{aligned} y_2(t) = \frac{k_1}{k_2}\frac{R_i(t)}{k_E} - \frac{\phi}{4k_2\delta}\left(\gamma y_{1,0} + \varepsilon \frac{R_i(t)}{k_E} - 2k_2 y_{2,0}\right) e^{-\frac{1}{2}\beta t} \\ + \frac{\gamma}{4k_2\delta}\left(\phi y_{1,0} + \eta \frac{R_i(t)}{k_E} - 2k_2 y_{2,0}\right) e^{-\frac{1}{2}\alpha t} \end{aligned}, \tag{2.8}$$

where $y_{1,0}$ and $y_{2,0}$ are the initial masses of Compartments I and II, respectively, and the Greek letters are defined as $\alpha = k_1 + k_2 + k_E + \delta$; $\beta = k_1 + k_2 + k_E - \delta$; $\gamma = k_1 - k_2 + k_E - \delta$; $\delta = \sqrt{(k_1 + k_2 + k_E)^2 - 4k_2 k_E}$; $\varepsilon = k_1 + k_2 - k_E + \delta$; $\phi = k_1 - k_2 + k_E + \delta$ and $\eta = k_1 + k_2 - k_E - \delta$. Since $(k_1 + k_2 + k_E)^2 - 4k_2 k_E > 0$ and thus δ is real, no oscillation in concentration is observed.

Suppose that N boluses, of sizes M_{b1}, M_{b2}, ..., M_{bN}, are injected at time points t_1(=0), t_2, ..., t_N prior to infusion, the number of subperiods is also N: the equations for the

first (N-1) subperiods are obtained by setting $R_i(t) = 0$; and the equation for the last one is derived by setting $R_i(t) = R_{i0}$. Consequently, the steady-state masses of Compartments I and II, for the N-th subperiod, are $y_{1,ss}^N = \frac{R_{i0}}{k_E}$ and $y_{2,ss}^N = \frac{k_1}{k_2}\frac{R_{i0}}{k_E}$, respectively. The initial masses are $y_{1,0}^I = M_{b1}$ and $y_{2,0}^I = 0$ for the first subperiod. The superscript number stands for the subperiod. At $t = t_2 + 0^-$, the final masses of the period become

$$y_1^I\left(t_2+0^-\right) = \frac{\phi M_{b1}}{2\delta}e^{-\frac{1}{2}\alpha t_2} - \frac{\gamma M_{b1}}{2\delta}e^{-\frac{1}{2}\beta t_2} \tag{2.9}$$

and

$$y_2^I\left(t_2+0^-\right) = \frac{\phi\gamma M_{b1}}{4k_2\delta}e^{-\frac{1}{2}\alpha t_2} - \frac{\phi\gamma M_{b1}}{4k_2\delta}e^{-\frac{1}{2}\beta t_2}, \tag{2.10}$$

where 0^- stands for the infinitesimal amount from the negative direction. Similarly, the initial masses of j-th subperiod (j=2, 3, ..., N) are

$$y_1^j\left(t_j\right) = y_1^{j-1}\left(t_j\right) + M_{bj} \tag{2.11}$$

and

$$y_2^j\left(t_j\right) = y_2^{j-1}\left(t_j\right). \tag{2.12}$$

Thus, masses of Compartments I and II in j-th subperiod are

$$
\begin{aligned}
y_1^j(t) = \frac{R_i(t)}{k_E} - \frac{1}{2\delta}\left(\gamma\left(y_1^{j-1}(t_j) + M_{bj}\right) + \varepsilon\frac{R_i(t)}{k_E} - 2k_2 y_2^{j-1}(t_j)\right) e^{-\frac{1}{2}\beta(t-t_j)} \\
+\frac{1}{2\delta}\left(\phi\left(y_1^{j-1}(t_j) + M_{bj}\right) + \eta\frac{R_i(t)}{k_E} - 2k_2 y_2^{j-1}(t_j)\right) e^{-\frac{1}{2}\alpha(t-t_j)}
\end{aligned}
\tag{2.13}
$$

and

$$
\begin{aligned}
y_2^j(t) = \frac{k_1}{k_2}\frac{R_i(t)}{k_E} - \frac{\phi}{4k_2\delta}\left(\gamma\left(y_1^{j-1}(t_j) + M_{bj}\right) + \varepsilon\frac{R_i(t)}{k_E} - 2k_2 y_2^{j-1}(t_j)\right) e^{-\frac{1}{2}\beta(t-t_j)} \\
+\frac{\gamma}{4k_2\delta}\left(\phi\left(y_1^{j-1}(t_j) + M_{bj}\right) + \eta\frac{R_i(t)}{k_E} - 2k_2 y_2^{j-1}(t_j)\right) e^{-\frac{1}{2}\alpha(t-t_j)}
\end{aligned}
,
\tag{2.14}
$$

respectively.

2.2.2 Elimination Rate Following Michaelis-Menten Kinetics

In this research, it is assumed that drug is administered directly to the systemic circulation (represented as Compartment I) without any delay caused by various types of biological barriers. Hence, the first pass metabolism is not considered. However, once a medicament is introduced into the systemic circulation, it undergoes degradation by a host of biochemical reactions [23]. The magnitudes of those two mechanisms affect the apparent kinetics of the overall metabolism. This section focuses specially on drugs subject to biodegradation by enzymes. The drug loss by chemical reactions with other blood components is considered less significant in the process. The Michaelis-Menten kinetics is often adopted to represent the rate of enzyme-involved metabolic consumption of drugs:

$$
E(t) = \frac{V_{\max} y_1}{K_M + y_1},
\tag{2.15}
$$

where V_{max} is the maximum rate and K_M is the Michaelis-Menten constant.

As in the previous case study where a linear-elimination kinetics was assumed, the constantly administered drug by infusion should be consumed by metabolic degradation in order to keep drug level in body steady. In other words, the infusion rate is obtained by setting Equations (2.1) and (2.2) with Equation (2.15) equal to zero at $y_1 = y_{1,ss}$ and $y_2 = y_{2,ss}$. As a result,

$$R_i(t) = \frac{V_{\max} y_{1,ss}}{K_M + y_{1,ss}}. \tag{2.16}$$

The analytical solutions of Equations (2.1) and (2.2) do not exist because of the nonlinearity of Equation (2.15), and a numerical method is required. However, the linearized system of Equations (2.1) and (2.2) about the steady state is still able to provide stability analysis [24]. The trace and the determinant of the Jacobian matrix of Equations (2.1) and (2.2) with Equation (2.15) are:

$$\tau = -(k_1 + k_2) - \frac{K_M V_{\max}}{(K_M + y_{1,ss})^2} < 0 \tag{2.17}$$

and

$$\Delta = \frac{k_2 K_M V_{\max}}{(K_M + y_{1,ss})^2} > 0 \tag{2.18}$$

respectively. The signs of those two parameters indicate that the steady state, i.e., fixed point in nonlinear dynamics, is a stable node, minimizing an accidental overdose or an insufficient dose administered to the patient.

Numerical solutions of Equations (2.1) and (2.2) with Equation (2.15) are pursued

by using the orthogonal collocations on finite element method. The integrations of those equations are carried out up to the treatment time, t_F. This time span is divided into N subperiods according to the administration times of N boluses, i.e., t_1(=0), t_2, ..., t_N. One subperiod is occupied by one finite element and, hence, there are N finite elements. In a collocation method, a domain, one finite element in OCFE, is rescaled to the range of 0 to 1. The collocation points are assigned according to the roots of Jacobi polynomials. Collocation method implements all these points to represent derivatives at one position, which improves accuracy with less computational load. Jumps are introduced between adjacent finite elements to represent corresponding concentration rises caused by bolus doses. Mathematica® (Wolfram Research, Inc.) provides the encoding platform best for concise programming of such a numerical procedure.

2.3 Optimal Dosage Regimens

The optimal dosage of a drug maximizes the efficacy and the safety of the therapy by maintaining the amount of drug in the body closest to the desired level. By using multiple boluses followed by infusion, the amount of drug in the body can remain as close as possible to the desired level. However, the frequent bolus doses may cause undesirable situations in clinical therapy such as severe injection pains. The model implemented in this study does not take those side-effects into account. Therefore, the number of the bolus injections, N, must depend entirely on the healthcare providersąŕ determination. Consequently, the design of the best dosage regimen focuses on the proper choice of the administration times of the bolus injections, t_i(i= 1, 2, ..., N), and the dosage sizes, M_{bj} (i= 1, 2, ..., N).

In the optimization, the times and the dosage sizes that lead to the minimum deviation of the mass in Compartment I from the desired level, y_{set}, are sought. The deviation is evaluated by the following object function:

$$\frac{\sqrt{\int_0^{t_F}\{y_1(t)-y_{set}\}^2 dt}}{\int_0^{t_F} y_{set} dt} = \frac{\sqrt{\sum_{j=1}^{N}\int_{t_j}^{t_{j+1}}\left\{y_1^j(t)-y_{set}\right\}^2 dt}}{t_F y_{set}} \tag{2.19}$$

where t_{N+1} is the total period of therapy, t_F. Three modules programmed by the author using Mathematica®: *prmts#.mx*, *objectfn.mx*, and *Optimizer.nb* are required to generate an optimal regimen. A set of the orthogonally collocated points over the normalized domain, 0 to 1, and weights for the Gaussian quadrature integration are defined in *prmts#.mx*. The # is the number of internal collocation points, and total number of collocation points is #+2 including the points at both boundaries. The extension ".mx" stands for a module coded as a Mathematica® Package as opposed to ".nb" as a script. By evaluating the module *objectfn.mx* with a suggested dosage regimen (function input) after *prmts#.mx* is run, the mass profiles in both compartments are calculated. The value of the object function, Equation (2.19), is also evaluated and returned (function output) to a calling function which implements an optimization procedure (*Optimizer.nb*). Once the number of boluses, duration of treatment, and desired level of theophylline are provided by users, the program automatically calculate the optimal dosage regimen.

2.3.1 Elimination Rate Proportional to Mass in Compartment I

In this case study, the analytical expression of Equation (2.19) is available because the closed-form solution for the mass of drug in Compartment I is given in Equation (2.13). For the j-th subperiod, the integration of squared error is given as

$$
\begin{aligned}
&\int_{t_j}^{t_{j+1}} \left\{ y_1^j(t) - y_{set} \right\}^2 dt \\
&= \int_{t_j}^{t_{j+1}} \left\{ \frac{R_i(t)}{k_E} - \frac{1}{2\delta} \left(\gamma \left(y_1^{j-1}(t_j) + M_{bj} \right) + \varepsilon \frac{R_i(t)}{k_E} - 2k_2 y_2^{j-1}(t_j) \right) e^{-\frac{1}{2}\beta(t-t_j)} \right. \\
&\qquad \left. + \frac{1}{2\delta} \left(\phi \left(y_1^{j-1}(t_j) + M_{bj} \right) + \eta \frac{R_i(t)}{k_E} - 2k_2 y_2^{j-1}(t_j) \right) e^{-\frac{1}{2}\alpha(t-t_j)} - y_{set} \right\}^2 dt \\
&= \frac{1}{4\alpha\delta^2} \left(\phi \left(y_1^{j-1}(t_j) + M_{bj} \right) + \eta \frac{R_i(t)}{k_E} - 2k_2 y_2^{j-1}(t_j) \right)^2 \left(1 - e^{-\alpha(t_{j+1}-t_j)} \right) \\
&\quad + \frac{1}{4\beta\delta^2} \left(\gamma \left(y_1^{j-1}(t_j) + M_{bj} \right) + \varepsilon \frac{R_i(t)}{k_E} - 2k_2 y_2^{j-1}(t_j) \right)^2 \left(1 - e^{-\beta(t_{j+1}-t_j)} \right) \\
&\quad - \frac{1}{(\alpha+\beta)\delta^2} \left(\phi \left(y_1^{j-1}(t_j) + M_{bj} \right) + \eta \frac{R_i(t)}{k_E} - 2k_2 y_2^{j-1}(t_j) \right) \\
&\qquad \times \left(\gamma \left(y_1^{j-1}(t_j) + M_{bj} \right) + \varepsilon \frac{R_i(t)}{k_E} - 2k_2 y_2^{j-1}(t_j) \right) \left(1 - e^{-\frac{1}{2}(\alpha+\beta)(t_{j+1}-t_j)} \right) \\
&\quad + (t_{j+1} - t_j) \left(\frac{R_i(t)}{k_E} - y_{set} \right)^2 + \left(\frac{R_i(t)}{k_E} - y_{set} \right) \\
&\quad \times \left\{ \frac{2}{\alpha\delta} \left(\phi \left(y_1^{j-1}(t_j) + M_{bj} \right) + \eta \frac{R_i(t)}{k_E} - 2k_2 y_2^{j-1}(t_j) \right) \left(1 - e^{-\frac{1}{2}\alpha(t_{j+1}-t_j)} \right) \right. \\
&\qquad \left. - \frac{2}{\beta\delta} \left(\gamma \left(y_1^{j-1}(t_j) + M_{bj} \right) + \varepsilon \frac{R_i(t)}{k_E} - 2k_2 y_2^{j-1}(t_j) \right) \left(1 - e^{-\frac{1}{2}\beta(t_{j+1}-t_j)} \right) \right\}.
\end{aligned}
\tag{2.20}
$$

Therefore, the deviation defined in Equation (2.19) is obtained by taking a square root on the summation of Equation (2.20) from j=1 to N and dividing it by $t_F y_{set}$.

The model constructed in this case study has been used to provide an optimal design of dosage regimen with the drug theophylline. Theophylline is used as a medicament against asthma, and the therapeutic range is known as 10-20 μg/mL [25]. Serious side-effects are reported when an accidental overdose occurs: symptoms such as nausea, vomiting and hypokalaemia with more than 25 μg/mL [25]; convulsions are apparent with more than 50 μg/mL [26]. The desired concentration of theophylline was set to 10 μg/mL, in accordance with several contributions [17, 18, 25]. This relatively low setting may result in a period of subtherapeutic drug amount in Compartment I before constant-infusion treatment

begins. However, it prevents the serious side effects from occurring and reduces the consumption of the expensive theophylline. The pharmacokinetic parameters of theophylline are reported by Wagner [18]: $k_1 = 2.73h^{-1}$, $k_2 = 3.11h^{-1}$, and $k_E = 0.321h^{-1}$. According to an apparent distribution volume of 0.277 L/kg, the desired level in mass, y_{set}, and the maximum therapeutic limit are set at 193.9 mg and 387.8 mg for an average body weight 70.0 kg. From Equation (2.5), the infusion rate is directly calculated as 60.5 mg/h.

A computer program, which evaluates Equations (2.19) and (2.20), and searches for the best dosage regimen, has been developed with Mathematica® (Wolfram Research, Inc.). Note that the constraint, such that the first dosage size does not exceed the maximum limit, is sufficient to guarantee that mass of Compartment I does not exceed the limit during the entire therapy because of the nature of the system represented by Equations (2.2) and (2.6): the mass of Compartment I always decreases right after a bolus injection and the mass of Compartment II does not exceed that of Compartment I. The regimens with 3 and 6 boluses have been tested for 3 hours of therapeutic period, and the results are presented in Figures 2.2 and 2.3. According to the optimization for 3-bolus treatment, the first bolus size was 241.74 mg followed by the second one of 74.8 mg in 10.1 minutes, and the third of 63.5 mg in 24.3 minutes. These dosage sizes are represented as three jumps of the mass of Compartment I (solid line) observed in Figure 2.2. After each jump, the mass of drug in the blood (Compartment I) declines due to distribution to the perfused tissues and elimination. With this regimen, the deviation, Equation (2.19), was estimated at 0.0309. It is worth noting that a small offset in the mass of Compartment I is observed in the third subperiod where a constant infusion is applied. However, the system represented by Equations (2.2) and (2.6) is stable at the fixed point, i.e., the desired level, and thus the mass is approaching the equilibrium value. When 6 bolus injections are used prior to the constant-rate infusion, the deviation, Equation (2.19), is improved up to 0.0174, and a much smaller offset is observed because of frequent doses of small amounts: the first of 218.6 mg; 43.2 mg at 5.1 min.; 39.6 mg at 11.2 min.; 35.9 mg at 18.5 min.; 32.3 mg at 27.5 min.; 29.3 mg at

38.7 min. Comparing the results of 3- and 6-boluses regimens, it is evident that more bolus administration lead to better performance or less deviation. Nevertheless, clinicians must pay careful attention to the prescriptions considering the unpleasant side-effects such as pain from a needle or that patients often forget to take medicine.

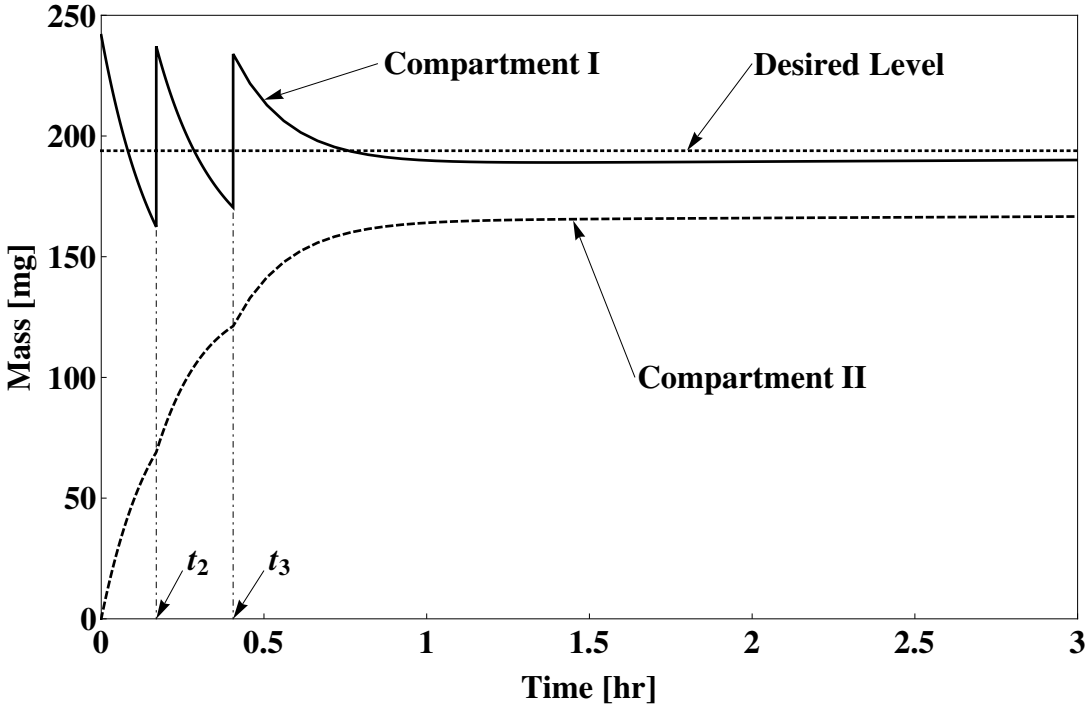

Figure 2.2 The time courses of masses of theophylline in Compartments I and II with the linear elimination rate model when the optimized 3-bolus/infusion regimen is applied.

The estimation of plasma drug mass profile in a post-therapy period is as important as knowing the amount of drug in the blood at any time because follow-up treatments, using the same or a different drug, must take into consideration the recently administered medications. Otherwise, another treatment applied before all theophylline disappears in the body may cause accidental overdose due to the underestimation of the initial drug content. In addition, undesired chemical reactions can occur when other drugs are administered in the presence of theophylline. These reactions may produce side-products that can act as poisons, or, at least, lessen the drug amount in the body, resulting in a sub-optimum treatment. To prevent these situations, it is important is to solve the governing equations,

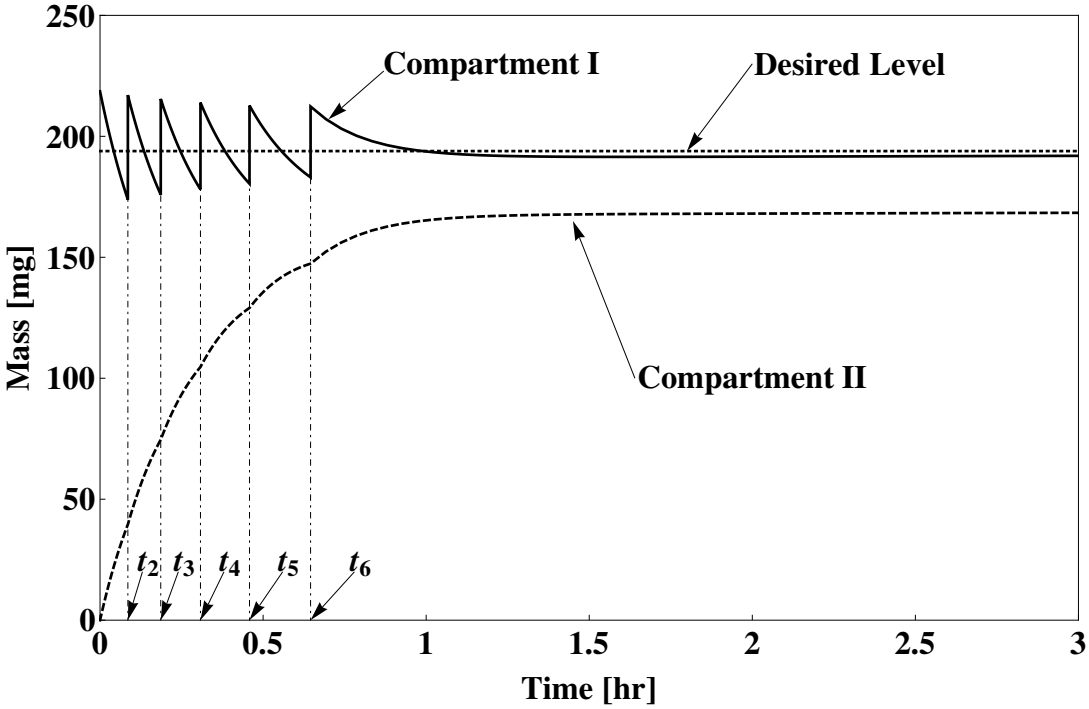

Figure 2.3 The time courses of masses of theophylline in Compartment I and II with the linear elimination model when the optimized 6-bolus/infusion regimen is applied.

Equations (2.1) and (2.2) until the mass in each compartment drops to an insignificant level. Alternatively, the decreasing mass of theophylline, at the end of the treatment, may be approximated by a first order exponential decay. This approach is valid only when drug elimination is the rate limiting mechanism. That is, the elimination rate is much smaller than the inter-compartmental distribution, and thus the masses of drug in both compartments are kept in equilibrium. Then, the mass in the blood, y_1, is expressed as:

$$y_1 = 10\exp(-k_E t)\,. \tag{2.21}$$

From Equation (2.21), the time to required for the elimination of 99 % of theophylline, t_{99}, is in hours:

$$t_{99} = \frac{1}{k_E}\ln\frac{1}{(1-0.99)} = \frac{\ln 100}{k_E} \tag{2.22}$$

According to Equation (2.22), it is not recommended to begin another treatment with theophylline or any other drug that is suspected to react with theophylline unless a period of time equal to t_{99} (14.7 hours with k_E=0.312 h^{-1}) has elapsed after the treatment ends.

The computer program is able to estimate optimized dosage regimen of different medicaments and for individual patients. For public access, this procedure is posted on the web <http://webmath.njit.edu/webMathematica/mathsimon/compartment2.jsp> powered by webMathematica® (Wolfram Research, Inc.). Hence, no mathematical or computational expertise is required to run the program. Once a user enters the pharmacokinetic data for a medicament, the optimal dosage schedule will be calculated. As noticed, it is still necessary to provide pharmacokinetic information in this first version of the program. In the future, collaborations with the other researchers around the world will lead to the development of the ready-to-use library of the pharmacokinetic data for a number of drugs. In this case, only the name of medication will be sufficient for estimating optimum dosage protocols.

2.3.2 Elimination Rate Following Michaelis-Menten Kinetics

The nonlinear Michaelis-Menten kinetic model of the drug, theophylline, was implemented by Ishizaki and Kubo [27] to explore the metabolic elimination. In a clinical experiment, the subjects consisted of 49 children and 21 adults. The kinetic parameters, V_{max} and K_M, recovered from the experiments vary from individual to individual. The average values are V_{max}=81.67 mg/h and K_M=467.3 mg. From Equation (2.16) and the desired level 193.9 mg, these average values lead to the constant infusion rate of 23.95 mg/h. For other parameters, the values that were used in the first case study were employed again.

The numerical strategy described in Section 2.2.2 and the object function, Equation (2.19), resulted in the optimal dosage regimen of three boluses followed by a constant infusion: the first bolus of size 240.8 mg; the second of 71.7 at 10.8 min; and the last of 58.4 mg at 27.6 min. The infusion therapy starts with the last bolus. The number of the

collocation points per finite element is 9, and the value of Equation (2.19) is 0.02948. With the obtained regimen, the time courses of the masses in both compartments are plotted in Figure 2.4. It is worth noting that a total 13 collocation points are used to better represent the amounts of drug in both compartments (Figure 2.4). The blank squares and circles stand for the collocation points. In this case, the value of Equation (2.19) is calculated at 0.02948 which is exactly the same as that calculated with 9 points. This shows the advantage of the orthogonal collocation method in solving differential equations as opposed to the finite difference method. For example, a total of 27 (actually 21 because the integrations are not performed for the outer two points) collocation points can provide an accurate solution for the domain of size 3, whereas a set of 30 evenly-spaced points, i.e., the size of finite difference is 0.1, would be a good usual starting in a finite difference method. The allocation of different number of collocation points on different finite element can also be implemented to reduce the computational load. As illustrated in Figure 2.4, the sizes of the first two finite elements, i.e., time spans from the first to second bolus and from the second to third ones, are relatively smaller than the last one, i.e., from the third bolus to the end of therapy. This is also observed in different systems regardless of the kinetic properties and number of boluses. It is well-known that a simulation of the system that has smaller domain requires less number of discretization points. Hence, the use of less collocation points is possible in the solutions for the first two subperiods, but it will not be demonstrated in this research.

Physiological properties, such as the drug distribution rates, elimination capacity, and volume of distribution, depend entirely on the individual patient: types of drugs that are being co-administered, gender, age, health (disease history) and diet. Hence, setting up a new dosage schedule of the prescribed drug requires running the programs that are developed in this research with the knowledge of the patient-specific pharmacokinetic information. However, unlike the first case study in which an analytical solution is available, the optimization of the dosage regimen requires extensive computational time, e.g., three or more hours depending on the numbers of boluses and the collocation points, in

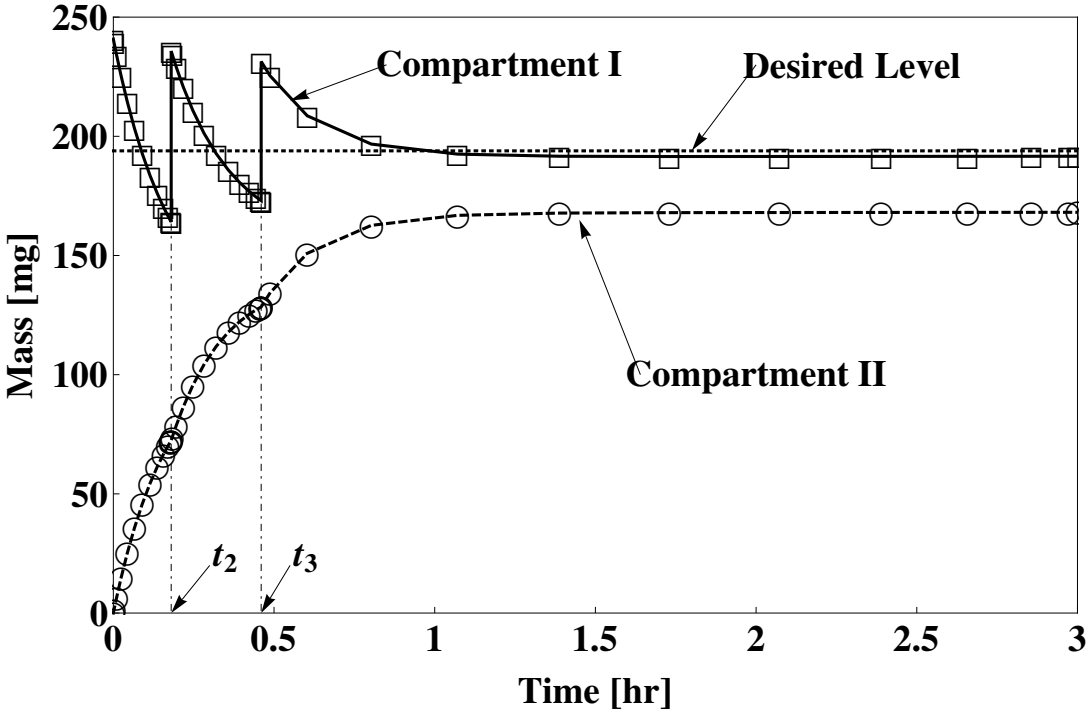

Figure 2.4 Time courses of masses of theophylline in Compartment I and II with the Michaelis-Menten elimination kinetics when the optimized 3-bolus-infusion regimen is used.

spite of the advantages of the OCFE approach and a high-performance computer. These time-consuming computations may not be acceptable to the potential users (clinicians and patients) even though the results are likely to lead to safe and efficient drug administration protocols. To circumvent this problem, best dosage regimens corresponding to specific pharmacokinetic parameters are pre-calculated and used to quickly estimate unknown doses and administration times for patients by interpolation (Table 2.1). The ten rows in Table 2-1 are generated as follows: the first row indicates the optimal dosage regimen at the nominal values of the pharmacokinetic parameters (i.e., Figure 2.4); the second and third ones show the regimen when the value of k_1 changes to 150 % and 50 % of the nominal value, respectively, with others remaining constant; the same variations are applied to k_2 in the fourth and fifth rows, to V_{max} in the sixth and seventh, and to K_M in the eighth and ninth. The last row of Table 2.1 uses interpolation based on the results of the first nine rows. For the test, k_1 is increased by 20 % of its nominal value while V_{max} and K_M are de-

creased by 20 % of their nominal values; k_2 remains unchanged. Linear regression and the optimization procedure described in this work (numbers in parenthesis) give similar results (Table 2.1). As a result, interpolation can be used to decide the administration times and dosages necessary to keep the plasma drug concentration at a desired level. It is worth noting that the estimation by a linear regression takes a thousandth of a second while showing close agreement with the results of the full-scheme optimization. This approach may allow researchers to fill a table, similar to Table 2.1, for different medicaments, which will reduce the time to market of drugs and avoid the collection of additional blood sample data from individual patients.

Table 2.1 Optimal Dosage Regimens with Different Values of Pharmacokinetic Parameters

k_1	k_2	V_{max}	K_M	Initial Dosage	Second Dosage		Third Dosage		Infusion Rate
[1/hr]	[1/hr]	[mg/h]	[mg]	Size [mg]	Size [mg]	Time [min]	Size [mg]	Time [min]	[mg/hr]
2.73	3.11	81.67	467.3	240.8	71.7	10.8	58.4	27.6	24.0
4.09	3.11	81.67	467.3	263.1	102.8	10.2	86.3	25.8	24.0
1.36	3.11	81.67	467.3	218.1	38.8	11.4	31.4	28.2	24.0
2.73	4.67	81.67	467.3	225.3	48.9	7.8	39.4	19.2	24.0
2.73	1.56	81.67	467.3	283.9	132.0	18.6	112.5	46.2	24.0
2.73	3.11	122.51	467.3	241.6	73.1	10.8	60.9	26.4	35.9
2.73	3.11	40.84	467.3	240.2	70.2	10.8	55.6	28.8	12.0
2.73	3.11	81.67	700.95	240.4	71.0	10.8	57.0	28.2	17.7
2.73	3.11	81.67	233.65	241.6	73.3	10.8	61.1	26.4	37.0
3.27	3.11	65.34	373.84	249.5 (249.5)	83.8 (83.5)	10.8 (10.6)	68.3 (68.4)	27.6 (27.4)	22.3

2.3.3 Other Case Studies

The strategy developed in this contribution can be applied to prescribe drugs with pharmacokinetics different from theophylline. For example, the Michaelis-Menten kinetics, the values of V_{max} and K_M, of ethanol, as an anesthetic agent, have been reported by other researchers [28, 29]. Transdermal drug delivery can be considered in the context of two-

compartment model in the presence of drug metabolisms in skin layers [30]. The strategy outlined can also be used to design drug dosage regimens that are based on time-dependent pharmacokinetic parameters. In this case, the drug kinetics needs to be well- formulated as a function of time. The approach is relevant to patients with chronic diseases whose treatment times are relatively long so that the body conditions are expected to change during the therapy. For example, experiments performed by Saadeddin et. al. show changes in the clearance rate of all-trans-retinoic acid (ARTA) occur at 180 min after an intravenous bolus injection [31]. As time elapses, the plasma drug concentrations shows an exponential decay followed by a linear decrease, after reaching a plateau, due to an increase in the elimination rate constant. Based on these observations, the elimination rate constant was expressed as a function of time [31]. This problem can be addressed in the present framework.

2.4 Conclusions

In this study, a two-compartment pharmacokinetic model was implemented to estimate optimal dosage regimens consisting of multiple intravenous boluses and a constant-rate infusion administration. Two different kinetic mechanisms for the theophylline elimination were used: linear and Michaelis-Menten metabolisms. Programs were written in a Mathematica® platform in order to estimate the administration time, dose sizes and infusion rate once the user inputs the number of boluses, treatment time and the desired mass of drug in the body. This contribution is posted on the Online Laboratory <http://webmath.njit .edu/webMathematica/mathsimon/compartment2.jsp>. Users can access and run the optimization program with minimum knowledge of mathematics, engineering or computer programming. Further versions of this program, developed in collaboration with clinicians, will include a library of pharmacokinetic parameters for a list of drugs. The creation of a platform that simulates plasma drug concentrations and calculates optimum dosage regimen will facilitate the development of safe and efficacious therapeutic strategies.

CHAPTER 3

HEAT-AIDED TRANSDERMAL DRUG DELIVERY

Transdermal drug delivery refers to a method of administration in which a therapeutic dose of medicine enters the systemic circulation through layers in skin. During the journey of drug to the systemic circulation through this dermal route, drugs do not undergo first-pass metabolism which is one of the biggest challenges in oral administration of medications. A patch is a sheet of drug-containing polymer, and is the most commonly consumed transdermal delivery device. By contacting with skin, it can provide continuous and steady dose of drug during a therapy: testosterone (Androderm®), sestrogen and progestogen (Ortho-Evra®), easing cigarette cravings (Nicoderm CQ®), and relieving motion sickness (Transderm-Scop®). This device can replace disposable hypodermal needle and minimize risks of infections and other diseases due to the reuse of the needles. In addition, the transdermal delivery device is usually placed outside the patient body during therapy. This way, the user is granted full access to the product so that quick changes in operational conditions can be made. Consequently, tighter control of drug release can be achieved by using the transdermal products compared to other types of delivery systems (e.g., implants or pills).

Nevertheless, low permeability of drug through skin imposes significant limitations to existing transdermal drug delivery technologies such as inevitable initial delay of drug release [32] and slow therapeutic effect. Stratum corneum is the outermost layer of skin that is composed of dry and dead cells. Although it is much thinner than other layers, it plays a great role in blocking drug passage to body. Therefore, continuous efforts to accelerate the delivery of drug through skin have been made by using chemical (e.g. water, oleic acid, and acetone) and physical enhancers (e.g. electric current, ultrasound, magnetic field, and heat). The chemical enhancers are applied on skin before patch and activate transport mechanism by widening openings in the stratum corneum. Chemicals for this purpose should not be expensive, harmful on skin, and must be used properly to prevent

side-effect such as skin irritation [33]. The release control in use of chemical enhancers depends largely on physical properties and application forms of the materials.

Iontophoresis [34, 35] uses mild electric current to force ionized or charged drugs through the stratum corneum. In sonophoresis, low-frequency ultrasounds are used to disturb lipid bilayers [36, 37, 38]. In these applications, precise and easy control of drug delivery rate can be achieved because patientąŕs requirement is almost instantaneously reflected to modules by microprocessors and electric signals. By the way, use of such electronics may increase volume and cost of product (note that the cheapest microprocessors are usually more expensive than a bundle of patches). This causes poor patientąŕs compliance and affordability. Especially, physically-challenged patients have difficulty to carry with big and heavy devices.

The enhancing medium employed in this research is heat from outside a patch. Elevated temperatures of patch and skin due to applied heat result in increased diffusions through the layers. Control of heat and, consequently, drug delivery is highly required since excessive heat causes thermal injury of skin (burn) and accidental overdose. Instead of heavy electronic, heat is available from a thin, light-weighted and, moreover, cheap heating pad where an exothermic reaction takes place. However, control protocol of drug release should be carefully prepared prior to taking such advantages. In this context, the point of this investigation is to understand the influence of applied heat on controlled release of drug through transdermal drug delivery and to know the role of mathematical model in detailed design of the heat-aided transdermal delivery device.

3.1 Problem Statements

Patch is the most popular transdermal delivery device due to its convenience. A sheet of patch is mainly composed of three layers: backing material, drug-loaded polymer, and adhesives. The backing material prevents loss of active pharmaceutical ingredients (API) blended in the polymer. On the opposite side, the adhesive helps to affix the patch to the

patientąŕs skin. It forms another layer between the drug-loaded polymer and the skin but also acts as a barrier to the drug delivery. In recent products, self-adhesive polymers are commonly adopted so that diffusion resistance through this region can be effectively ignored compared to transport in the drug-loaded polymer or in the skin. Consequently, a mathematical representation of the transport phenomena does not consider the presence of the adhesive. Once the patch is worn on the skin, the API and other materials begin to move by passive diffusion toward the depth of the skin until they are absorbed to the systemic circulation. The skin is composed of different physiological layers: stratum corneum, epidermis, dermis and others. The layers exhibit different transport properties. In practice, a single-layer model, with uniform properties, is usually implemented to simulate drug transport through the skin.

In this work, a sheet of heating pad is placed in the backing material in order to promote release of the medicine. The heat released from the pad increases the temperatures of the patch and the skin which leads to increases in drug diffusivities in those layers (active diffusion). Hence, controlled release of the drug can be achieved by manipulating the design parameters of the heating pad. The heating pad, modeled in this research, is composed of powder mixture of iron as solid reactant, charcoal, salt and moisture as catalyses, and vermiculite as insulator. Those materials are packed by an air-permeable pouching material. The shape of the pad is similar to that of the patch: an adhesive helps to affix the pad to the backing material on one side; an air-tight seal is attached on the other side. Once the seal is removed, oxygen begins to penetrate into the pouch and an exothermic oxidation of iron takes place. Other materials in the heating pad do not participate in the reaction but are still important because they determine thermal characteristics, such as overall heat capacity. These components also initiate and promote the exothermic reaction. Two design parameters are associated with the use of the heating pad: the maximum temperature and the duration of the pad application. Because the human skin is composed of viable proteins, excessive heat may result in irritation, redness, shock and/or burn. It is reported that

exposure to a heating pad producing more than 55 $^{\circ}C$can cause a serious thermal injury [39]. In light of this, clinical experiments have focused on a maximum skin temperature of 55 $^{\circ}C$. In practice, several applications of the pad may be required for effective therapy due to the time it takes the constituents to completely react. In fact, the reaction in a pad does not last more than 6 hours while the temperature of the system starts decreasing before that time. With a patch, such as Duragesic®, which is applied for more than 36 hours, the delivery enhancement is observed only at the beginning of the treatment. In this case, multiple applications of the heating pads are more likely to induce enhanced release of the medicament than a single application. This research deals primarily with the case of a single application of the heating pad. The findings of this work may be extrapolated to the repeated application protocol. Also, this strategy is critical in reducing the initial time lag [40, 41].

The configuration described above is shown in Figure 3.1. Since a patch with a heating pad usually forms a thin layer, but a wide surface area, on a skin, transverse transports of heat and drug are only considered. The boundary between the drug loaded polymer (patch hereafter) and the backing material (back hereafter) lies at $x = -L_{II}$. The outer surface of the heating pad is at $x = -L_I$ so that the thickness of the pad is $L_I - L_{II}$. From a physiological standpoint, the interface between the skin and the body core is not clearly defined. Nevertheless, this model places the boundary at L_{III}, where the capillary vessels are found and the drug absorption begins. At that position, instantaneous uptake of the drug (i.e., the perfect sink condition) is assumed.

In Figure 3.2, the expected profiles of temperature (dashed line) and concentration (solid line) are shown for a better understanding of the system treated in this research. Since the backing material is impermeable to the drug ingredient, the concentration of drug in the heating pad is always zero. The instant-drug absorption assumption at the boundary between skin and body core (see Figure 3.1), leads to the zero concentration at that position. The discontinuity in the concentration observed at the patch-skin boundary is

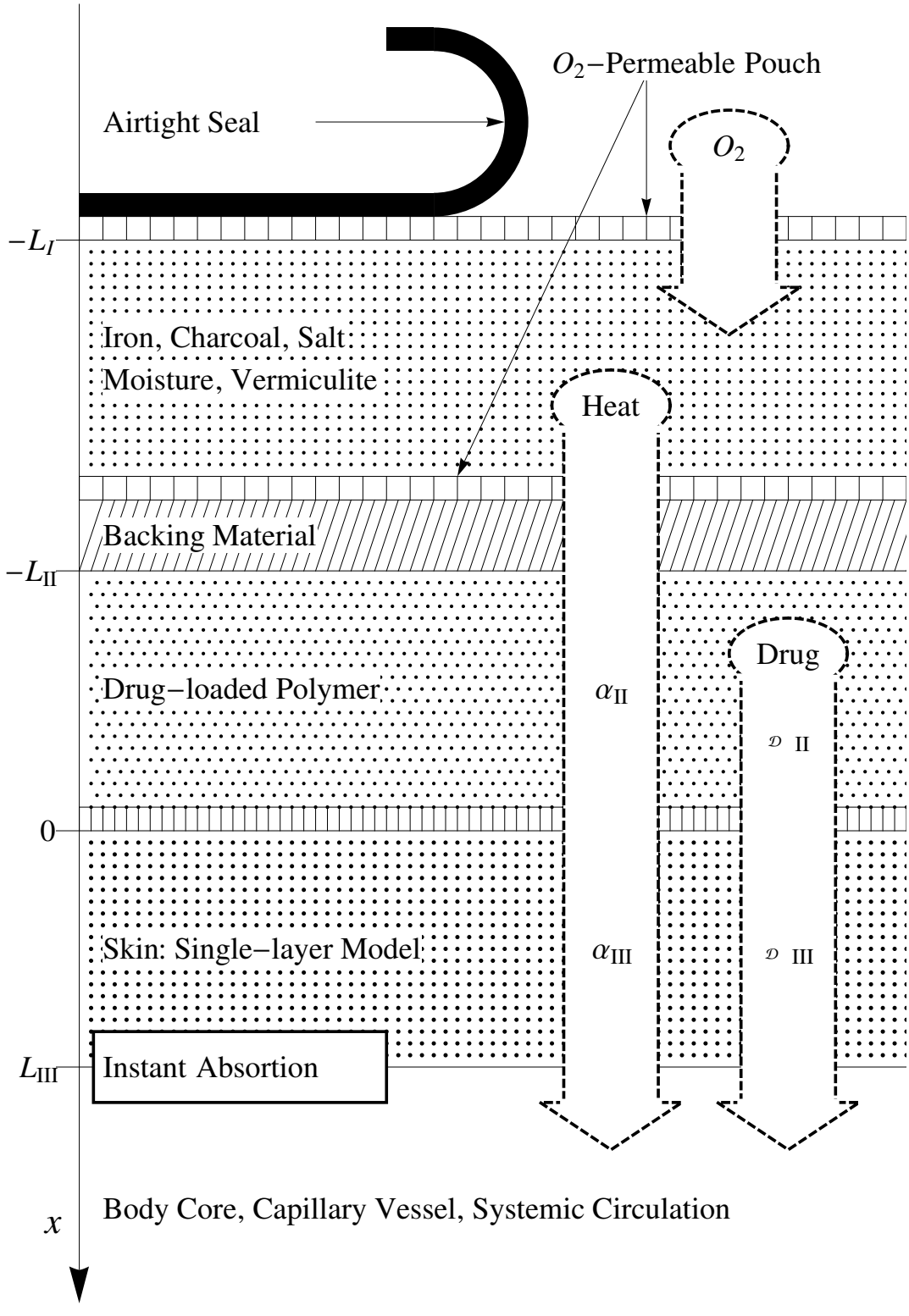

Figure 3.1 Physical configuration of a heat-enhanced transdermal drug delivery protocol.

due to the equilibrium between two media, which is called partitioning. On the other hand, the temperature distribution in the pad is considered uniform. No partitioning is observed and the temperature is continuous at every position. The temperature beyond the skin layer is not shown, but is kept unchanged far from the patch (at $x \to \infty$). This configuration does not take the thicknesses of the pouch and backing materials into account.

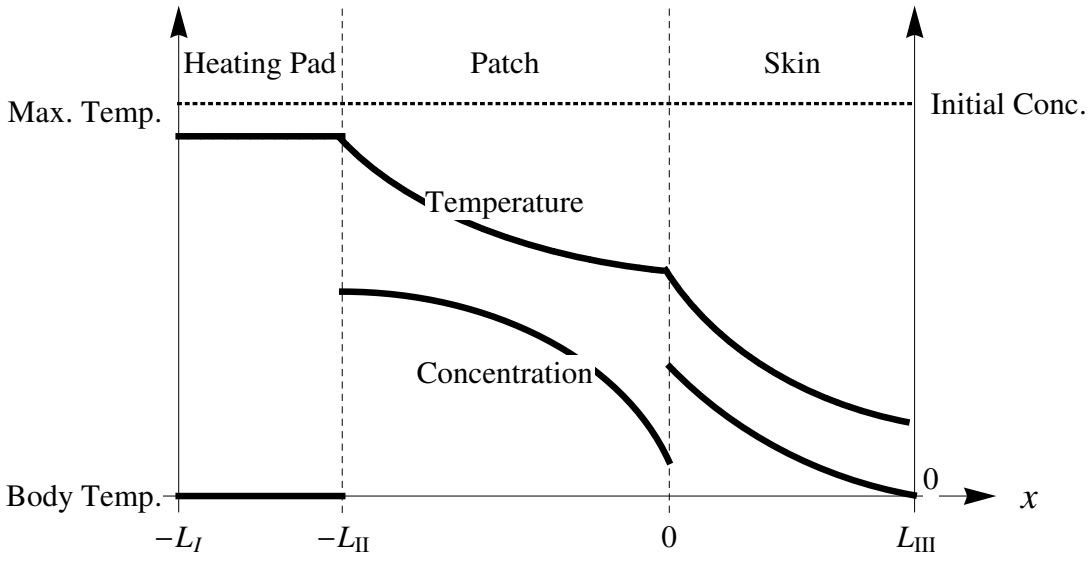

Figure 3.2 Expected temperature and concentration profiles observed throughout the treatment by the transdermal drug delivery protocol used in this research.

The one-dimensional analysis on the transdermal drug delivery configured in Figure 3.1 is already available in the work done by Kim and Simon [3]. In the previous work, four design parameters defined by virtue of the mathematical model were implemented to i) analyze the dynamic transports of heat and drug to the body, ii) explore optimum designs and sort the relative sensitivity of those parameters to the optimum design. The results led to the conclusion that the initial concentration of corticosterone in a patch is of most importance than other factors such as, in a descending order, initial reaction rate of a heating pad, total mass of the pad, and overall heat transfer coefficient of the patch. However, the model is constructed under the assumption that the domain of heat transfer is same as that of mass transfer. Thus, the temperature at the boundary between skin and capillary region was kept

constant. This represents benefits of the application of heating pad in the diffusion of drug to the capillary region (body core or systemic circulation), but cannot show any change in drug absorption. Therefore, modifications in the mathematical model are now required to maximize the applicability of the suggested heat-enhanced transdermal drug delivery protocol. First, the domain of the heat transfer is considered semi-infinite (from heating pad to somewhere in the body). Second, Arrhenius-type diffusivities are adopted as opposed to the linear model. Those changes allow the mathematical model to be validated using the experimental results published by [9].

In the following sections, the governing equations and the conditions are derived and a numerical solution methodology will be outlined. The constructions of those equations allow the identification of design factors that can affect the release profile. The solutions first provide insights into the dynamics of heat and mass transfers throughout the therapy and will facilitate qualitative and quantitative studies of the effects of the design parameters on the release profile. The findings of this contribution will also help in the fabrication of transdermal drug delivery systems.

3.2 Mathematical Formulations

In drug delivery research, mathematical-modeling study provides a deeper understanding of phenomena that cannot be observed with naked eyes or detected by sensors. For example, in the absence of an analytical model, it would be very difficult and expensive to monitor the temperature profile through the skin. In this case, a mathematical representation, based on mass and energy balances, can be instrumental as it represents the distribution of concentration and temperature through the skin or much thinner viable membrane. The process described in Figure 3.1 is translated into a set of mathematical equations that address the transport of heat and mass throughout the system in addition to boundary and initial conditions that refer to external factors influencing the drug delivery. The results of the mathematical modelings can contribute to the optimal designs of new pharmaceutical

devices and treatment schedules to specific diseases and patients. A dimensional analysis of the model can provide the design factors which can later be used in developing guideline for the best therapy protocol.

3.2.1 Mass and Energy Balances in Heating Pad

The heating pad neither contains any active pharmaceutical ingredient nor contributes to the therapeutic treatment directly. The role of the pad in this protocol is to provide a barrier of drug delivery with an extra heat to facilitate the passage of medication to the systemic circulation. In order to accomplish this purpose, an exothermic chemical reaction (oxidation of iron) is commonly used such that

$$4Fe + 3O_2 \rightarrow 2Fe_2O_3 \tag{3.1}$$

The heterogeneous reaction is initiated by the exposure of the iron powder to the oxygen in the air. One kilogram of iron is known to release 7436 kJ of heat when it completely oxidized to iron oxide [42]. It is assumed that only three fifths of this energy contributes to warm a heating pad up, and the rest is lost to outer environment. Note that the net oxidation energy is still large so that even slow oxidation may result in an extremely high temperature of a heating pad. Unless it is controlled properly, the reaction can cause serious injury such as burned skin. For this reason, the pad also includes charcoal, vermiculite, salt and sometimes a small amount of moisture. Those filler materials do not affect any thermodynamic properties of the reaction, Equation (3.1). However, those materials increase the heat capacity of the pad to prevent the temperature from rising sharply. Moisture and salt act as catalysts of the reaction.

In the case of heterogeneous reaction, two rate-determination steps must be considered: 1) mass transfer limitation due to the poor mixing oxygen with and the slow move-

ment of the gas, 2) chemical reaction rate limitation due to the slow reaction rate. In this work, it is hypothesized that the oxidation of iron powder controls the reaction rate. Since oxygen is abundant in the air (about 20 %), it is also assumed that its concentration is kept constant during the process. This consideration leads to two consequences: Consequently, first, the iron powder is treated as the limiting reactant. Second, the reaction rate is a function of only the concentration of iron, more specifically, the remaining amount of iron in the pad such that

$$-r_{Iron} = -\frac{dC_{Iron}}{dt} = k_1 C_{Iron}^n \tag{3.2}$$

where k_1 is the rate constant and n is the order of the reaction rate. The rate constant is a function of only temperature. An Arrhenius-type dependency has been a good candidate in many non-isothermal reaction kinetics studies [43]. In this drug delivery protocol, however, it is set constant because the range of the temperature change is too narrow to show a significant variation. The order of reaction can be only determined only by conducting experiments. The introduction of the conversion of iron powder, ξ, and the dimensionless time, τ, result in

$$\frac{d\xi}{d\tau} = \tau_0 k_1 C_{Iron,0}^{n-1}(1-\xi)^n \tag{3.3}$$

where τ_0 is a characteristic time that will be defined later. With an arbitrary choice of n=2, the solution of Equation (3.3) is

$$\xi = 1 - \frac{1}{(1+A\tau)} \tag{3.4}$$

with $A = \tau_0 k_1 C_{Iron,0}$. From Equation (3.4), the estimation of the time for the iron powder

to be exhausted is possible. To write an energy balance for the heating pad, it is worth noticing that the heat released by the oxidation of iron is

$$-\Delta H^R \left[\frac{J}{kg}\right] \times C_{Iron,0} \left[\frac{kg}{m^3}\right] \times V \left[m^3\right] \times \xi \left[-\right] \tag{3.5}$$

where V is the volume of the pad. The negative sign is used to state the total enthalpy of the reactants and the products decreases as a result of the exothermic reaction. The heat of reaction, ΔH^R, is a function of temperature such as

$$\begin{aligned}\Delta H^R(T) = &\left[\tfrac{1}{2}H^o_{f,Fe_2O_3} - \tfrac{3}{4}H^o_{f,O_2} - H^o_{f,Fe}\right] \\ &- \left[\int_{T_R}^{T}\left(\tfrac{1}{2}C_{p,Fe_2O_3}(t) - \tfrac{3}{4}C_{p,O_2}(t) - C_{p,Fe}(t)\right)dt\right]\end{aligned} \tag{3.6}$$

The first bracket of Equation (3.6) is the heat of oxidation of iron at standard condition (1 atm and T_R= 25 $^\circ C$) that is obtained from the heats of formation of the reactants and the product. The second bracket denotes the deviation from the reference temperature, T_R. The heat capacities of the reactants and the product are available as polynomial functions of temperature. It is worth noticing that the mild change of temperature does not significantly influence the heat of reaction and the effect can be ignored. For example, a 100 $^\circ C$temperature difference results in only 1kJ/kg (the first term is 7436 kJ/kg) [42].

The energy balance for the heating pad is written as

$$m\hat{C}_{p,Iron}\frac{d\bar{T}_I}{dt} = -\Delta H^R C_{Iron,0} V\left(\frac{d\xi}{dt}\right) + UA\left(\bar{T}_{II} - \bar{T}_I\right)\big|_{x=-L_{II}} \tag{3.7}$$

where m and $\hat{C}_{p,Iron}$ are the mass and the heat capacity of the pad; U and A are the overall heat transfer coefficient and the surface area of a backing material of the patch, respectively. The subscripts I and II denote the heating pad and the patch, respectively. The initial temperature of the pad is set equal to the body temperature (T_0 =37 $^\circ C$)

$$\bar{T}_I\,(t=0) = T_0 \tag{3.8}$$

Defining the maximum temperature T_{max} as the highest temperature that does not cause any thermal injury to the viable skin (55 $^{\circ}C$), dimensionless expression of temperature is written as

$$T = \frac{\bar{T}_I - T_0}{T_{\max} - T_0}. \tag{3.9}$$

Therefore, dimensionless form of Equation (3.7) is

$$\frac{dT_I}{d\tau} = (1-\xi)^2 + B\,(T_{II} - T_I)|_{\zeta=-1} \tag{3.10}$$

where τ_0 is defined as time required for the pad to reach the maximum temperature, T_{max}, by chemical reaction: $\tau_0 = \frac{m\hat{C}_{p,Iron}(T_{\max}-T_0)}{(-\Delta H^R)k_1 C_{Iron,0}^2 V}$. The dimensionless parameter, $B = \frac{U(T_{\max}-T_0)}{L_I(-\Delta H^R)k_1 C_{Iron,0}^2}$, measures the ratio of the rates of heat loss to generation by the reaction. The dimensionless coordinate is $\zeta = {}^{x}/_{L_{III}}$. Note that the mass of pad is used instead of the density because the density of the mixture varies with the composition and the particle size. Then, the initial condition becomes at τ=0,

$$T_I = 0. \tag{3.11}$$

3.2.2 Mass and Energy Balances in Patch

A common transdermal patch contains a thin film of polymer matrix uniformly blended with a drug. During the medical treatment, the adhesive side of the patch is in contact with a small area of bare skin and releases the active pharmaceutical ingredient. The decrease in the amount of drug results in a concentration gradient and, consequently, the movement of medication by diffusion. Because diffusivity is an increasing function of temperature, the presence of an external heat source should promote drug delivery. For the non-isothermal diffusion of drug,

$$\frac{\partial \bar{C}_{II}}{\partial t} = \frac{\partial}{\partial x}\left(D_{II}\left(\bar{T}_{II}\right)\frac{\partial \bar{C}_{II}}{\partial x}\right), \tag{3.12}$$

where $\bar{C}_{II}$ is the drug concentration in the polymer matrix and $D_{II}\left(\bar{T}_{II}\right)$ is the diffusivity through the polymer matrix as a function of temperature.

The backing material is designed in such a way that it is impermeable to the drug resulting in a zero-flux condition at $x = -L_{II}$:

$$\left.\frac{\partial \bar{C}_{II}}{\partial x}\right|_{x=-L_{II}} = 0. \tag{3.13}$$

On the other side of the patch (patch-skin interface), it is assumed that equilibrium between the concentrations exists:

$$\bar{C}_{II}\big|_{x=0} = K_M\,\bar{C}_{III}\big|_{x=0}, \tag{3.14}$$

where $\bar{C}_{III}$ is the concentration of drug in the skin, and K_M is the partition coefficient which measures the hydrophobicity. The polymer matrix is blended uniformly at t=0:

$$\bar{C}_{II}\big|_{t=0} = C_0. \tag{3.15}$$

When the heating pad is in contact with the backing material and the air-tight seal is removed, the temperature in the patch, at the backing material, begins to increase subsequent to a rise in the pad. The established temperature gradient induces heat conduction throughout the polymer:

$$\rho_{II}\hat{C}_{p,II}\frac{\partial \bar{T}_{II}}{\partial t} = \kappa_{II}\frac{\partial^2 \bar{T}_{II}}{\partial x^2}, \tag{3.16}$$

where κ_{II} is the heat conductivity of the polymer. At the pad-patch boundary, the energy flux is conserved:

$$-\kappa_{II}\left(\frac{\partial \bar{T}_{II}}{\partial x}\right)\bigg|_{x=-L_{II}} = -U\left(\bar{T}_{II}|_{x=-L_{II}} - \bar{T}_I\right). \tag{3.17}$$

The temperature at the patch-skin boundary is equal to each other:

$$\bar{T}_{II}|_{x=0} = \bar{T}_{III}|_{x=0}. \tag{3.18}$$

The temperature of the patch before treatment begins is kept at body temperature:

$$\bar{T}_{II}|_{t=0} = T_0. \tag{3.19}$$

Following a method similar to the one adopted in the energy balance for the pad, dimensionless equations are obtained:

$$\frac{\partial C_{II}}{\partial \tau} = \frac{\partial}{\partial \zeta}\left(\mathscr{D}_{II}\left(T_{II}\right)\frac{\partial C_{II}}{\partial \zeta}\right), \tag{3.20}$$

$$\left.\frac{\partial C_{II}}{\partial \zeta}\right|_{\zeta=-L_{II}/L_{III}} = 0, \tag{3.21}$$

$$C_{II}|_{\zeta=0} = K_M C_{III}|_{\zeta=0}, \tag{3.22}$$

$$C_{II}|_{\tau=0} = 1, \tag{3.23}$$

$$\frac{\partial T_{II}}{\partial \tau} = \alpha_{II}\frac{\partial^2 T_{II}}{\partial \zeta^2}, \tag{3.24}$$

$$\left.\left(\frac{\partial T_{II}}{\partial \zeta}\right)\right|_{\zeta=-1} = \mathscr{C}\left(T_{II}|_{\zeta=-1} - T_I\right), \tag{3.25}$$

$$T_{II}|_{\zeta=0} = T_{III}|_{\zeta=0}, \tag{3.26}$$

and

$$T_{II}\big|_{\tau=0} = 0. \tag{3.27}$$

The dimensionless diffusivity is $\mathscr{D}_{II} = \frac{\tau_0 D_{II}}{L_{III}^2}$; the concentrations in the two layers are $C_{II} = \bar{C}_{II}/C_0$ and $C_{III} = \bar{C}_{III}/C_0$; the dimensionless thermal diffusivity of patch is $\alpha_{II} = \frac{\tau_0 \kappa_{II}}{L_{III}^2 \rho_{II} \hat{C}_{p,II}}$. The new constant $\mathscr{C}$ is defined as $\mathscr{C} = \frac{U L_{III}}{\kappa_{II}}$.

3.2.3 Mass and Energy Balances in Skin

The transport mechanisms through the skin are similar to those in the patch: drug diffusion and heat conduction. However, the skin contains several different layers with unique transport properties. For example, the stratum corneum (SC) is the outermost layer of skin and is composed by dry, dead cells [7]. Although the SC is a very thin layer of skin, it offers the most resistance to drug penetration when compared to the epidermis and dermis. Nevertheless, this study proposes a single layer model where the physical properties are uniform throughout the skin. In spite of the simplicity of the single layer model, it can provide valuable results that can be incorporated in clinical drug permeation tests because many of these studies focus on the overall skin instead of the distinct layers. Medication that is transported to the deep skin is subjected to absorption to the systemic circulation through the capillary vessels.

The mass balance for the skin layer is written as

$$\frac{\partial \bar{C}_{III}}{\partial t} = \frac{\partial}{\partial x}\left(D_{III}\left(\bar{T}_{III}\right) \frac{\partial \bar{C}_{III}}{\partial x} \right). \tag{3.28}$$

At the patch-skin boundary, the flux should be conserved:

$$-D_{II}\left(\frac{\partial \bar{C}_{II}}{\partial x}\right)\bigg|_{x=0} = -D_{III}\left(\frac{\partial \bar{C}_{III}}{\partial x}\right)\bigg|_{x=0}. \tag{3.29}$$

At the end of the skin where drug absorption takes place, a perfect sink condition is used:

$$\bar{C}_{III}\big|_{x=L_{III}} = 0. \tag{3.30}$$

The concentration of drug in the skin before treatment begins is set equal to zero:

$$\bar{C}_{III}\big|_{t=0} = 0. \tag{3.31}$$

Conduction is the main heat transfer mechanism through the skin and body core:

$$\rho_{III}\hat{C}_{p,III}\frac{\partial \bar{T}_{III}}{\partial t} = \kappa_{III}\frac{\partial^2 \bar{T}_{III}}{\partial x^2}, \tag{3.32}$$

where ρ_{III} and $\hat{C}_{p,III}$ are the density and heat capacity of skin, respectively. The heat conductivity of skin, κ_{III}, is assumed constant. At the patch-skin boundary, the heat flux should be continuous:

$$-\kappa_{II}\left(\frac{\partial \bar{T}_{II}}{\partial x}\right)\bigg|_{x=0} = -\kappa_{III}\left(\frac{\partial \bar{T}_{III}}{\partial x}\right)\bigg|_{x=0}. \tag{3.33}$$

Far from the surface of skin, it is assumed that the temperature is kept at the body temperature:

$$\bar{T}_{III}\big|_{x\to\infty} = T_0. \tag{3.34}$$

Initially, the skin temperature is set equal to the body temperature:

$$\bar{T}_{III}|_{t=0} = T_0. \tag{3.35}$$

The perfect sink condition employed in Equation (4.36) allows a simple analysis on the drug delivery system, although it is valid only when the blood circulation rate is sufficiently high so that drug concentration in blood can remain very low. This assumption is made in in-vitro experiments and mathematical simulations [72, 73]. In the case of insufficient circulation, however, drug will be accumulated around the capillary vessel and other analysis should be considered [74, 75, 76].

The dimensionless equations are briefly given:

$$\frac{\partial C_{III}}{\partial \tau} = \frac{\partial}{\partial \zeta}\left(\mathscr{D}_{III}\left(T_{III}\right)\frac{\partial C_{III}}{\partial \zeta}\right), \tag{3.36}$$

$$\left(\frac{\partial C_{II}}{\partial \zeta}\right)\bigg|_{\zeta=0} = \mathscr{E}\left(\frac{\partial C_{III}}{\partial \zeta}\right)\bigg|_{\zeta=0}, \tag{3.37}$$

$$C_{III}|_{\zeta=1} = 0, \tag{3.38}$$

$$C_{III}|_{\tau=0} = 0, \tag{3.39}$$

$$\frac{\partial T_{III}}{\partial \tau} = \alpha_{III} \frac{\partial^2 T_{III}}{\partial \zeta^2}, \tag{3.40}$$

$$\left(\frac{\partial T_{II}}{\partial \zeta}\right)\bigg|_{\zeta=0} = \mathscr{F} \left(\frac{\partial T_{III}}{\partial \zeta}\right)\bigg|_{\zeta=0}, \tag{3.41}$$

$$T_{III}|_{\zeta\to\infty} = 0, \tag{3.42}$$

and

$$T_{III}|_{\tau=0} = 0. \tag{3.43}$$

The dimensionless parameters are: the diffusivity of drug in skin is $\mathscr{D}_{III} = \frac{\tau_0}{L_{III}^2} D_{III}$; the ratio of the diffusivities at the patch-skin interface is $\mathscr{E} = \frac{D_{III}}{D_{II}}$; the dimensionless thermal diffusivity of skin is $\alpha_{III} = \frac{\tau_0 \kappa_{III}}{L_{III}^2 \rho_{III} \hat{C}_{p,III}}$ and the ratio of thermal conductivities at the patch-skin interface is $\mathscr{F} = \frac{\kappa_{III}}{\kappa_{II}}$.

3.2.4 Optimization Protocol

Solutions of the partial differential equations and the boundary and initial conditions, i.e., Equations (3.9), (3.10), (3.19) to (3.25) and (3.35) to (3.42), allow researchers to monitor the following variables: 1) concentrations through patch and skin, 2) temperature of heating pad, patch and skin, 3) flux of drug to body, 4) cumulative amount of drug, and so forth. Among them, flux is the most associated factor to rate of drug absorption. After patch is applied, flux appears four characteristic period: Dormant Period; Exponential Period; Quasi

Steady Period; and Declining Period. In dormant period, flux is negligible since drug is yet available at the depth where capillaries are found. Time required for drug to be absorbed significantly is called "lag time." In the transdermal drug delivery, the estimation of the lag time by method of eigenvalue is addressed in the literature [56]. Absorption of drug begins in exponential period so that flux increases gradually up to a certain level. When flux reaches maximum, quasi steady period comes. During that period, drug release rate is subjected to a relatively small change until remaining drug in the patch is not sufficient to maintain the desired flux. Finally, in declining period, flux decreases steadily until the remaining amount of drug in the patch and the skin is completely consumed. Based on such observation, therapy should end before the declining period, and a long-period therapy may consist of multiple applications of transdermal patches.

The mathematical representation of flux at the end of skin ($x = L_{III}$) discussed above is given by

$$J = -D_{III}\left(\bar{T}_{III}\left(L_{III}, t\right)\right)\frac{\partial \bar{C}_{III}}{\partial x}. \tag{3.44}$$

Due to the elimination of drug by metabolism and renal clearance, this flux should be maintained at a desired level in order to keep patient within a therapeutic range. Therefore, effectiveness of design will be assessed by the integral of square error (ISE) such that

$$ISE = \frac{1}{\tau_T}\int_0^{\tau_T}\left(\frac{J - J_{set}}{J_{set}}\right)^2 dt \tag{3.45}$$

where τ_T is the duration of a treatment with a single patch, and J_{set} is the desired flux of drug. The same procedure used in the optimization in Chapter 2 has been followed. Significant factors that affect flux are determined. Flux and ISE are repeatedly calculated with randomly or systematically chosen values of those factors until minimum ISE is found.

3.3 Physical Properties and Design Parameters

The benefits of the mathematical modeling implemented in this research are: 1) the non-invasive monitoring of drug transport through the patch and skin, 2) the quantitative assessment of the effect of an external heat source on the enhanced drug delivery, 3) the broad applications of the findings to the controlled release of medications and 4) significant improvements in the design of controlled-release devices for various drugs. For the purpose of simulations and to increase the applicability of the results, information on the physical properties of drug, pad, patch and skin is required. The related experiments and products developed for the enhanced drug delivery up to date do not provide all the physical properties necessary in this study. For example, the temperature dependency of the diffusivity of a drug in a biomaterial is not published. Because of the complexity in the analysis of drug transport through the skin, only the overall permeability is measured in most of the clinical experiments. The results of such experiments are applicable to specific purposes and products but are not suitable for general designs. Estimation equations are often used to estimate parameters in the absence of experimental data. The literatures offer empirical diffusivity equations such as Wilke-Chang [44, 45], Tyn-Calus [46] and Chen-Chen [42] correlations. Although those theories are valid for a range of chemical engineering processes, they usually involve constraints that make them unsuitable for biosystems. For example, the most frequently-used model in the diffusivity estimation is the Wilke-Chang equation:

$$D_{AB} = \frac{7.4 \times 10^{-8} (\phi_A M_B)^{1/2} T}{\eta V_A^{0.6}}. \tag{3.46}$$

Equation (3.46) provides reliable estimation (within 10 % error) for the diffusivity of very large molecules (M_B>1000) in a dilute liquid [42]. But note that drugs such as

fentanyl or corticosterone have molecular weight of only 200-400 Daltons. In addition, Equation (3.46) is not a linear function of temperature since viscosity of media, η, also varies with temperature. Thus, process designers must deal with the viscosities of the formulation medium. It is also impractical to prepare tables for the diffusivities of thousands of drugs in a large number of possible media for given temperatures. Therefore, in this research, estimation models will be selected to compute parameters that are not available in the literature. Although these correlations may not be accurate for the systems used in the study, the findings, however, can also be applied in controlled-release research to help identify important design features. The equations can also lead to the development of methods for extracting key properties. The simulation platform will help researchers reduce the number of experiments which will to save valuable time and efforts.

In the design of a transdermal drug delivery patch enhanced by an external heat, a host of parameters affect the release profile, e.g., from the composition of the pad material to the thickness of patch. As a result, medical device manufacturers are charged with the task of carefully selecting among several options, process and design parameters, at their optimum levels, for a particular application. Not all possible combinations of these variables are tested in the laboratory. Instead, a few important factors (called "design parameters hereafter") are selected and tested to produce a desired therapeutic effect. The general guidelines for choosing the design parameters are 1) the value of the parameter can be controlled easily, e.g., simply by changing the material, thickness, composition or size, 2) the parameters are independent of each other, 3) the release profile must be more sensitive to changes in the design parameters compared to the influence of other specifications. In this context, the results of this investigation can help manufacturers of controlled release devices develop strategies to identify the design parameters, determine the best combination and assess the effects of those parameters on the release profile. Such analysis will also provide the relative importance of the selected design parameters. Further process design experiments and clinical tests can be performed based on the relative importance measures.

3.3.1 Material Properties

As a model drug, corticosterone is selected. Corticosterone is a steroid hormone secreted by the adrenal glands. Steroid hormones, such as corticosterone, play important roles in the regulation metabolism and affect the immune system and behaviors. Recent studies found that a prenatal administration of corticosterone to the common lizard results in less dispersal life style of its juvenile [47, 48]. Other investigation also found that excessive corticosterone indirectly affects abdominal obesity since it stimulates calorie intake [49]. Hence, the administration of corticosterone requires careful considerations. The results of this research will contribute to the controlled-release of corticosterone.

The patch is assumed to be made of poly (ethylene-co-vinyl acetate) polymer (so called EVA polymer). EVA polymer is a good candidate of transdermal patch material since it has high flexibility and adhesion characteristics at a low temperature. The thickness of EVA polymer is set to 5×10^{-3} m (5 mm). Thermal conductivity [50], density [51], heat capacity [50] and diffusivity [52] of commonly used EVA polymer are available in the literature. Based on those values, the thermal diffusivity of EVA polymer is estimated at $5.483 \times 10^{-7} m^2/s$. This value is assumed to be constant in the narrow temperature range of 37-55 $°C$. This choice is supported by publications demonstrating a weak functionality of thermal diffusivity, e.g., $\kappa \propto T^{0.5}$ and $C_p \propto T^{0.73}$ [50]. Only the effect of heat on the drug diffusivity is studied in this contribution.

The partition coefficient is defined as the ratio of the concentrations of a material (corticosterone) in two immiscible, contiguous media at equilibrium. In pharmaceutical sciences, the octanol-water partition coefficient is often referred as a measurement of hydrophobicity of a drug. Even though the drug delivery model in this study does not describes the equilibrium system, the boundary condition as Equation (3.14) is valid since it is assumed that the equilibrium is achieved much faster than the outflow of drug at the boundary. The reciprocal of the partition coefficient, $1/K_M$, of corticosterone in lipid bilayers of stratum corneum is reported as 39 [53].

3.3.2 Temperature Dependence of Diffusivity

The Arrhenius-type temperature dependence of diffusivity has been used in the analyses involving the non-isothermal transport of drug through polymeric membranes [43]. In studies on the moisture loss in heat, a spherical model was implemented and predicted results were compared with experimental data [54]. The results showed a linear relationship between the natural logarithm of diffusivity and the reciprocal of the absolute temperature (Arrhenius-type).

In the absence of the complete set of data for the diffusivities of drug in the EVA polymer and skin, this research proposes to implement the Arrhenius-type functionality [40, 43] such that

$$D(T) = D_0 e^{-\frac{E_a}{RT_0}\left(\frac{T_0}{T}-1\right)} \tag{3.47}$$

where D_0 is the diffusivity of drug at reference temperature (body temperature, T_0, herein), and E_a is activation energy of diffusion. The diffusivities of corticosterone in the EVA polymer ($5.9 \times 10^{-13} m^2/sec$) and skin ($4.4 \times 10^{-12} m^2/sec$) were measured at 37 $^\circ C$. To obtain the activation energy, the diffusivities at different temperature are required. Instead, it is assumed that the diffusivity is doubled in the skin and tripled in the EVA polymer for the temperature elevation by 10 $^\circ C$(i.e., a rule of thumb used in chemical reaction kinetics). From Equation (3.46), this assumption leads to E_a of 57.17 kJ/mol for the skin and 90.607 kJ/mol for the patch, respectively. These values show similar orders of magnitude to those reported for desoxycorticosterone and testosterone in a silicone membrane [43].

3.3.3 Design Parameters

In line with the previous definition, a design parameter is a factor that has a strong influence (compared with other parameters) on the transdermal delivery of corticosterone to the systemic circulation. It can also be easily manipulated in the device design. In the heat-enhanced transdermal delivery protocol, five design parameters are suggested: initial reaction rate; mass of pad; overall heat transfer coefficient; and initial concentration.

Initial reaction rate (IR=$k_1 C^2_{Iron,0}$) refers to the chemical reaction rate when iron powder is just exposed to the oxygen gas. This determines the speed of the oxidation of iron and estimates how long the exothermic reaction persists during the treatment. The control of the initial reaction rate is very important. A sonophoresis or an iontophoresis contains an electronic device to control the magnitude of the enhancement. However, the chemical reaction, once it is initiated, takes place spontaneously and cannot be stopped by an external factor. Fast initial reaction rate will result in a fast release of heat in a short time, and thus high temperature will be quickly achieved. Without a proper control of the reaction rate, an extremely high temperature can cause thermal injury. In addition, the exothermic reaction will not persist longer, and thus the thermal effect will vanish earlier than necessary due to the quicker cooling down of the pad. The amount of heat released is related to the amount of iron powder. The concentration notation in the initial reaction rate is valid for a homogeneous reaction. In the heterogeneous reaction, reaction rate depends more on the surface area. In other word, the initial reaction rate can be controlled by manipulating the particle size distribution of iron powder.

Mass of pad (MS=m) refers to the amount of the contents included in the heating pad except iron powder: the filler materials. As mentioned before, the filler material plays a role in deciding the heat capacity of the pad and also controls the release of heat to the patch. A commonly-used hand warmer contains 12.5 g of iron powder and the filler materials in a pouch. A patent shows that the weight ratio is 5 (activated carbon) : 16 (iron powder) : 3 (saw dust) : 2 (sodium chloride) : 6 (water) [55]. Hence, the efficacy of

transdermal delivery protocol can be examined in two ways: 1) considering the contents as pseudo-binary mixture (iron powder and the filler materials), the protocol is tested for various amounts of the filler materials with the amount of iron powder fixed, 2) the protocol is tested without changing the mass of pad. In the former case, the mass ratio in the filler materials is conserved. The manipulation of the mass of the pad is achieved by simply adding the filler materials to the pouch.

Overall heat transfer coefficient (OH=U) is the reciprocal of the resistance to the transport of energy through the layer located between the heating pad and the drug-loaded polymer. Since the backing material acts as a valve of the flow of heat from the pad to the patch and the skin, the overall heat transfer coefficient has significant influence on the temperature profiles in the patch and the skin and, as such, influence the enhancement of drug delivery. The manipulation of the overall heat transfer coefficient can be achieved by the choice of the backing material. A thick backing material provides high resistance to heat transport (small overall heat transfer coefficient). In addition to the thickness, the type of backing material also affects heat transport.

Initial concentration (IC=C_0) of corticosterone in the patch is related to the rate of drug release to the body since the diffusion is a transport mechanism driven by the concentration gradient. If the EVA polymer is blended with a large amount of corticosterone, the initial concentration will be high, and thus fast drug absorption can be achieved. However, the initial concentration is directly related to the dosing size (i.e., financial factors). Even though this research does not take the economics of the drug delivery protocol into account, the price of the active pharmaceutical ingredient (corticosterone in this study) is one of the most important factors in the development of new products. Therefore, the protocol in this research needs to be developed considering the minimal use of valuable drugs to avoid wastes.

Finally, *thickness of patch* (L_{II}) is also considerable. It accounts for ratio of amount of API remaining after treatment to the initial dose. Especially, the diffusivity of corti-

costerone is much smaller than other transdermally-transported materials such as fentanyl citrate. Slow diffusion causes a boundary-layer-like concentration profile through a thick patch, which means drug release has taken place only at the front (to the side contacting with the skin). And thus great amount of corticosterone blended in the polymer will be unused. On the other hand, too much thin patch may be able to minimize waste of drug after a treatment. However, the desired supply (flux to systemic circulation) of APIs may not persist long. It is worth noticing that thickness of patch was not a design parameter in the previous study.

3.4 Results and Discussions

In this research, the analysis on a heat-aided transdermal corticosterone delivery has been performed for one-time application of patch. Period of therapy is set to 7 days (a week). A week-long therapy is common for such hormone as corticosterone since required flux is very small ($J_{set} = 1.2 \times 10^{-5}$ mg/cm^{2}hr [57]). The repeated applications of transdermal patches keep a patient in a continuous therapeutic range (quasi steady period). This problem was addressed in a prior research [3].

Prior to proceeding with the mathematical model derived early in this study, the validation of the theoretical model is required to support feasibility of rest of the research. For this purpose, data of serum concentration as time obtained from set of clinical experiments are employed. Since the experimental conditions are quite different from that described so far, the modification of the original mathematical model has been made.

3.4.1 Validation of Mathematical Model

The mathematical model developed so far is used to provide information on design of transdermal corticosterone (or any other drug) delivery patch with an external heating source. In spite of useful advantages of the protocol, the validation of the modeling approach should

be done before releasing it for ongoing pharmaceutical researches. In the validation, clinical experimental results are critically required.

Clinical data, retrieved from [9], are used in the validation of the proposed mathematical model. In the experiments in [9], a transdermal patch (Duragesic®) that delivered 25 μg/h of fentanyl to 10 healthy subjects was applied. The serum concentrations were monitored for 36 hours during which blood samples were taken, analyzed and recorded every hour. The tests were performed in four sessions (called A, B, C and D, respectively). In sessions A and B, a patch is worn to each subject for first 30 hours, and is removed then. In session A, a heating pad is applied over patch for 1 hour starting at 24 hour. In session B, a heating pad is applied for the first 4 hours and removed. Then another heating pad is applied again during the 24 to 25 hour period. Temperature of a heating pad is assumed to be 42 $^{\circ}C$. Sessions C and D are not suitable for this validation. Serum concentrations as time in each session that will be used in the rest of this study are taken from Figure 1 of [9].

The modification of the original mathematical model is also required to suit the experimental data. Although the heating pads worn by the subjects were identical to that described in this work, no detailed description of the pad is given except a temperature rise of 42 $^{\circ}C$. In addition, Duragesic® is a reservoir-type patch whereas a matrix-type patch is used in the original model. A reservoir-type patch can maintain a constant drug concentration in the polymer material for a long time. In this case, the existence of the polymer material is not significant, and thus the mass and heat transports through the patch are ignored. The original model is modified accordingly:

$$\frac{\partial \bar{C}_{III}}{\partial t} = \frac{\partial}{\partial x}\left(D_{III}\left(\bar{T}_{III}\right)\frac{\partial \bar{C}_{III}}{\partial x}\right), \tag{3.48}$$

$$\frac{\partial \bar{T}_{III}}{\partial t} = \alpha_{III}\frac{\partial^2 \bar{T}_{III}}{\partial x^2}, \tag{3.49}$$

$$\begin{cases} \bar{C}_{III}\big|_{x=0} = K_M C_0 & 0 \le t < 30\text{hr} \\ \frac{\partial \bar{C}_{III}}{\partial x}\Big|_{x=0} = 0 & t \ge 30\text{hr} \end{cases}, \tag{3.50}$$

$$\bar{C}_{III}\big|_{x=L_{III}} = 0, \tag{3.51}$$

$$\begin{cases} \bar{T}_{III}\big|_{x=0} = 42^{\text{o}}\text{C} & 0 \le t < 4,\ 24 \le t < 25 \\ \frac{\partial \bar{T}_{III}}{\partial x}\Big|_{x=0} = \frac{h}{\kappa_{II}}\left(\bar{T}_{II} - T_a\right) & \text{others} \end{cases}, \tag{3.52}$$

$$\bar{T}_{III}\big|_{x\to\infty} = 37^{\text{o}}\text{C}, \tag{3.53}$$

$$\bar{C}_{III}\big|_{t=0} = 0, \tag{3.54}$$

and

$$\bar{T}_{III}\big|_{t=0} = 37^{\text{o}}\text{C}. \tag{3.55}$$

The temperature of air, T_a, is kept at 25 $^{\circ}C$, and the heat transfer coefficient is 20 W/m^{2}K [58]. The heat conductivity of the patch, κ_{II}, is not known, and hence the same value as used in the original model is assumed. The dimensionless expression is not

used in this modified model. The partition coefficient of fentanyl is 860, and the constant concentration of the patch is 164 μg/mL [59]. Even though the model that is intended to be validated has been slightly simplified, the important feature of the original model (i.e., the thermal enhancement of diffusion) is still represented well by the new equations. The serum concentration is expressed by

$$\frac{dC_{serum}}{dt} = \frac{-D_{III}\left(\bar{T}_{III}\big|_{x=L_{III}}\right)A\left(\frac{\partial \bar{C}_{III}}{\partial x}\right)_{x=L_{III}}}{V_B} - k_E C_{serum} \tag{3.56}$$

where C_{serum} is a serum concentration of fentanyl, V_B and k_E are the volume of distribution and the elimination rate constant of fentanyl, respectively. Specific steps to validate the original model using the modified system, Equations (3.48) to (3.56), is summarized as following: 1) the serum concentrations up to first 12 hours in sessions A and B are involved in the study, 2) as many physical and other properties as possible are collected from literatures, 3) the modified model with applied local heat is fitted to the serum concentrations in session B (some uncollected parameters may be determined here), 4) using the physical property values in step 3), the modified model without heat is predicted for the first 12 hours, 5) the modified model is successfully validated if the predictions in step 4) agree with the experimental data. The implementation of only the first 12-hours data is relevant because unchanged physiological conditions of human subject are expected for such short period. Unlike the mathematical model, biological conditions of human are continuously changing due to various factors. One and half day (i.e., 36 hours) is too long period for those conditions to remain unchanged. They eat, move, and even sleep during that time. And continued exposure to a drug also changes pharmacokinetic parameters of that drug. In these reasons, unexplainable behaviors (e.g., jump of serum concentrations) are often observed in Figure 1 of [9].

The result of the steps 1) to 5) are shown in Figure 3.3. The volume of distribution,

V_B, and the elimination rate constant, k_E, of fentanyl are set 3 L and 0.6 hr^{-1}, respectively. When fitting the modified model to the data of session A, two pharmacokinetic parameters are estimated: effective diffusivity of fentanyl, D_{III}=1.45$\times$10^{-9} m^2/s, and the activation energy of the effective diffusivity of fentanyl through skin, E_a=114.34 kJ/mol. With these values and the same model, the experimental data of session A are predicted and the results are shown in Figure 3.3. In Figure 3.3, a good agreement is observed between the model prediction and the experimental data. Therefore, the modified and original models of the transdermal drug delivery system with heat enhancement are verified. This finding justifies the development of a design protocol based on the mathematical representation. The model may help address questions relevant to researchers and device manufacturers.

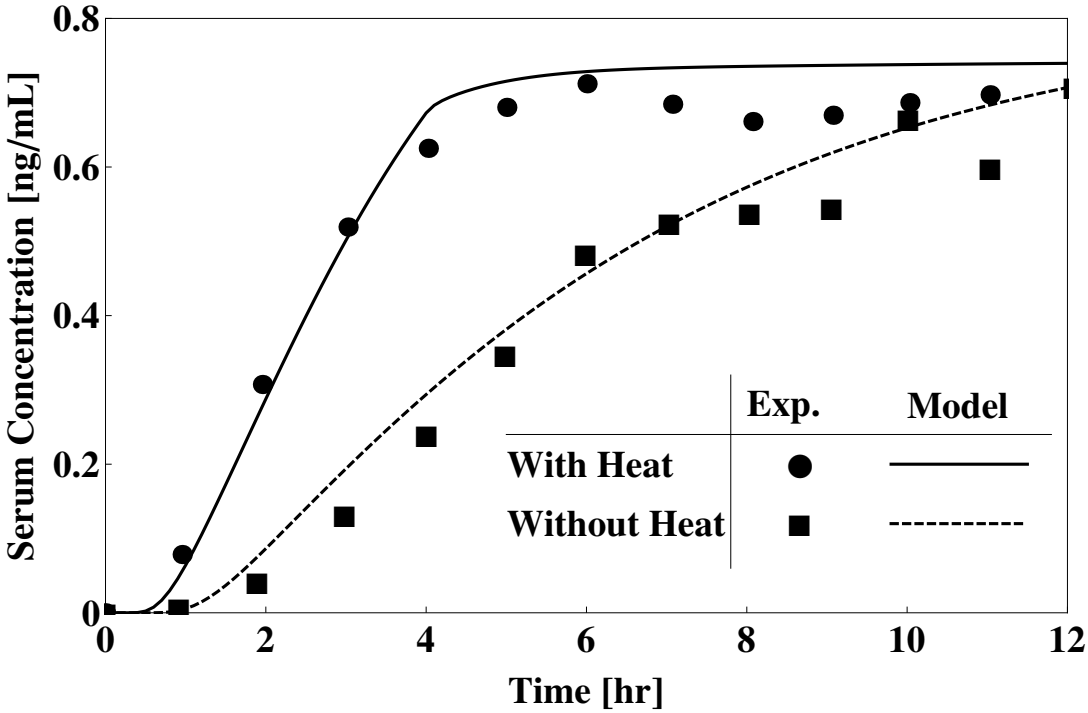

Figure 3.3 Expected temperature and concentration profiles observed throughout the treatment by the transdermal drug delivery protocol used in this research.

3.4.2 Optimal Design of Heat-Enhanced Transdermal Drug Delivery

The design parameters defined are the initial reaction rate (IR), mass of heating pad (MS), overall heat transfer coefficient (OH), initial concentration of patch (IC), and thickness of patch (TH). For the patch thickness, specific values of 0.5 mm, 1 mm, 2 mm and 3 mm are selected in the optimization. Compared to other factors, variation in TH contributes less to the flux. Rather, the patch thickness is related to the effective use of drug. Consequently, no high-precision tuning is required for TH. The values of IR and MS are fixed at 12.375 g/cm^{3}hr and 12.5 g. In previous work, the two factors, IR and MS, were ranked 2nd and 3rd, respectively, among four parameters as having the most significant impact on the desired flux [3]. Nevertheless, from experiences and theoretical considerations, these parameters were excluded from the list of design parameters and set at specific values for the following reasons. Because the diffusion of corticosterone through either patch or skin is very slow, the treatment period is long. Under this condition, simulation results showed long dormant and exponential periods. In order to shorten these periods, the initial oxidation rate is likely to increase so that a high temperature can be achieved. Also, the mass of the heating pad also tends to increase to ensure a prolonged effect of an external heat source. Those trends that cannot be controlled systematically by the developed computer program yield two disadvantages: skin burn due to the high temperature and an inconveniently heavy device. To circumvent these drawbacks, the analysis should be more case specific so that the problem is solved for a limited number of design parameters. Therefore, the mass of pad (MS) is fixed to 12.5 g, which is the weight of common hand-warmer [55]. Also, to avoid thermal injury, the initial oxidation rate (IR) is determined so that the 99 % conversion of iron powder is achieved 10 hours after the treatment begins; this leads to an IR of 12.375 g/cm^{3}hr. The program is designed to display whether the input parameters cause skin burn or not. The sets of values of design parameters that result in thermal injury are excluded in the optimization.

With the patch of 0.5 mm thick, the optimum design is obtained: OH=1.881 J/cm^{2}hrK and IC=65.02 μg/cm^3 with the resulting ISE=0.1097. Note that the units of mass, length and time are gram, centimeter and hour, respectively while and others follow SI units. The unconventional unit selection has benefits in the numerical solutions of the governing equations and decreases the optimization time. At the end of the simulations and optimizations, those values are reported in the SI units. Concentration profiles in the patch and skin over the treatment period are showed in Figure 3.3. The discontinuity at the boundary between patch and skin is observed due to the equilibrium condition applied at the interface. After the treatment ends, around 2 % of the initial corticosterone remains. The temperature distributions and the flux at this optimal design are shown in Figures 3.5 and 3.6, respectively. Since this transdermal drug delivery system is cooled down nearly to the initial temperature within the first 12 hours of the treatment, it is said that the heat is used merely to promote the initial diffusion and absorption of drug to the capillary. The maximum allowed temperature is 55 $^{\circ}C$, and no skin burn will occur. It takes about 2 days for the flux to reach the desired level, and it persists for 3 days. Hence, parallel administration with other dosage form should be suggested to maintain the serum concentration of corticosterone during this time. Note that the flux does not meet the need for the remaining 2 days.

With a 1 mm-thick patch, the optimum design is obtained OH=1.646 J/cm^{2}hrK; and IC=51.74 μg/cm^3. The concentrations of corticosterone are shown in Figure 3.7. Those settings lead to 68.9 % of the drug consumed during 7 days. The remaining corticosterone may be helpful in case a patient forgets to replace the patch with a new one. According to Figure 3.8, no skin burn occurs, and the system is cooled down in the first 12 hours. Figure 3.9 shows that it needs 3 days to reach the desired flux. This is longer than 2 days with a 0.5 mm patch. However, the overshoot of flux is moderate and the flux changes within a narrow range in the quasi-steady region. Moreover, after the end of treatment, the flux still meets the need of the patient.

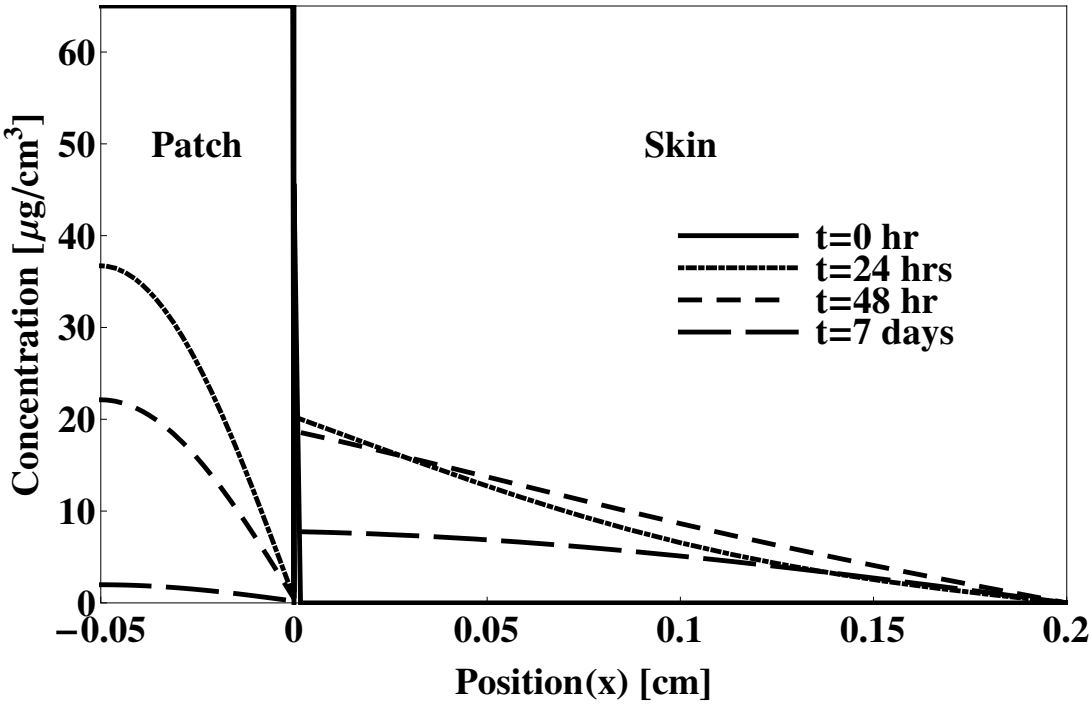

Figure 3.4 The concentrations of corticosterone in the patch and the skin during the treatment with the 0.5 mm-thick patch at its optimum design.

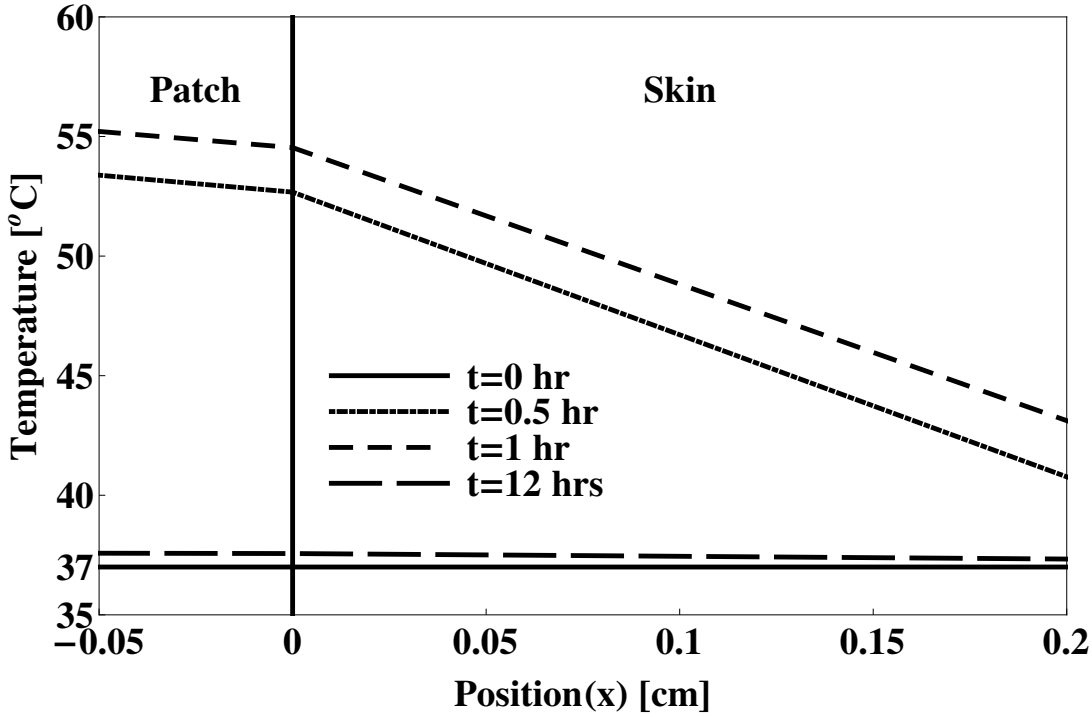

Figure 3.5 The temperature distributions in the 0.5 mm-thick patch and the skin.

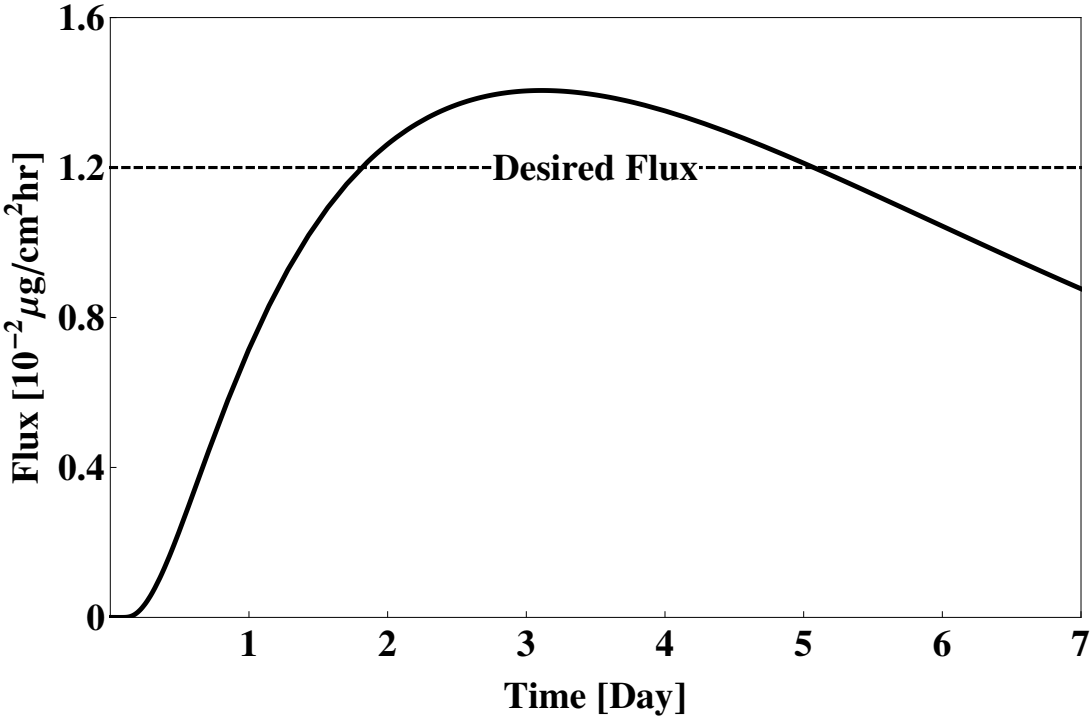

Figure 3.6 Flux during the treatment period with the optimally designed 0.5 mm-thick patch.

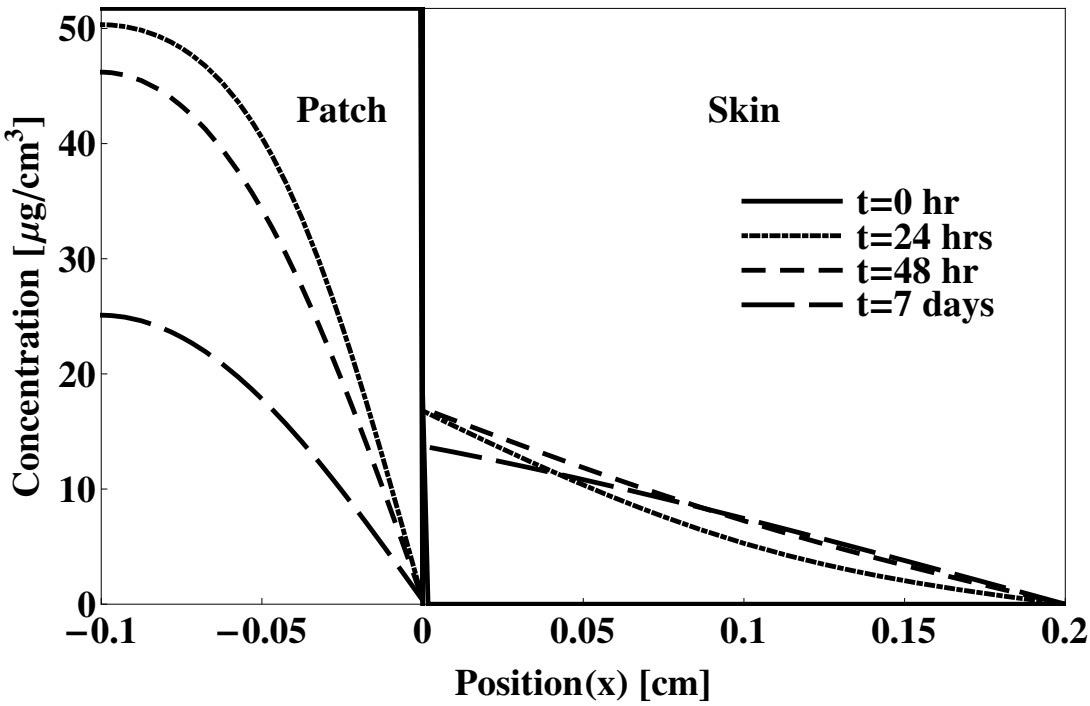

Figure 3.7 The concentrations of corticosterone in the patch and the skin during the treatment with the 1.0 mm-thick patch at its optimum design.

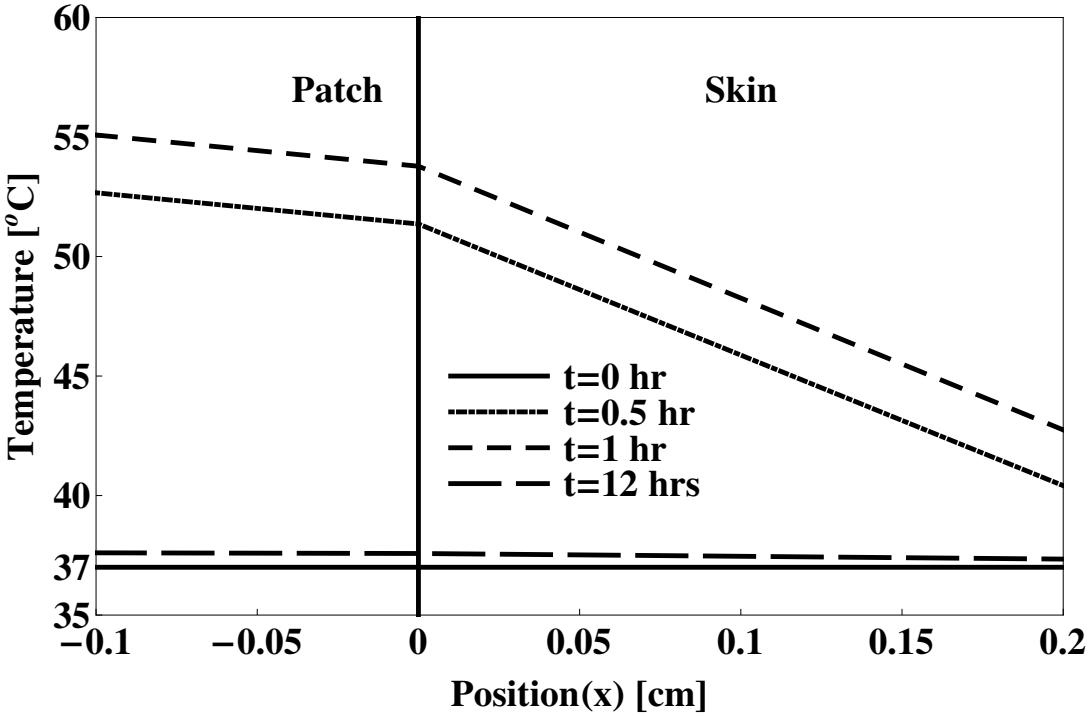

Figure 3.8 The temperature distributions in the 1.0 mm-thick patch and the skin.

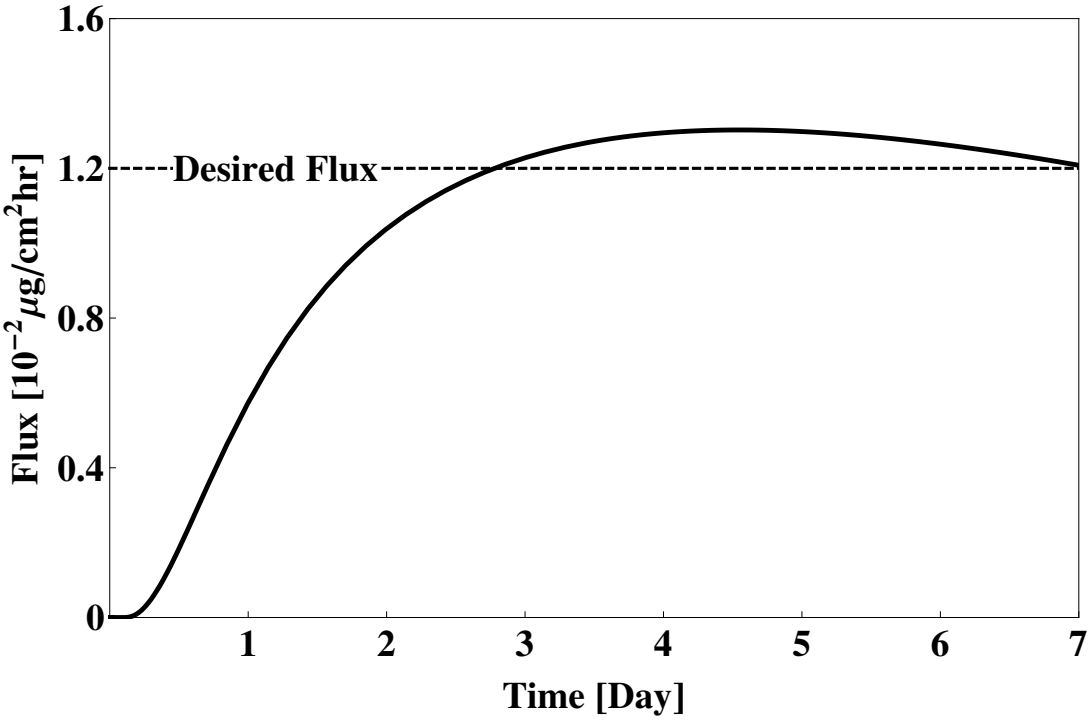

Figure 3.9 Flux during the treatment period with the optimally designed 1.0 mm-thick patch.

The concentration distributions, temperature distributions and the fluxes of corticosterone are illustrated in Figures 3.10 to 3.12 for a 1.5 mm. Similar profiles are shown in Figures 3.13 to 3.15 for TH=2.0 mm; Figures 3.16 to 3.18 for TH=2.5 mm; Figures 3.19 to 3.21 for TH=3.0 mm-thick patches at their optimum design. For those setups, no skin burn is observed, moderate overshoots in the fluxes are obtained and the final fluxes are all above the desired level. The temperatures of the systems get back to the body temperature after around 12 hours. This shows that the determination of the initial reaction rate (IR) is reasonable since the reaction is completed before the system cools down. Two to three days are inevitably required to achieve the desired flux level. Therefore, it is concluded that a proper dose of corticosterone is administered in the form of bolus for an immediate therapeutic action.

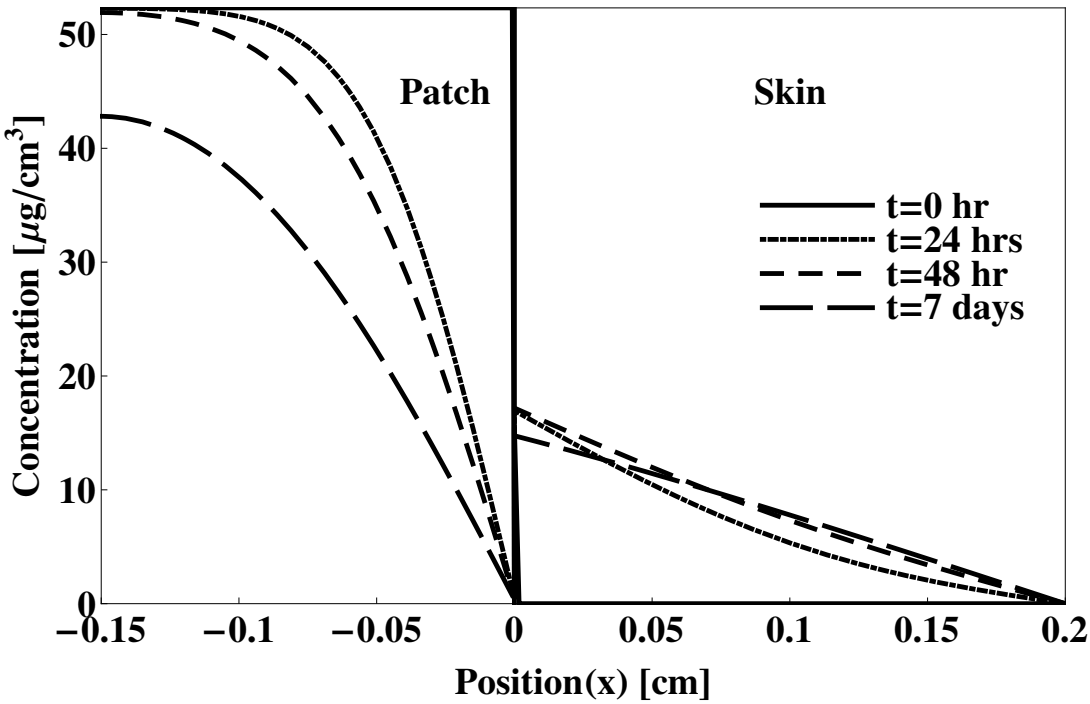

Figure 3.10 The concentrations of corticosterone in patch and skin during the treatment with the 1.5 mm-thick patch at its optimum design.

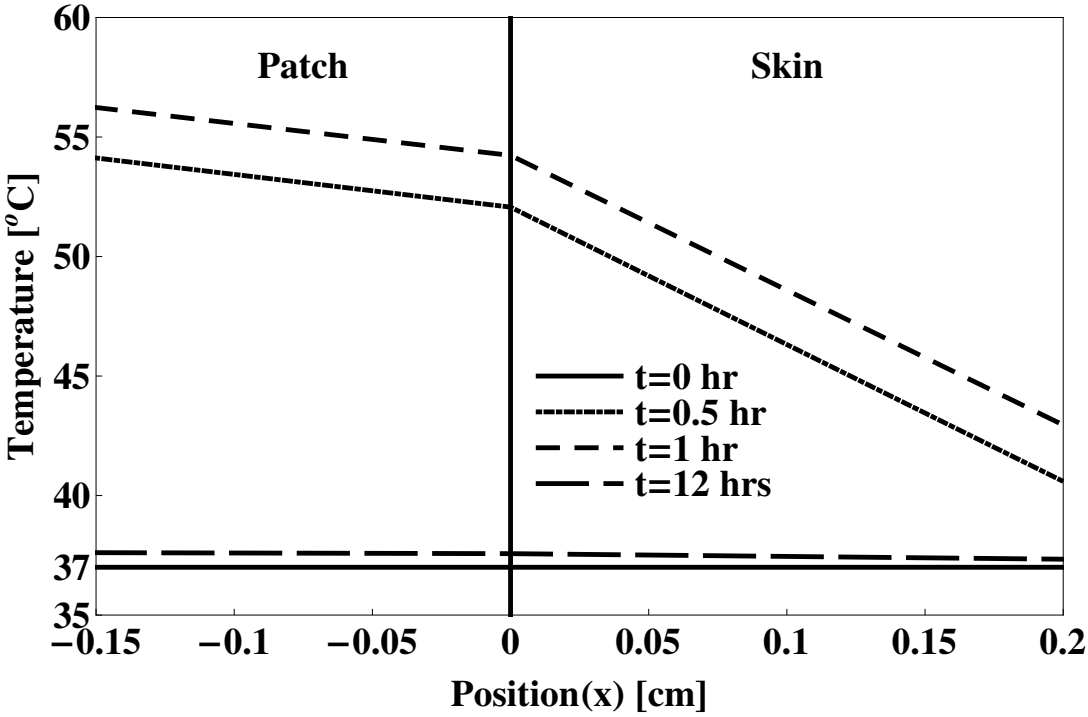

Figure 3.11 The temperature distributions in the 1.5 mm-thick patch and the skin.

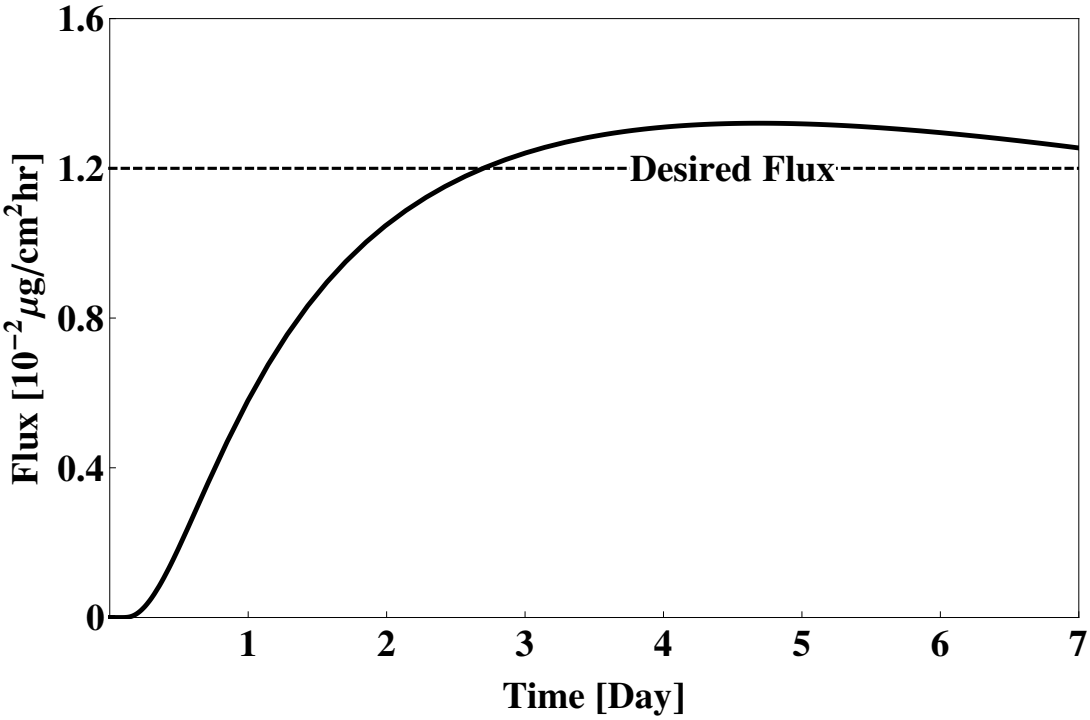

Figure 3.12 Flux during the treatment period with the optimally designed 1.5 mm-thick patch.

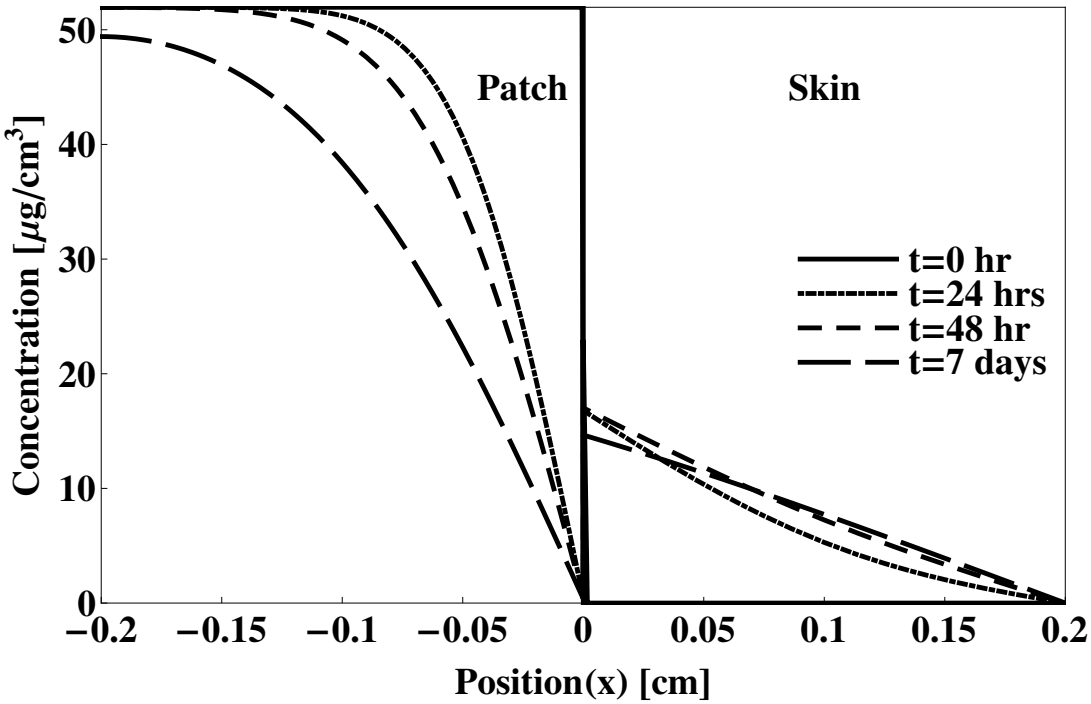

Figure 3.13 The concentrations of corticosterone in patch and skin during the treatment with the 2.0 mm-thick patch at its optimum design.

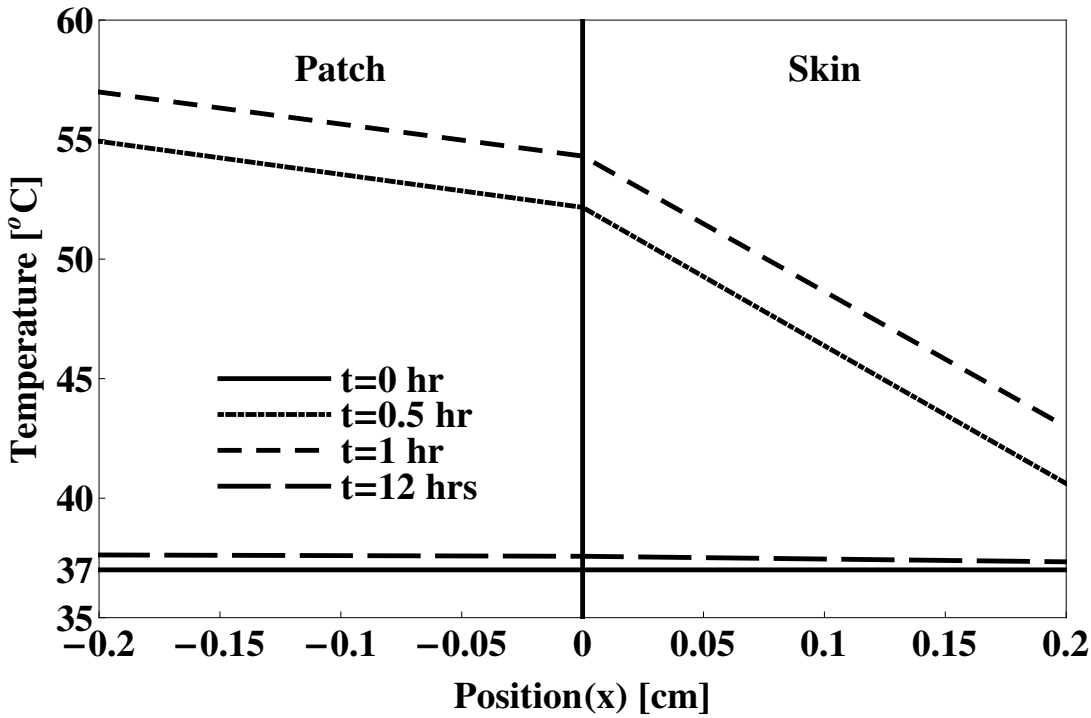

Figure 3.14 The temperature distributions in the 2.0 mm-thick patch and the skin.

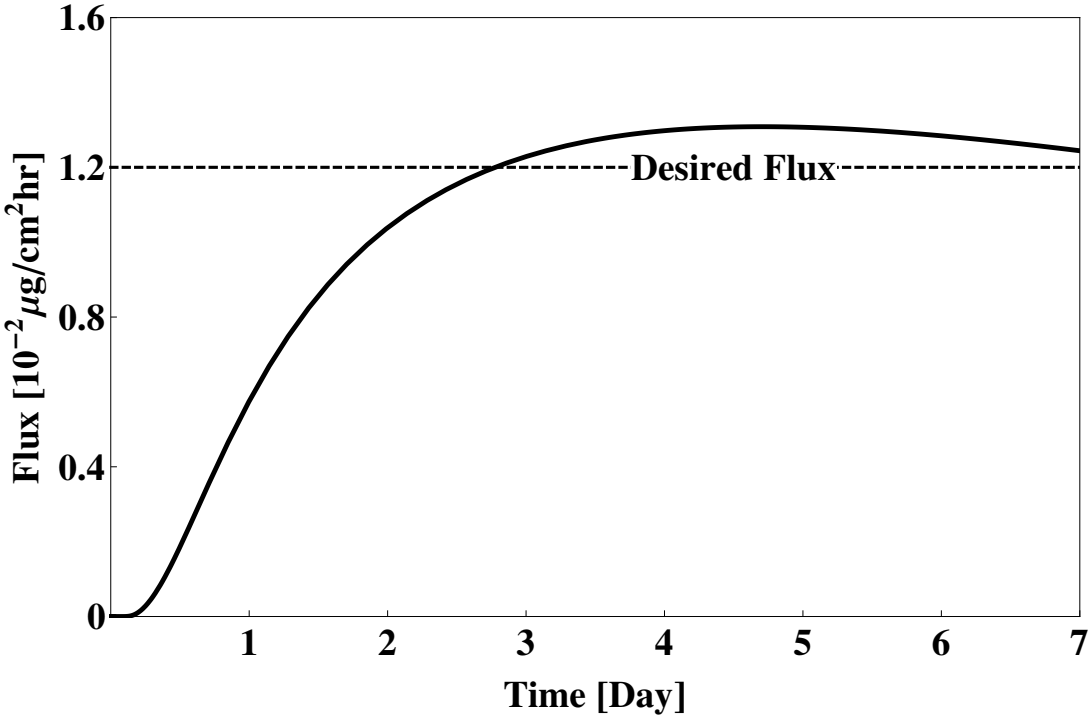

Figure 3.15 Flux during the treatment period with the optimally designed 2.0 mm-thick patch.

The optimal designs for all case studies are summarized in Table 3.1. The ISE represents a measure of the drug therapy to reach the desired delivery rate. The smaller the ISE, the closer the actual flux target is to the target or prescribed flux. Table 3.1 shows that the ISE value increases with the patch thickness at the exception of the 3.0 mm-thick patch. The implication is that a thinner patch if preferred to effectively deliver corticosterone into body.

Table 3.1 Optimum Design Parameters of Transdermal Corticosterone Delivery System Enhanced by External Heat Source

Thickness [mm]	IR [g/cm^{3}hr]	MS [g]	OH [J/cm^{2}hrK]	IC [μg/cm^3]	ISE
0.5	12.375	12.50	1.8809	65.02	0.109653
1.0	12.375	12.50	1.6458	51.74	0.116883
1.5	12.375	12.50	1.7872	52.33	0.117121
2.0	12.375	12.50	1.8190	51.96	0.117232
2.5	12.375	12.50	1.7758	53.12	0.117333
3.0	12.375	12.50	1.7707	52.62	0.117156

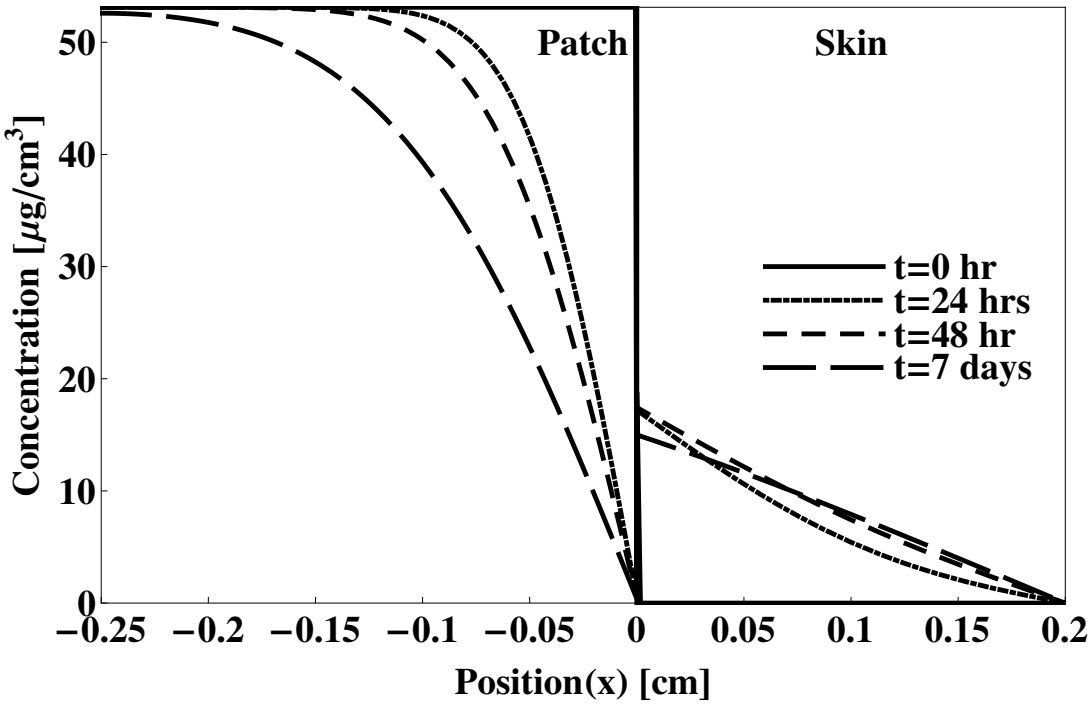

Figure 3.16 The concentrations of corticosterone in patch and skin during the treatment with the 2.5 mm-thick patch at its optimum design.

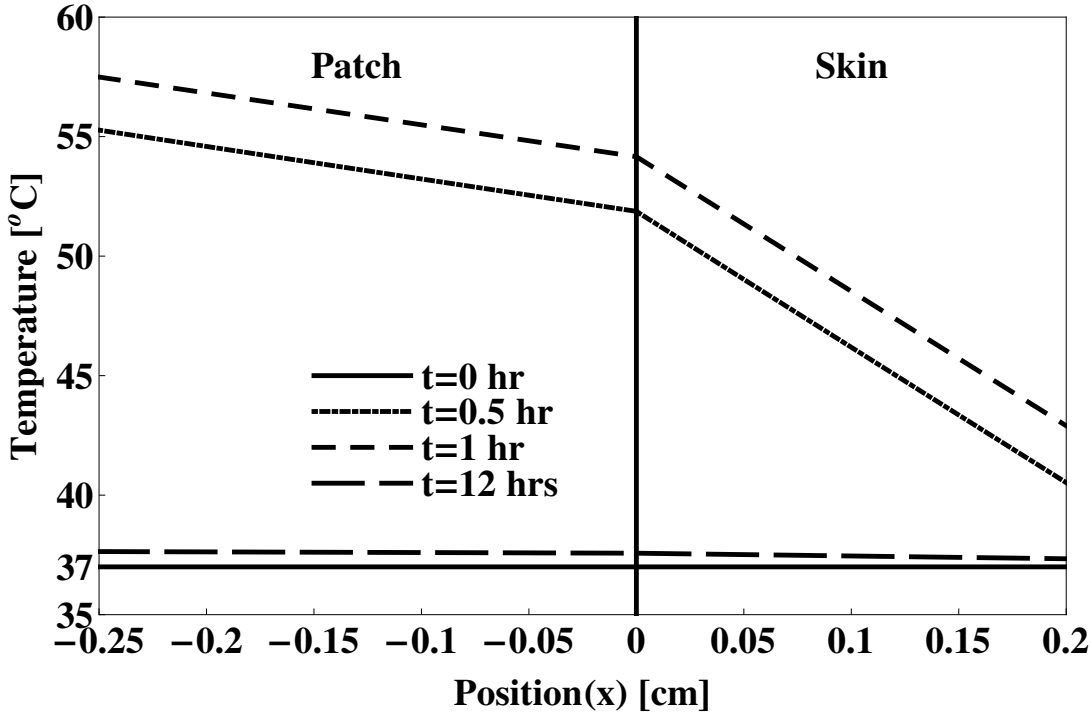

Figure 3.17 The temperature distributions in the 2.5 mm-thick patch and the skin.

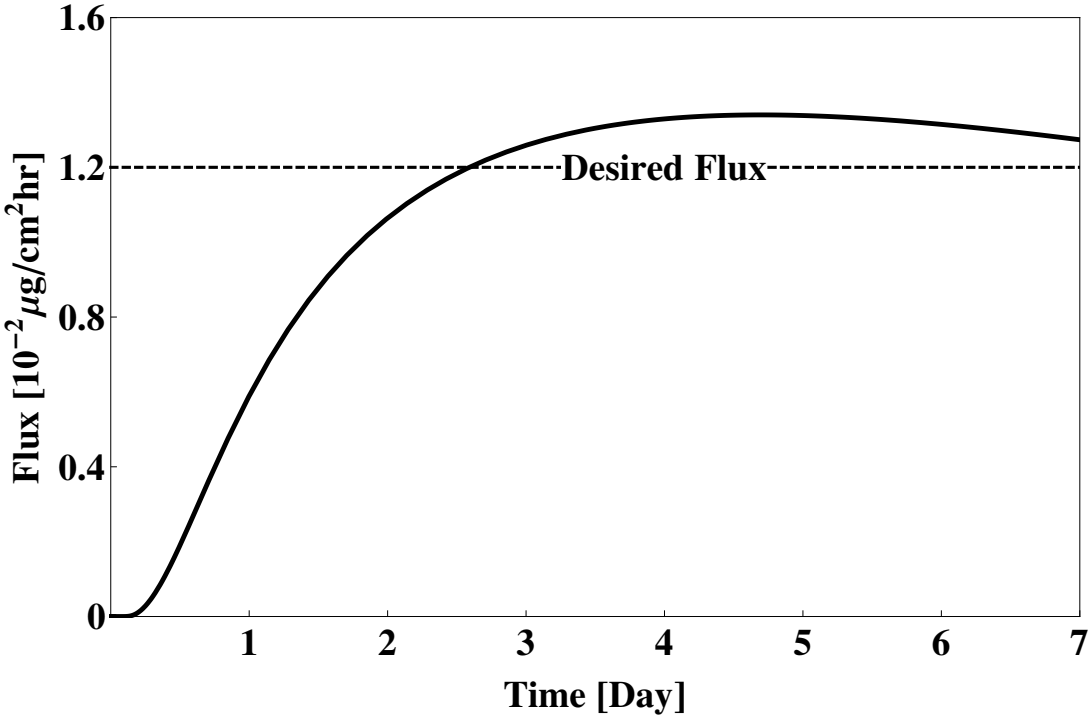

Figure 3.18 Flux during the treatment period with the optimally designed 2.5 mm-thick patch.

Table 3.1 lists other useful quantities resulting from the design. In Table 3.1, the "drug consumption" denotes the amount of drug to be blended with the polymer in a unit area of patch, and is calculated by multiplying the initial drug concentration by the thickness of the patch. Note that the use of thicker patch increases the expenses of corticosterone. The "ratio released" is the percentage of corticosterone that has been released during the treatment out of the total amount embedded initially. The amount of corticosterone that is released from the patch (including the fraction that is absorbed into the body and the residual amount that remains in the skin) does not change significantly from one design to another. On the other hand, the "residue" (defined as the amount of corticosterone remaining in patch per square centimeter after treatment) monotonically decreases with increasing TH. As a result, even though a very thin patch is the best option, from a financial perspective, the 0.5 mm-patch does not satisfy the therapeutic need for the last 2 days, which may cause serious health problems (see Figure 3.9. According to Table 3.2, the patches that are

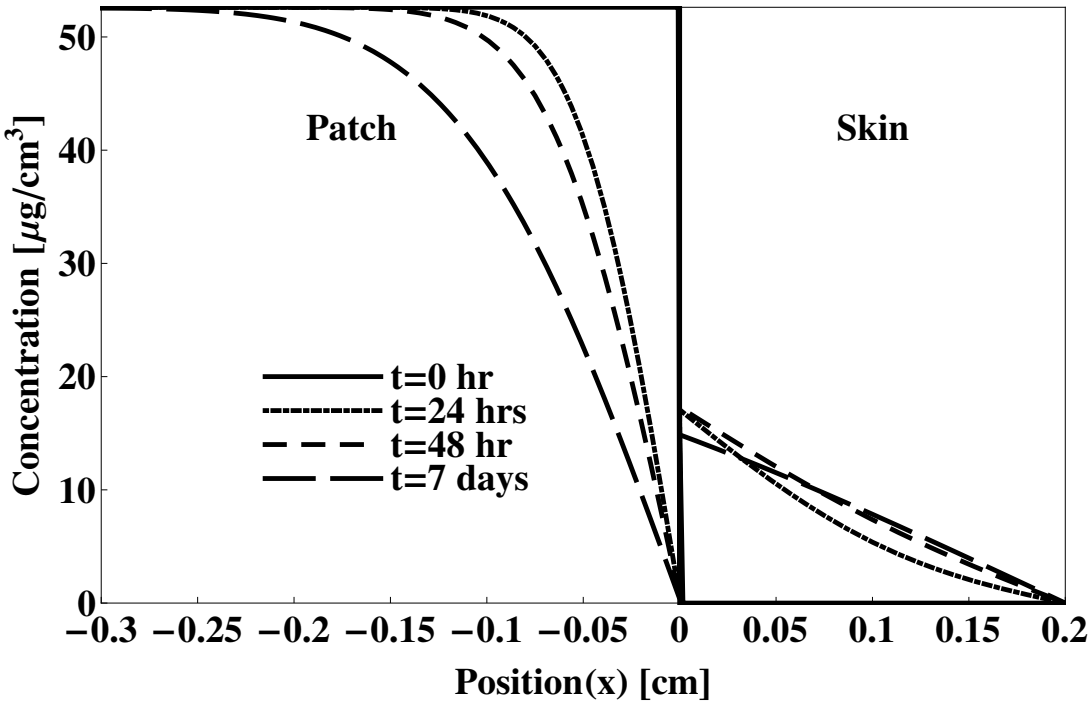

Figure 3.19 The concentrations of corticosterone in patch and skin during the treatment with the 3.0 mm-thick patch at its optimum design.

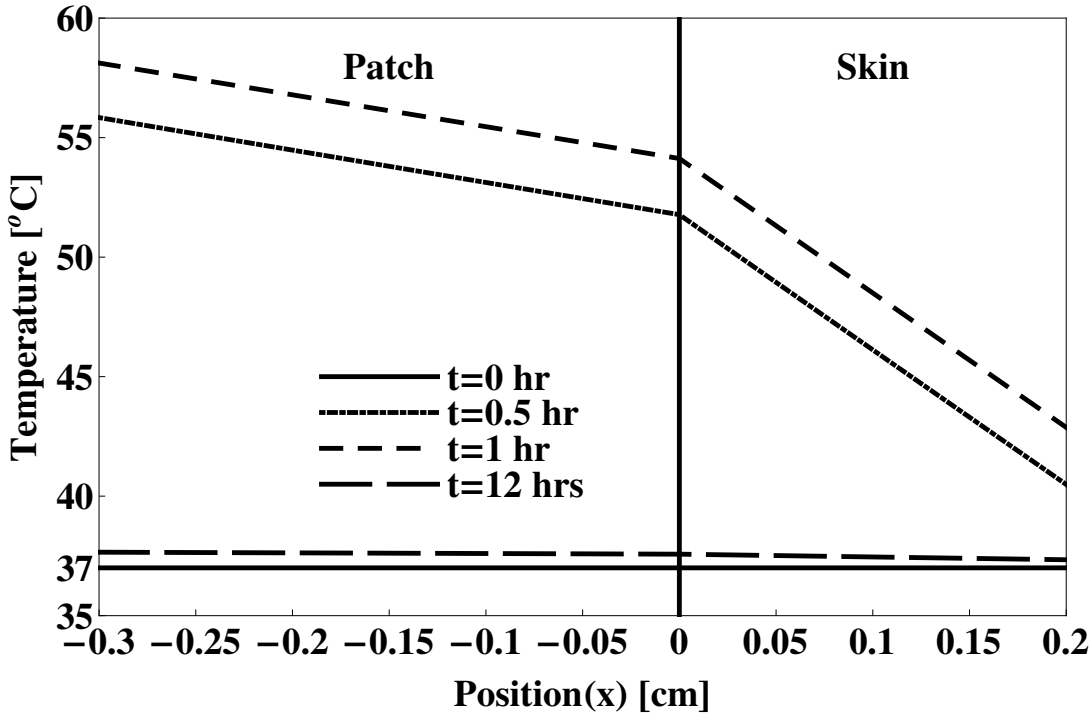

Figure 3.20 The temperature distributions in the 3.0 mm-thick patch and the skin.

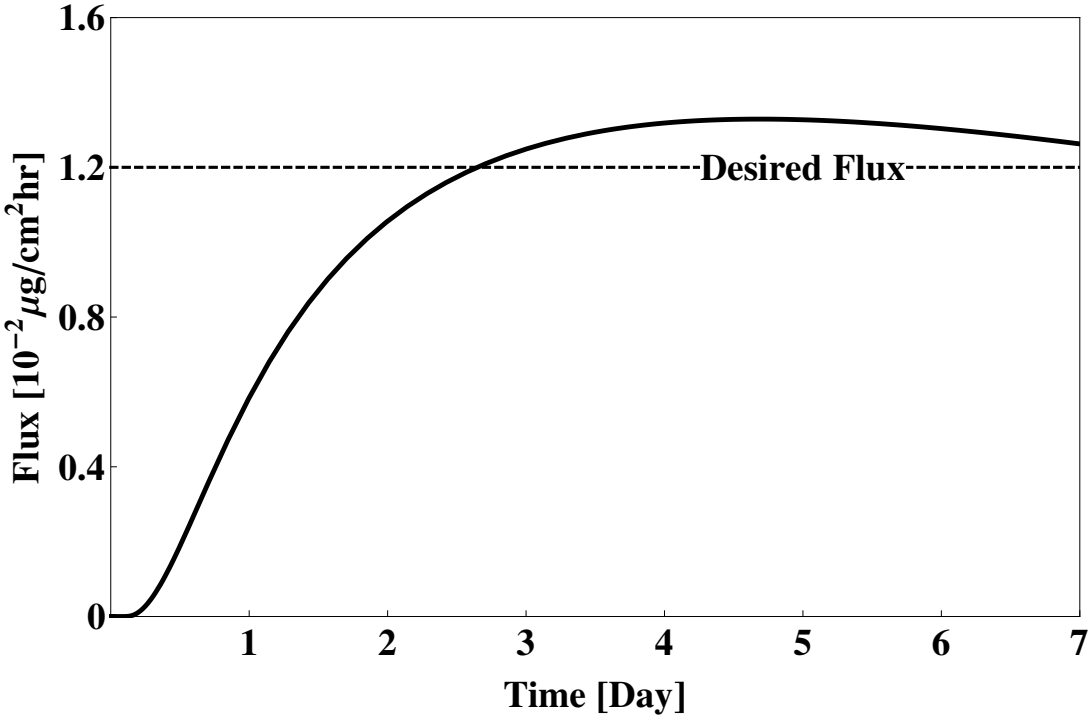

Figure 3.21 Flux during the treatment period with the optimally designed 3.0 mm-thick patch.

1.0 mm or thicker can provide sufficient drug for a 7-day treatment. Therefore, taking the efficiency and the safety issues into account, a 1.0 mm-thick, corticosterone-loaded patch with its optimal design parameters is the best choice for a week-long therapeutic treatment.

Table 3.2 Summary of Transdermal Corticosterone Delivery System Enhanced by External Heat Source with Optimum Design

Thickness [mm]	Drug Consumption [μg/cm^2]	Ratio Released [%]	Amount Released [μg/cm^2]	Residue [μg/cm^2]	Prolonged Release
0.5	3.25	97.95	3.18	0.07	No
1.0	5.17	68.9	3.57	1.61	Yes
1.5	7.85	46.99	3.69	4.16	Yes
2.0	10.39	35.29	3.67	6.72	Yes
2.5	13.28	28.23	3.75	9.53	Yes
3.0	15.79	23.52	3.71	12.07	Yes

3.4.3 Relative Impacts of Design Parameters on Drug Delivery

An optimum design for a heat-assisted transdermal patch was developed using mathematical modeling. A 1.0 mm-thick patch, that enhances the effectiveness of the treatment and addresses safety issues, was recommended. The next task is to assess the relative impacts of design parameters on the desired drug delivery rate. This analysis is important to manufacturers because it will show to what extent deviations of some critical parameters from their nominal values influence the performance of the device.

Similar analyses were performed for the heat-enhanced transdermal drug delivery in [3]. Nevertheless, the mathematical model was slightly modified: infinite domain defined for heat transfer. Hence, it is important to check whether the change made here affects the relative impacts of the design parameters.

Two parameters (i.e., p_1 and p_2) are first selected. A three-dimensional Cartesian coordinate system is used so that two axes are occupied by p_1 and p_2, respectively. The domains of p_1 and p_2 are defined from 80 % to 120 % of the optimum values for p_1 and p_s. The other model parameters are set at their nominal (i.e., optimum) values. The error (ISE) is plotted on the third axis. This error is evaluated at points (p_1, p_2) to produce a surface. Since the center of the p_1-p_2 plane denotes the optimal setting (i.e., the lowest ISE), the expected shape of the ISE surface is a cup which is open to the top. The vertex is placed at the center. However, experiences show different results (e.g., planar). This is because the optimization procedure searches for parameter values that do not violate certain constraints. To facilitate the mathematical optimization, proper domains of variables should be predetermined. On the other hand, this study does not provide such domains until the equations are solved using the given parameters. The program script is written in such a way that a given set of parameters is omitted if the results cause thermal injury. Therefore, assessment of the impacts of two parameters is not straightforward. Some suggestions are given below:

- with a planar surface, the higher-impact parameter shows larger magnitude of gradi-

ent along the associated axis,

- with a bent surface, the higher-impact parameter forms a U-shaped cross-section when the surface is cut by a plane perpendicular to the axis associated with the other parameter,
- with a cup-shaped surface, the higher-impact parameter yields greater second partial derivatives along the associated axis at the center.

In the prior study, six combinations were compared to rank the four design parameters [3]. The results were (from the most to the least influential parameter): initial concentration (IC), initial reaction rate (IR), mass of heating pad (MS) and overall heat transfer coefficient (OH). Although IR and MS were not supplied to the optimization routine, their relative contributions are important to the process. Therefore, six tests are performed in this study, as well.

The optimum design with the 1.0 mm-thick patch is used in the analysis. The results of six tests are: $S_{MS} > S_{IR}$ (Figure 3.22, $S_{IR} > S_{OH}$ (Figure 3.23, $S_{IC} > S_{IR}$ (Figure 3.24, $S_{MS} > S_{OH}$ (Figure 3.25, $S_{IC} > S_{MS}$ (Figure 3.26 and $S_{IC} > S_{OH}$ (Figure 3.27 where S_p is the sensitivity of a parameter p. Consequently, the ranking of the relative impacts is: $S_{IC} > S_{MS} > S_{IR} > S_{OH}$. The overall trend is similar to that of the previous work; the only difference is that MS precedes IR with this model. However, this does not invalidate the conclusions from the two models. Compared to the model outlined in [3], the temperature-dependent absorption of corticosterone at the boundary between the skin and the body core contributes much more to the overall drug delivery. Thus, the duration of a high temperature of skin, as well as the patch and heating pad, is of importance. Note that, in the old model, the boundary is isothermal, and hence, the absorption is not affected by the persistence of heating. It should be noted that the factor controlling the duration of heating is the mass of heating pad, i.e., MS (or amount of fuel). Therefore, the sensitivity test with the new model results in MS having more impact on the corticosterone delivery than IR.

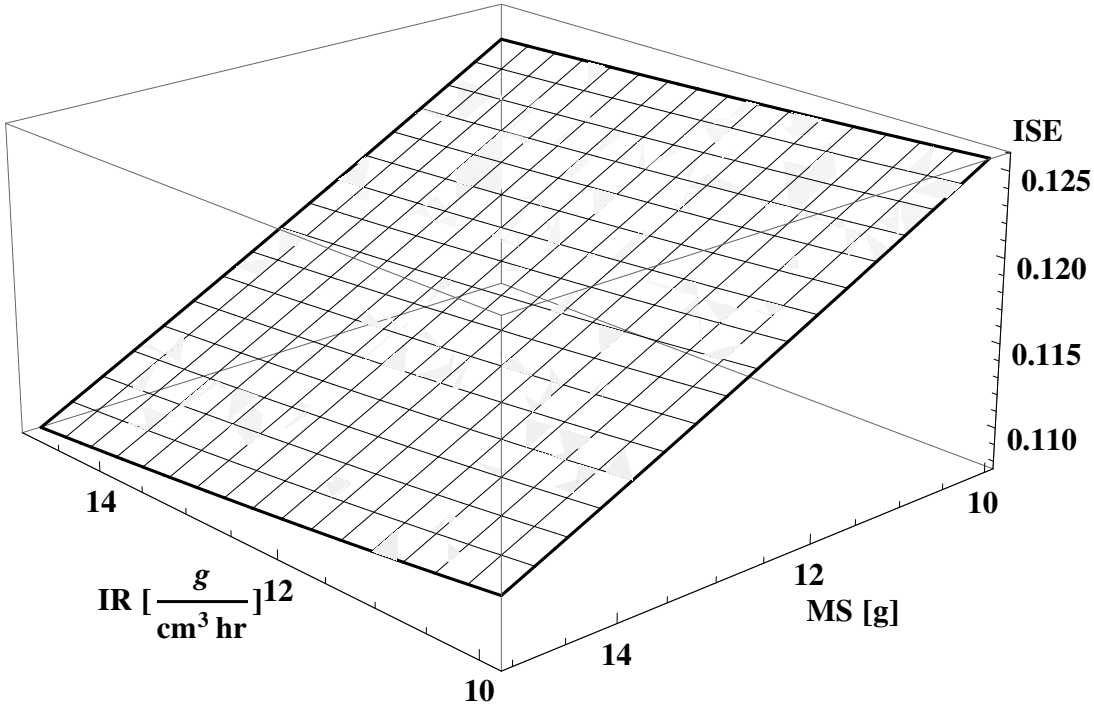

Figure 3.22 ISE surface on the IR-MS domain.

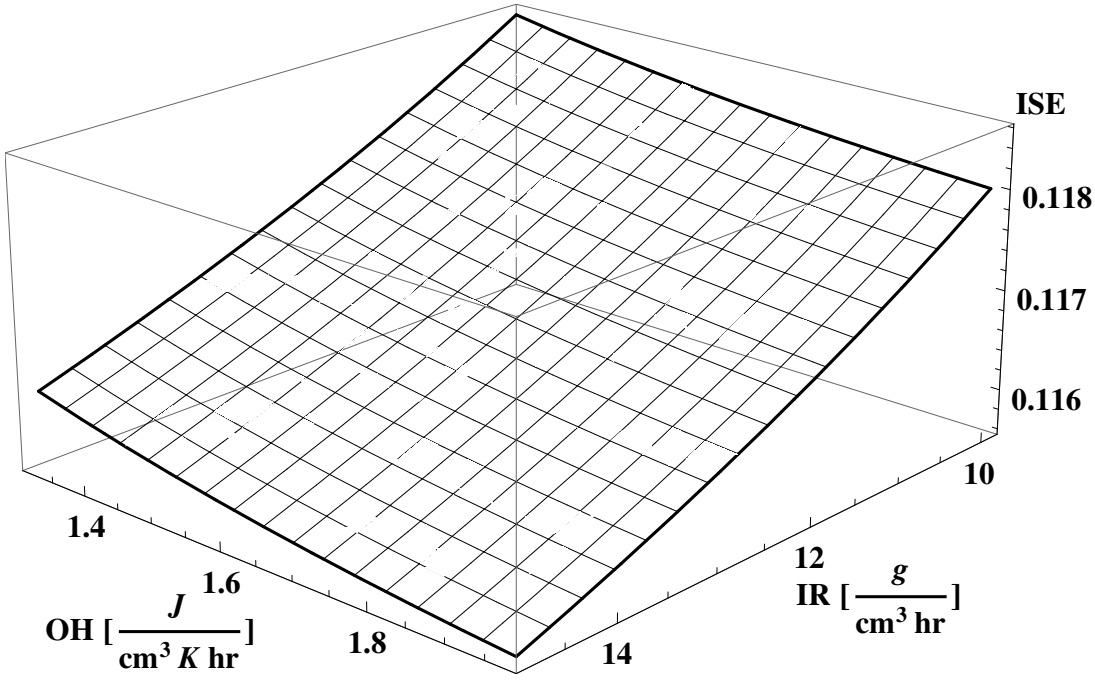

Figure 3.23 ISE surface on the OH-IR domain.

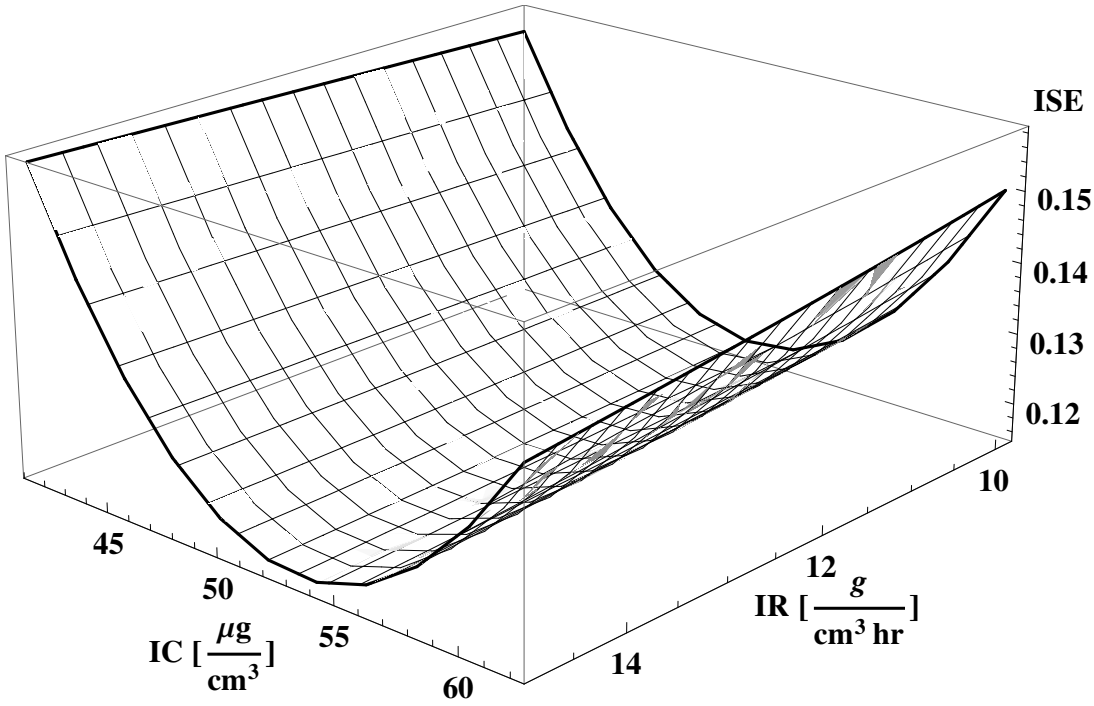

Figure 3.24 ISE surface on the IC-IR domain.

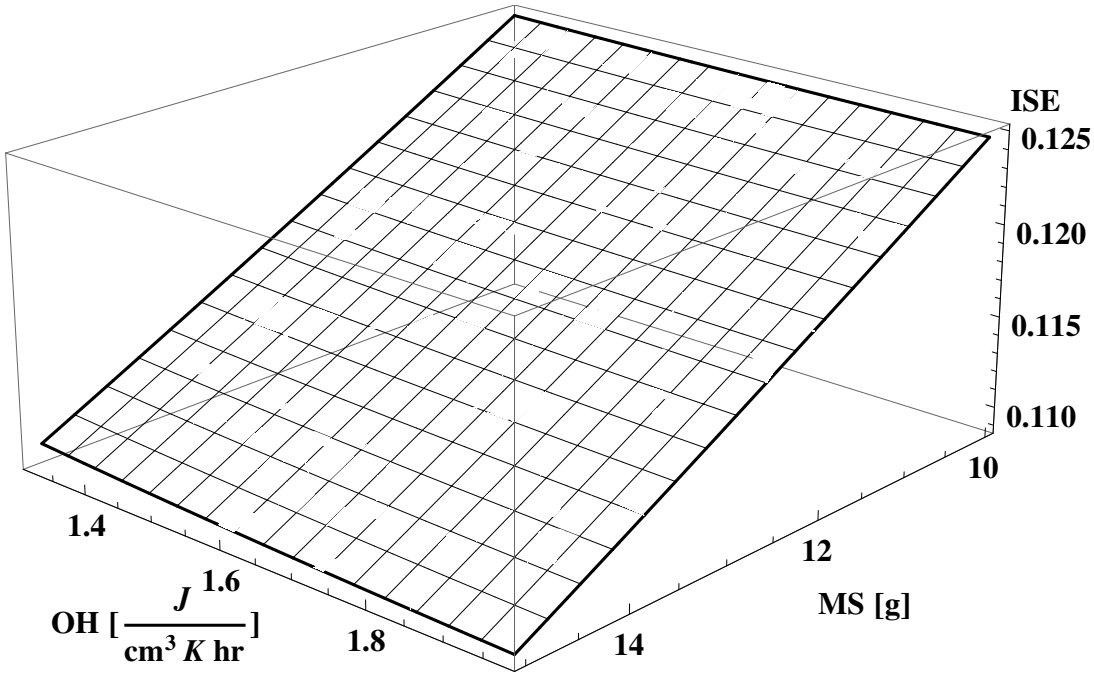

Figure 3.25 ISE surface on the OH-MS domain.

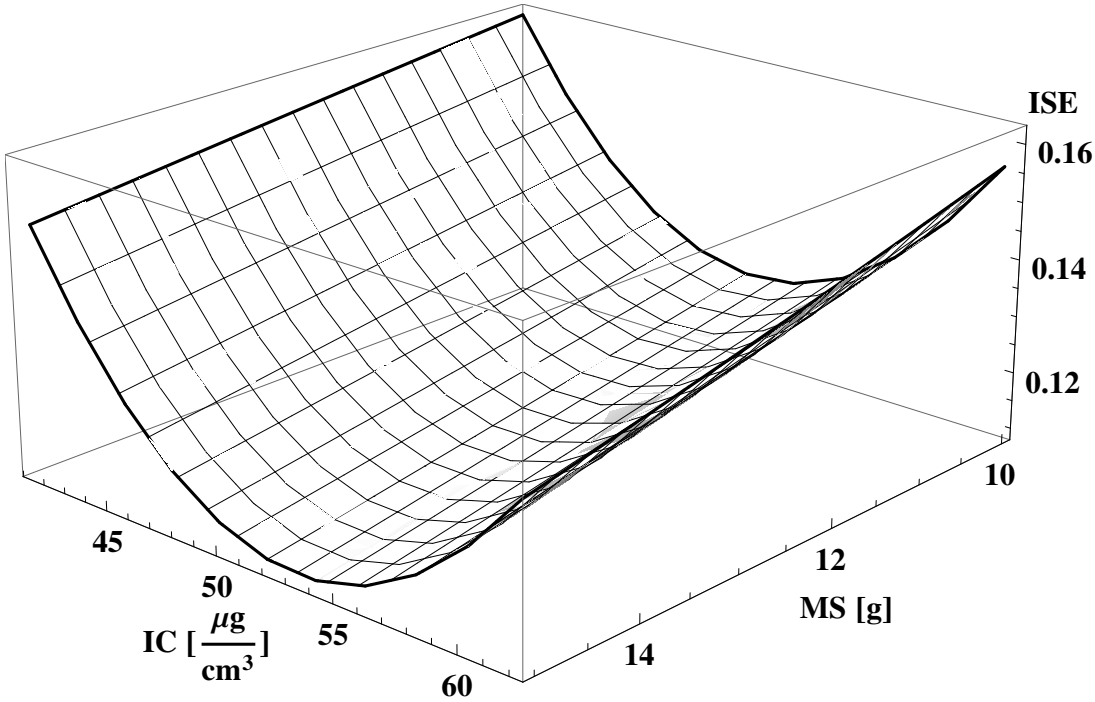

Figure 3.26 ISE surface on the IC-MS domain.

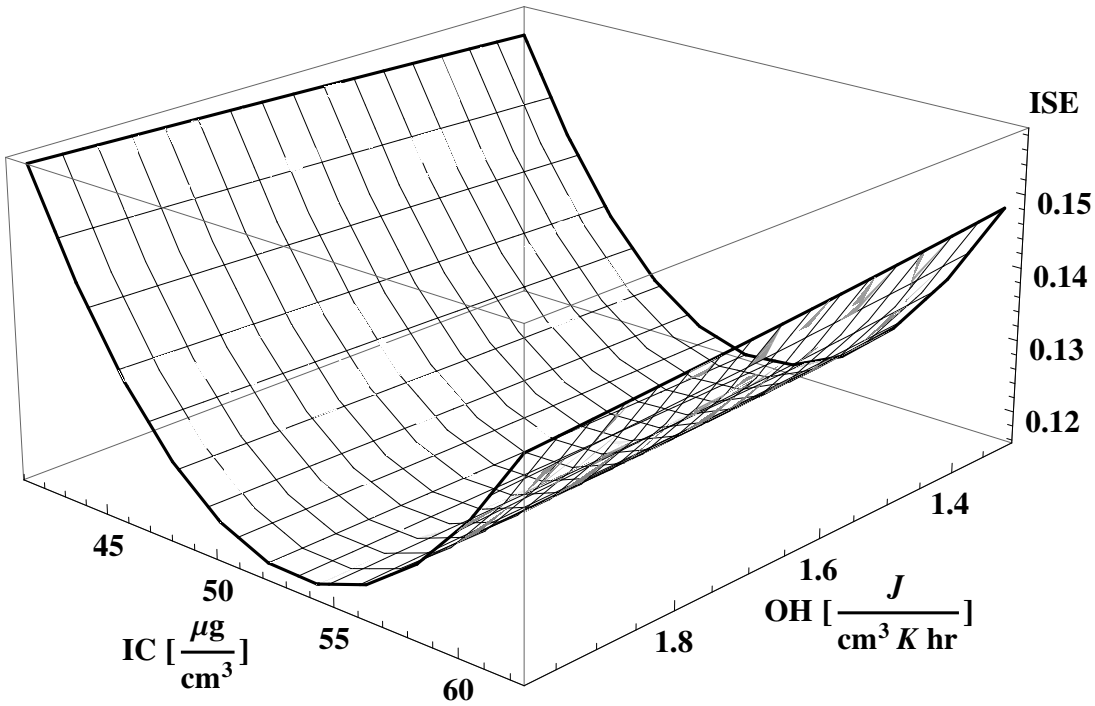

Figure 3.27 ISE surface on the IC-OH domain.

3.5 Conclusions

A mathematical model was derived to investigate the dynamics and the design problems in the transdermal drug delivery system enhanced by the external heat source. The mathematical expressions describe key pharmacokinetic phenomena that take place in a transdermal route:

1. change in temperature of an external heating pad due to an oxidation of iron and heat loss to a patch,
2. the diffusion of an API and the conduction of heat through two adjacent membranes, i.e., patch and skin,
3. a pseudo equilibrium of an API at the interface between the two membranes,
4. flux of an API due to absorption through capillaries.

Validation of the mathematical model based on clinical experimental data shows that the modified model agrees well with the real pharmacokinetics of the transdermal fentanyl delivery with and without heat. This result is used as a good evidence that the mathematical model and subsequent design protocol can be implemented for answering questions in the related pharmaceutical sectors.

The numerical solutions of the partial differential equations are the transient distributions of concentrations and temperatures through the patch and the skin. Mass and energy were conserved which showed the integrity of the model, solution procedure and computer program. The implementation of these solutions in the design of the suggested protocol is performed by 1) identifying a set of design factors and discussing how they can be manipulated [3], 2) finding optimal values of those parameters based on how close the flux is to a desired level, and 3) listing them in the order of the relative sensitivity to the optimal delivery. There are five design parameters [3] that show priorities in controlled release of corticosterone: mass of a heating pad (MS), initial oxidation rate (IR), overall heat

transfer coefficient (OH), thickness of patch (TH), and initial corticosterone concentration in a patch (IC).

Due to the modifications made in the model of this research from that of the previous work [3], i.e., heat is transported deeper into the body than corticosterone. Infinitely large values of the first two design parameters, MS and IR, are required, in theory, for the mathematically optimal release, which would cause a thermal injury in the practical therapy. To prevent the undesired skin burn, three actions are taken in the computer program written in Mathematica® environment: MS is fixed at 12.5 g based on the patent [55], IR is determined 12.375 g/cm^{3}hr based on the setting that 0.99 conversion of iron is achieved for 10 hours, and the optimization process is designed so that it monitors the maximum skin temperature every single iteration and gives a warning sign when the temperature is over the safety margin (55 $^\circ C$). As a result, the optimal release of corticosterone is achieved by making the suggested transdermal delivery protocol so that OH=1.6458 J/cm^{2}hrK, TH=1.0 mm, and IC=51.74 μg/cm^3. The decision is made to take into account not only the ability to reach a desired flux (see Table 3.1) but also the safety and the effectiveness of the treatment (see Table 3.2).

CHAPTER 4

ELECTRICALLY-ENHANCED SOLUBLE MICRONEEDLE PATCH

Microneedle Therapy System (MTS) is one category of transdermal drug delivery system where medicine is transported through the skin by diffusion [59-64]. As discussed in Chapter3, stratum corneum is the thinnest layer but definitely the most significant barrier in transdermal delivery. In spite of difficulties associated with the transport of substances through the stratum corneum, the transdermal route remains a very favorable alternative to other forms of administration. Hence, in addition to applied heat treated in Chapter 3,there have been continued efforts to control and accelerate drug passage through this layer by introducing various drug delivery enhancers. For instance, some non-toxic chemicals (e.g., simply water) have an ability to loosen textures, widen and hydrate pores of skin when it is mixed with or applied prior to APIs (chemical enhancers). With such tunnel-making mechanisms, molecules of APIs can be easily diffused into deeper skin. As a physical enhancer, low-frequency ultrasound is widely used because the sound waves are capable of increasing the skin permeability [69, 70]. Weak electric current can be applied to facilitate the active transport of molecules through the stratum corneum [68, 66, 67]. Drug delivery improvement mechanism of MTS is to pierce stratum corneum with an array of microneedles to make micropores through which medicine passes without resistance of stratum corneum [61, 60]. Despite poking small holes in the skin, microneedles cause no pain or serious injury because nerves are not irritated by microneedle of length ranging from 200 μm to 2 mm according to specific purpose [61].

There are two representative types of microneedles:

Solid microneedle The major function of this kind is to *pierce* stratum corneum to make microchannel. After insertion, the patch is removed for following treatment with medicine. For this reason, it is fabricated by etching metal or molding polymer [61,

77]. Cone, pyramid or other shape of microneedle is possible [78]. Recently, coated microneedle with APIs is also available so that drug can be introduced quickly into skin [79, 80, 81].

Hollow microneedle This microneedle contains microchannel which serves for the release of APIs or the suction of body fluid through micropump (Poiseuille flow) after insertion [82, 83, 84, 85]. When it is connected to lab-on-a-chip analyzer, this kind of microneedle can be implemented as probe of biosensor monitoring and diagnosing body glucose level of patients who have diabetes [86, 71].

Self-dissolving microneedles are advanced forms of solid microneedles. The needles are made of water-soluble substances such as glucose or biodegradable polymers mixed with APIs. After insertion, the microneedle starts to degrade releasing medicine beneath skin. This patch is removed when all needles disappear.

At this point, new transdermal drug delivery system needs to be suggested for achieving low cost and promoting greater patient compliance. In addition, development of mathematical model that can be used in analysis and control of the drug delivery system is required. Simulations based on developed mathematical model provide future experimental and manufacturing guidelines.

4.1 Problem Statements

In this research, the author proposes a parallel use of electric current (iontophoresis) and self-dissolving microneedles. Figure 4.1 illustrates the structure of the proposed patch. The cathode is also an insoluble microneedle made of metal or conductive polymer. The anode is placed at the center of drug-loaded soluble microneedle. Two lines from cathodes to anodes are connected via power supply (not shown). To avoid any confusion caused by long names, hereafter, let *electrode* refer to cathode, *microneedle* to drug-loaded soluble microneedle containing anode at its center, *body* to the depth where capillary vessels and

nerves are found (in some cases, it also denotes systemic circulation), and *epidermis* to space between stratum corneum and *body*.

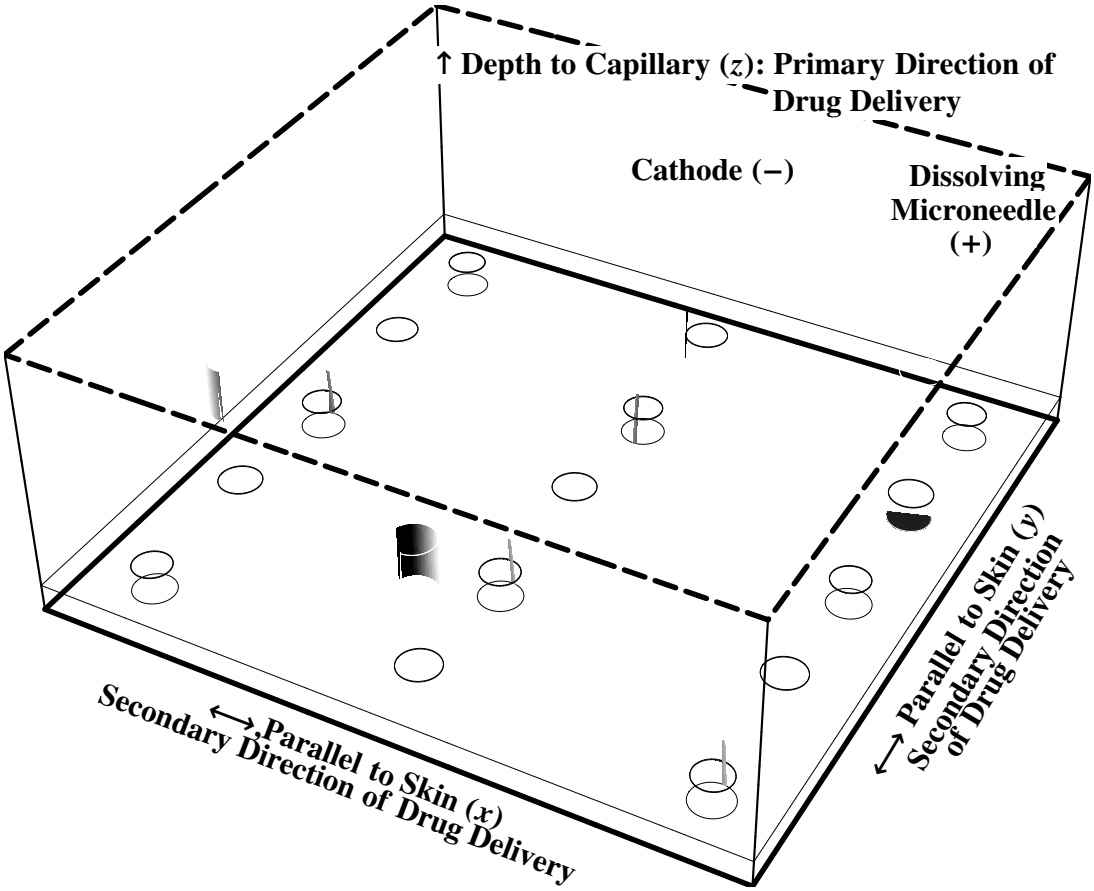

Figure 4.1 Array of microneedles and electrodes in alternate order on patch substrate (figure not drawn to scale).

Despite the curvature in a real skin surface, Cartesian coordinates can be employed because of the very short height of microneedle compared to the width of the patch. In Figure 4.1, two horizontal axes, x and y, denote a direction parallel to surface of skin, while vertical axis is perpendicular to the skin surface. On a single patch substrate (at the bottom enclosed by thick line), electrodes and microneedles are placed in an alternating order and inserted simultaneously. Drug absorption takes place at the boundary between epidermis and body (i.e., top face of Figure 4.1 which is encompassed by thick dashed line). The space between the patch substrate and the layer encircled by thin line denotes the stratum corneum. Although the skin is composed of various layers that have different

physiological functions, a single layer assumption has been adopted. It will provide a good and convenient approximation of drug delivery from an engineering standpoint. The primary direction of drug delivery is determined based on a sense that drug transport in the direction is directly related to drug absorption. Note that cathode is expressed as a negative terminal, which implies this study focuses on the drug delivery through skin.

Synergistic effects of coupled physical enhancers (soluble microneedles and iontophoresis) had already analyzed in prior work [12]. In in-vivo tests, soluble-microneedle patch was first placed on a hairless rat skin for 90 seconds during which all microneedles disappear. After the patch was removed from the skin, a constant electric current was applied for 60 minutes using iontophoresis device. The results were positive: a 25-fold enhancement was achieved using both microneedle and iontophoresis in the delivery of methotrexate compared to individual application of iontophoresis or microneedle [12].

Although a sequential application of two individual drug-delivery systems has already been attempted, the newly proposed platform has the following differences when compared to the old technology:

1. the electrodes and the microneedles are inserted into skin,
2. the electric current is applied while the microneedles are being dissolved,
3. thus, distance between the cathode and the anode is very close.

Drug carrier in both platforms is a space charge (i.e., electrically charged particle). Ions are the best candidates for the carriers. However, nonpolar particles can also serve as drug carriers since induced dipole makes them polar temporarily under an electric field depending on the polarity of the species. As a result, drug-delivery enhancement scenario of the proposed platform is as follows:

1. first, applied electric field accelerates diffusion of drug molecule from microneedles toward electrodes (i.e., secondary direction of drug delivery in Figure 4.1),

2. increased diffusion leads to
    a. fast outspread of drug over skin,
    b. lower drug concentration around microneedle,
3. drug absorption is enhanced due to
    a. wider area of diffusion to primary direction of drug delivery in Figure 4.1,
    b. increased dissolution of microneedle.

A quicker dissolution by applied electric field is achieved since the driving force for dissolution is the deviation of drug concentration around the solid from its solubility. Using sequential applications of microneedle patch and iontophoresis [12], this effect cannot be attained. For this reason, the term "electrically-enhanced" or equivalents will be used to describe current platform instead of iontophoresis, although both share the same physical mechanism.

Another design of parallel applications of microneedle and electric current is also possible as shown in Figure 4.2. Unlike the original platform, cathode and anode are not inserted into skin. Indeed, after soluble-microneedle patch has been worn on the skin, the patch substrate is covered with a sheet of anode while a sheet of cathode is attached to a different location on the skin, as in iontophoretic delivery. In Figure 4.2, dashed line from microneedles to the cathode represents an electric field, with an electromotive force tangential to it. Drug absorption occurs due to diffusion to the body (primary direction of drug delivery). For both platforms, the role of the electric field is to activate drug motion in the secondary delivery direction (i.e., along the skin).

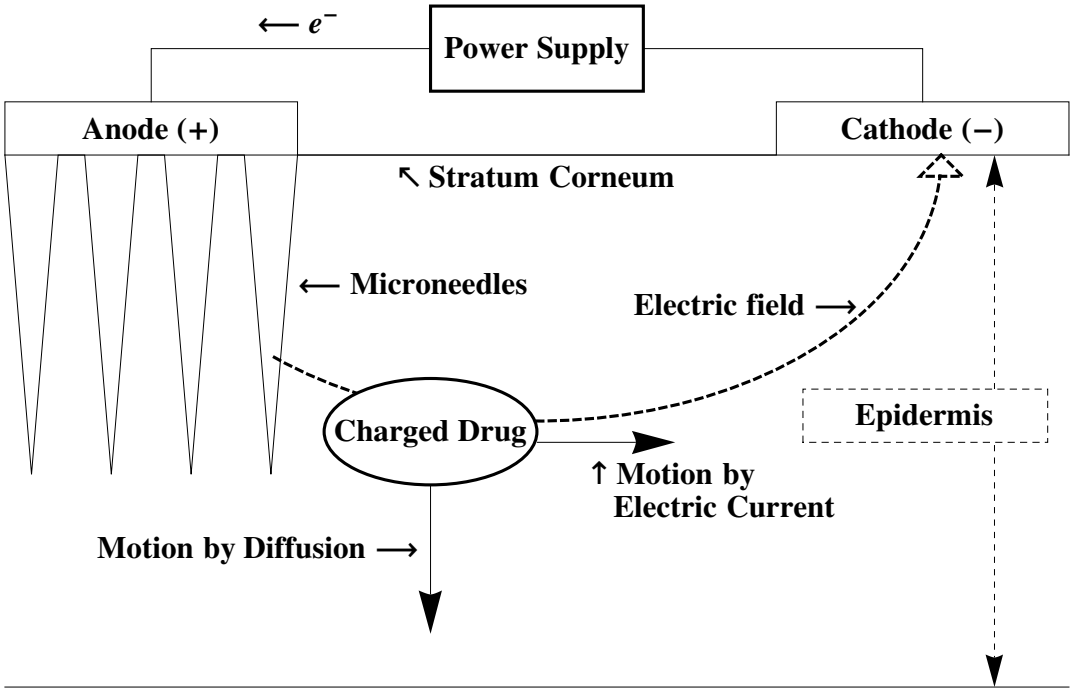

Figure 4.2 Different design of parallel application of microneedle and electric current in transdermal drug delivery.

Advantages of this design are that the fabrication of the microneedle array is much simpler, and that currently-developed products can be utilized in treatment. However, in patients' (in other word, customers') point of view, the original platform can be much more beneficial because of:

- low energy consumption,
- no console may be required,
- light-weighted unit.

The key difference between the two platforms is the distance between cathode and anode, ∼500 μm (i.e., 0.5 mm) in the original design and ∼1 cm (i.e., 10 mm) in the other option. This difference results in a lower energy consumption. According to Ohm's law, the current is directly proportional to the voltage and inversely proportional to the resistance. The latter is directly proportional to the distance between the electrodes. Based on this

observation, only one twentieth voltage is required for the original system to produce the same current as design shown in Figure 4.2. Even though the actual energy saving may be less than the estimated value, it should be significant.

Iontophoresis modules, e.g., LidoSite^{TM} (Vyteris Inc.), usually require consoles for controlling electric current. These consoles contain expensive preprogrammed microprocessors [87, 88], which increases not only controllability of drug delivery but also manufacturing cost.

The above features can also result in reduced battery size and, consequently, a smaller product. The proposed drug delivery platform consists of only a single patch and a power supply. To fully appreciate the benefits of the device, it is necessary to derive analytical models and develop computational tools to facilitate simulations.

4.2 Preliminary Studies

Even though the advantages of microneedle combined with electric current are qualitatively shown above, no clinical data has been found to support the feasibility of the proposed platform and to be used for model validation. The absence of relevant experimental results to be compared with outcomes of this research may raise issues that can make further investigations useless. Therefore, sets of preliminary studies are conducted to indirectly prove drug delivery enhancement of the new platform.

4.2.1 Pilot Experiment I: Electrically Activated Diffusion of Ink

Active diffusion of dissolved Indigo Carmine powder (Matheson Coleman & Bell, Gardena, CA) by a DC power supply (Hewlett Packard, Harrison 6202B) is qualitatively compared to passive diffusion. Indigo Carmine is a pH indicator that shows blue color in a neutral solution. To conduct the experiment, two 1 7/8” ID Petri dishes are filled with

pieces of cheesecloths (VWR Scientific, Bridgeport, NJ) and water (mimicking immobile viable cells and body fluid), respectively. Electrodes are 3/8” wide and 1” long aluminum foil. They are immersed in one Petri dish. The voltage is kept at 38V. Instrumental setup is illustrated in the left picture of Figure 4.3. The left electrode is cathode (+).

Evolutions of inks are shown in pictures on the right in Figure 4.3. Indigo Carmine powder is initially placed at the center of each Petri dish. Electrodes are placed only on one dish. A stopwatch is used to record movements of inks as time. After five minutes, ink on the right dish has diffused out more than that on the other dish has toward cathode. From the observations, it is proven that applied electric field improves molecular diffusion. In addition, it is important to note that direction of motion is toward cathode which is same as that of electron.

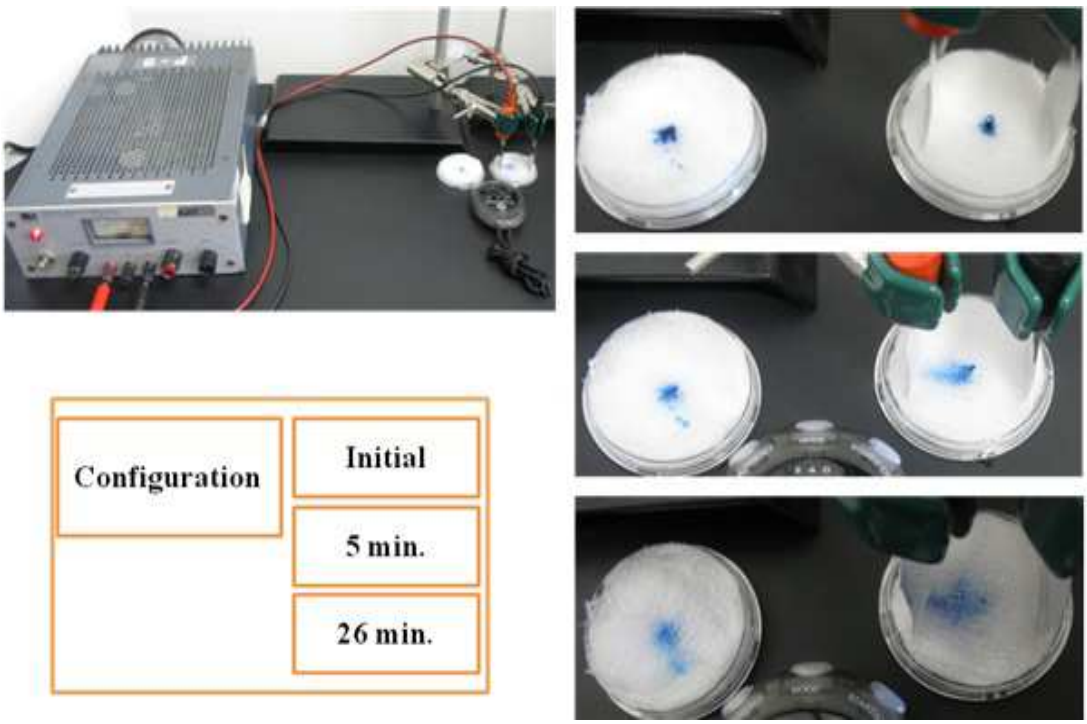

Figure 4.3 Experimental setup (left) and observations (right) of the first preliminary study.

4.2.2 Pilot Experiment II: Dissolution Enhanced by an Electric Field

Another feature of the proposed platform is that applied electric current improves dissolution rate of microneedle. To validate this scenario, an experiment has been performed with cough drops containing 6 mg of benzocaine. Similar instrumental setup to the previous experiment has been used. Instead of Indigo Carmine powder, cough drop is placed at the center of each dish. Weights of two lozenge have been carefully measured at specific times during experiment for calculations of fractional releases of benzocaine. It is assumed that 6 mg of benzocaine is uniformly distributed in a lozenge.

Experiments are conducted twice: during the first experiment, weights of lozenges are measured with caution for 27 minutes. In the second test, only initial and final weights are measured. The reason is that measuring actions inevitably cause disturbances to tranquil lozenges and may result in unexpected drug loss, the impact of which to dissolution of lozenge may be unpredictable or sometimes suppress effect of electric field. Thus, the first experiment should be repeated until weights of lozenges at 27 minutes are acceptably close to those in the second experiment (e.g., $\pm 5\%$) in order to guarantee that the first experiment is performed under a disturbance-free condition as much as possible. Another reason of the second experiment is to investigate processes of changing shapes of lozenges, which can provide helpful insight into enhancement scenario of dissolution by electric current.

The results of the first experiment are shown in Figure 4.4, in which fractional-release profiles of benzocaine from each lozenge are shown and extents of enhancements in percentage are also plotted. The lozenge under an influence of applied electric field released more benzocaine than the counterpart did. An averaged enhancement for 27 minutes is 5.84 %, it is calculated by dividing area under curve by 27 minutes.

As a result of the second experiment, approximately 72 % of benzocaine is released in the presence of electric field which is induced by DC 40V, while 70 % is released without electric current. Only 2% improvement in this in vitro lozenge dissolution test seems not to be in favor of any breakthrough by the proposed delivery platform. However, in light

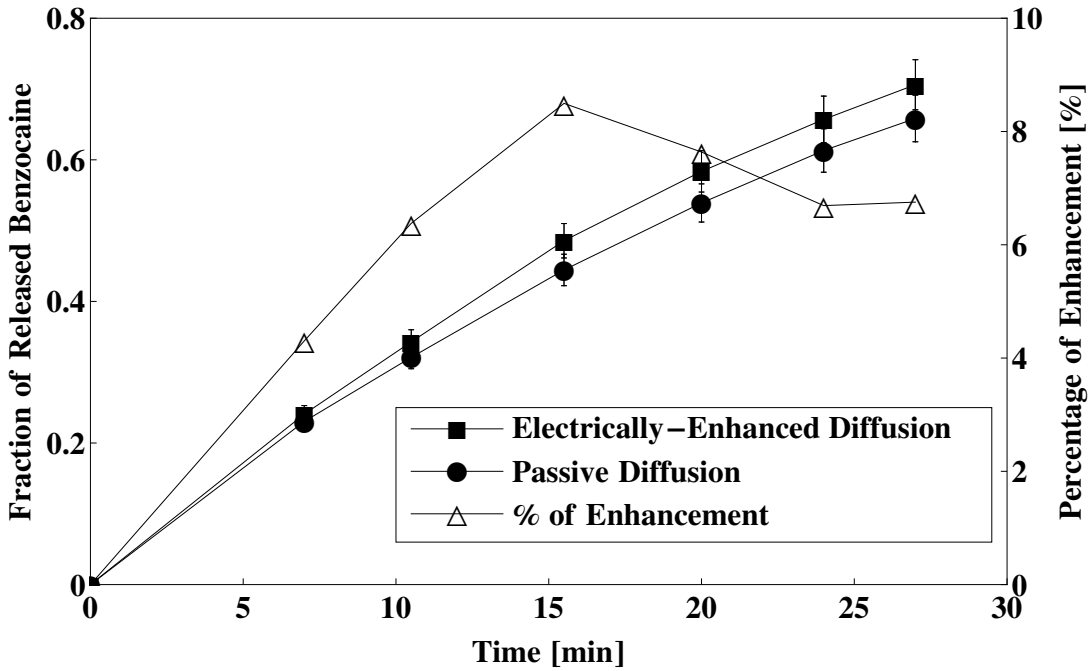

Figure 4.4 Fractions of benzocaine released from two lozenges and percentage of enhancement by applied electric field.

that effect of electric field is magnified in smaller scale, significant enhancement can still be expected with a real microneedle patch.

Also, comparison of the shapes of remaining lozenges provides much more important information for advocating the proposed drug delivery enhancement scenario. In Figure 4.5 (a), the lozenge is placed between electrodes (cathode is at left), while no electric current is applied in Figure 4.5 (b). Lower right corner of lozenge in Figure 4.5 (a) definitely seems to be much more degraded than the other corner of the same lozenge. The cheesecloth around cathode is much darker (i.e., more concentrated with dissolved lozenge) than that around anode. This can be explained by the theory such that dissolved lozenge moves toward cathode (to the left), this causes lower concentration around that corner than used to be, and thus, dissolution occurs at higher rate. On the other hand in Figure 4.5 (b), dissolution of lozenge takes place evenly on entire wet surface because diffusion, in this case, occurs only in radial direction.

(a)

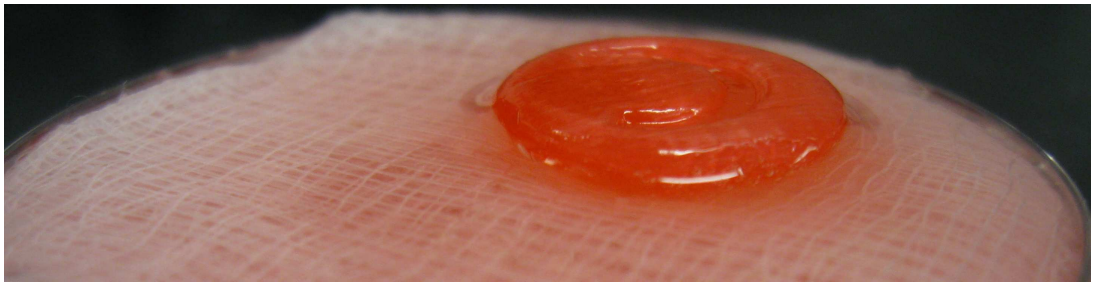

(b)

Figure 4.5 Shapes of remaining lozenges after 27 minutes in the second experiment.

4.2.3 Theoretical Consideration of a Dissolving Microneedle

In addition to the previous laboratory experiments, a mathematical model of a dissolving conical needle has been considered. In this model, a conical needle is submerged into a container filled with liquid of volume v_E. Liquid represents epithelial fluid and is agitated well so that drug concentration, c, in liquid is assumed to be uniform. Dissolution of drug-containing cone (rate constant=k_D) results in supply of drug into liquid. First-order elimination of drug takes place in liquid (rate constant=k_L). Side-view description of this model is given in Figure 4.6. Degradation of cone is assumed not to change the apex angle, 2θ. Thus, the size of remaining microneedle can be expressed only by its height, h. The equations for microneedle height and drug concentration in epidermis are given as:

$$\frac{dh}{dt} = -\frac{k_D}{\rho \sin\theta}(c_s - c), \tag{4.1}$$

and

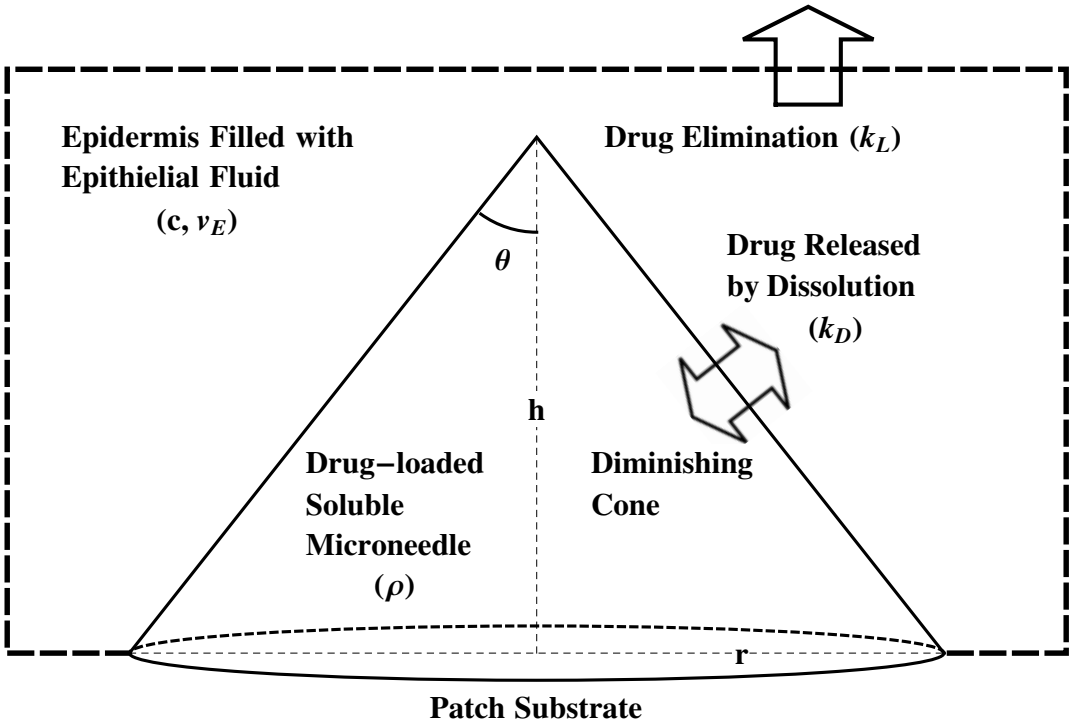

Figure 4.6 Physical configuration of a dissolving conical microneedle in epidermis.

$$\frac{dc}{dt} = -\left(k_L c\right) + \frac{(\rho - c)}{v_{E,0} + v_{C,0} - v_C(t)} \left(\pi \tan\theta \frac{h^2}{\cos\theta} \frac{k_D}{\rho} (c_s - c)\right), \tag{4.2}$$

where ρ and c_s are density and solubility of cone, respectively. Volume of cone is denoted by v_C Initial value of every variable is marked with subscript 0. Before dissolution, no drug exist in epidermis, i.e., $c_0 = 0$.

Dimensionless expressions provided below may offer easier analysis and insight to the given system:

$$\frac{dH}{d\tau} = -(1 - C), \tag{4.3}$$

and

$$\frac{dC}{d\tau} = -k_1 C + 3\frac{(\bar{\rho} - C)(1 - C)H^2}{(\alpha + 1 - H^3)}. \tag{4.4}$$

Dimensionless height of cone and concentration are $H = \frac{h}{h_0}$ and $C = \frac{c}{c_s}$, respectively. Characteristic time is defined as $\tau_0 = \frac{\rho h_0 \sin\theta}{k_D c_s}$, the dimensionless elimination rate constant is $k_1 = \frac{k_L}{k_D}\frac{\rho}{c_s} h_0 \sin\theta = k_L \tau_0$, capacity of epidermis is defined as $\alpha = \frac{c_s}{(\rho - c_s)}\frac{v_{E,0}}{v_{C,0}}$, and $\bar{\rho} = \frac{\rho}{c_s}$ is dimensionless density. The capacity α is the ratio of maximum amount of drug that can be accommodated in initial volume of epidermis to dosage size. Initial conditions are given at τ=0 as

$$H = 1, \tag{4.5}$$

and

$$C = 0, \tag{4.6}$$

respectively.

Two limited cases are analyzed: infinitesimal k_1 and large α. In the former case where $k_1 \to 0$ (i.e., negligible elimination, concentration and cone height after long time, C_∞ and H_∞, respectively, depend on α. If $\alpha < (\bar{\rho} - 1)$, epidermis becomes saturated with drug before complete dissolution of microneedle. Consequently, $C_\infty = 1$ (i.e., solubility) and $H_\infty = \left(1 - \frac{\alpha}{(\bar{\rho}-1)}\right)^{\frac{1}{3}}$. And if $\alpha > (\bar{\rho} - 1)$, dosage size contained in the cone is not sufficient to saturate liquid in epidermis, and $C_\infty = \frac{\bar{\rho}}{(\alpha+1)}$ and $H_\infty = 0$ (i.e., complete dissolution). In the second case, where $\alpha \to \infty$, the volume of epidermis is very large enough to neglect change in drug concentration, i.e., C=0. This is attained when tip-to-tip distance in an array of microneedles is sufficiently long. Applying these restrictions to Equations (4.3)

and (4.4) leads to

$$H = 1 - \tau. \tag{4.7}$$

By letting H=0 in Equation (4.7), the time lapsed before microneedle disappears, τ_D, is obtained

$$\tau_D = \tau_0 = \frac{\rho h_0 \sin\theta}{k_D c_s}. \tag{4.8}$$

This value can be used to estimate dissolution rate constant of a microneedle from experimental data such that

$$k_D = \frac{\Delta V}{\Delta t} \frac{\sin\theta}{c_s \pi h_0^2 \tan^2\theta}, \tag{4.9}$$

where ΔV is difference in volumes of a microneedle measured at different times (interval is Δt).

Numerical simulations of Equations (4.3) and (4.4) with initial conditions, Equations (4.5) and (4.6), have been performed using fourth order Runge-Kutta method. Results with $H_0 = 0.5 \times 10^{-3}$ m, $\theta = \frac{\pi}{6}$, $k_D = 10^{-4}$ m/s, ρ=2 kg/m^3, c_s=1 kg/m^3 and α=1.5 are plotted in Figure 4.7. In Figure 4.7, concentrations are denoted as dashed lines and microneedle heights are in solid lines. Each line passes through label that shows value of k_1 used in its simulation. Each simulation ends when H reaches zero. From the trend observed in Figure 4.7, fast elimination of drug out of epidermis increases the dissolution of the microneedle. In the context of Chapter 4, an applied electric current is expected to increase the elimination of drug away from microneedles, and thus, enhance diffusion and dissolution of medicine.

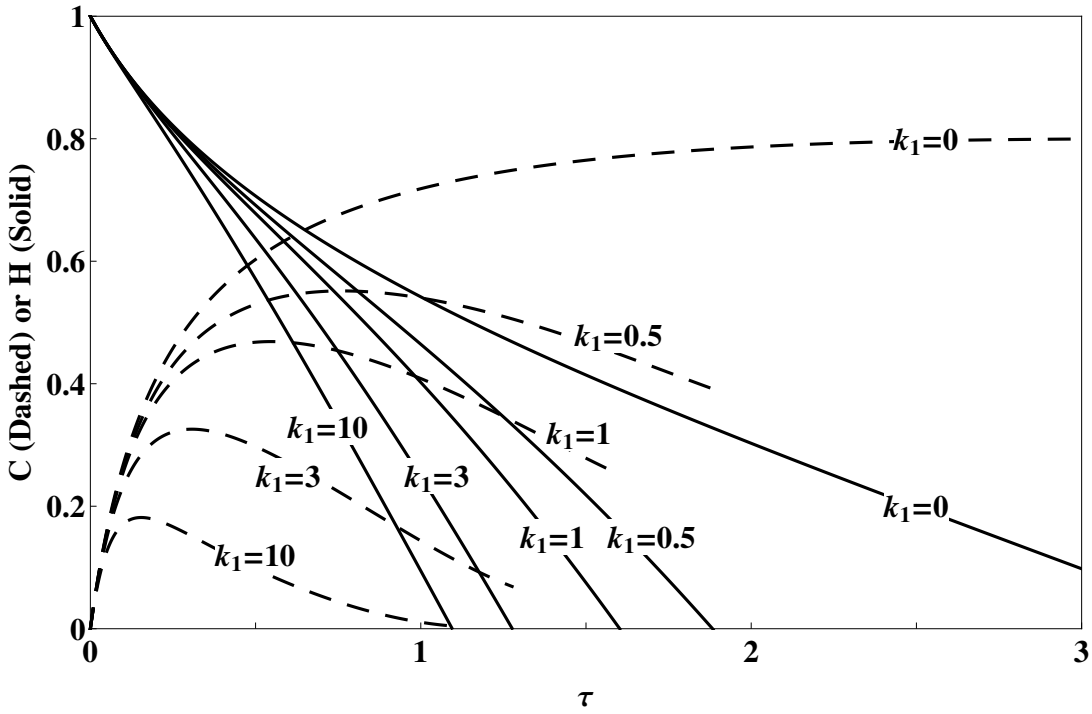

Figure 4.7 Effect of drug elimination rate constant on dissolution of soluble microneedle.

4.3 Mathematical Formulations and Simulations

Feasibility of the proposed transdermal drug delivery using soluble microneedle patch plus electric current simultaneously has been indirectly proven through set of preliminary studies, although data obtained from in vivo experiments are not present. Therefore, the rest of this chapter will be dedicated to development of mathematical model describing motion of drug in epidermis, to computer-assisted simulation and to comments on future experimental and manufacturing tasks.

4.3.1 Electrohydrodynamic Equations

An electrohydrodynamics is a class of studies in which effect of electric field on fluid dynamics and/or species transport is investigated [89, 90, 91]. For example, attempts to involve equations of electrohydrodynamics in dynamics of a falling liquid film down an in-

clined plane have been made so far [92, 93, 94, 95]. Drug delivery system discussed in this research also contains epithelial fluid and drug species under an applied electric field, and thus, equations developed in electrohydrodynamics should be employed in mathematical model. Equations already used in the analyses on iontophoresis [96, 97, 98, 99, 100] are also based on the electrohydrodynamics.

Considering the involved transport mechanisms of drug molecules, diffusion, convection and electromotive motion contribute to total flux such that

$$[J_{\text{total}}] = [J_{\text{diffusion}}] + [J_{\text{convective}}] + [J_{\text{electromotive}}]\,. \tag{4.10}$$

Square brackets are used to denote for vectors. Mass transfer only by diffusion in Equation (4.10) is called *passive* diffusion to emphasize that no external force is exerted to motions of drug molecules and transporting speed is commonly slow. The flux due to diffusion follows the Fick's law:

$$[J_{\text{diffusion}}] = -D\,[\nabla C]\,, \tag{4.11}$$

where D is apparent (or effective) diffusivity of drug through epithelial and C is drug concentration. The negative sign means that drug moves from high to low drug concentration, regardless of choice of coordinate system. The nabla, ∇, stands for gradient in coordinates. Flux of drug molecules by convection is directly proportional to concentration and velocity of epithelial fluid, $[u]$:

$$[J_{\text{convective}}] = C\,[u]\,. \tag{4.12}$$

The electromotive motion is caused by the Coulomb's force exerted between charged mat-

ters. Such motion by applied electric field, $[\varepsilon E]$, yields electric current (density) $[I]$ such that

$$[I] = q\,[\varepsilon E]\,, \tag{4.13}$$

where q is charge density. Permittivity of epithelial fluid, ε, is defined as $\varepsilon_r \varepsilon_0$ in which ε_r is a dielectric constant of the fluid and ε_0(=8.854 $\times$ 10^{-12} F/m) is the electric constant. For examples, dielectric constant is 1 for vacuum (or air) and 80.4 for water. Drug carrier is space charge [94] (i.e., charged particle), and thus,

$$[J_{electromotive}] = Cp\mu\,[\varepsilon E]\,. \tag{4.14}$$

Here, p represents induced dipole moment of space charge and μ is its ionic mobility. Note that the SI units of the dipole moment and the ionic mobility are C·m (C is Coulomb) and $\frac{\mathrm{m}^2}{\mathrm{V{\cdot}s}}$, respectively.

By recalling Equation (4.10), the total flux of drug is rewritten as

$$[J_{total}] = -D\,[\nabla C_i] + C\,[u] + Cp\mu\,[\varepsilon E]\,. \tag{4.15}$$

Applying the Gauss Theorem into Equation (4.15) yields partial differential equation governing motion of drug such that

$$\frac{dC}{dt} = -\nabla \cdot J_{totoal} = D\nabla^2 C_i - \nabla \cdot (C\,[u]) - \nabla \cdot (Cp\mu\,[\varepsilon E])\,. \tag{4.16}$$

Identity relations in vector calculus simplify Equation (4.16) to

$$\frac{dC}{dt} = D\nabla^2 C - ([u] + p\mu\,[\varepsilon E]) \cdot [\nabla C] - Cp\mu\,[\varepsilon \nabla \cdot E]\,. \tag{4.17}$$

Space charge, q, also affects electric field, and the interaction is given by the Maxwell's equation

$$\nabla \cdot E = \frac{q}{\varepsilon}. \tag{4.18}$$

Since the space charge is induced by electric field, charge density can be written as

$$q = pC. \tag{4.19}$$

The velocity of epithelial fluid also contribute to convective transport of drug, and it is governed by the Navier-Stokes equation under an electric field such as

$$\rho \frac{d\,[u]}{dt} = \eta\,\left[\nabla^2 u\right] + q\,[\varepsilon E]\,, \tag{4.20}$$

where ρ and η are density and effective viscosity of fluid, respectively. Deriving Equation (4.20), effect of gravity or pressure drop can be ignored because epithelial fluid is bounded by closed system (i.e., skin). Plugging Equation (4.19) in to Equation (4.20), it is rewritten to

$$\rho \frac{d\,[u]}{dt} = \eta\,\left[\nabla^2 u\right] + pC\,[\varepsilon E]\,. \tag{4.21}$$

Using the Cartesian coordinates, Equation (4.17) is rewritten in the scalar form:

$$\begin{aligned}\frac{\partial C}{\partial t} =& D\left(\frac{\partial^2 C}{\partial x^2}+\frac{\partial^2 C}{\partial y^2}+\frac{\partial^2 C}{\partial z^2}\right)-\left\{\left(u_x-p\mu\varepsilon\left(\frac{\partial\phi}{\partial x}\right)\right)\frac{\partial C}{\partial x}\right.\\ &\left.+\left(u_y-p\mu\varepsilon\left(\frac{\partial\phi}{\partial y}\right)\right)\frac{\partial C}{\partial y}+\left(u_z-p\mu\varepsilon\left(\frac{\partial\phi}{\partial z}\right)\right)\frac{\partial C}{\partial z}\right\}-\mu(pC)^2. \qquad (4.22)\end{aligned}$$

And for Equation (4.20),

$$\frac{\partial u_x}{\partial t}=\nu\left(\frac{\partial^2 u_x}{\partial x^2}+\frac{\partial^2 u_x}{\partial y^2}+\frac{\partial^2 u_x}{\partial z^2}\right)+\frac{pC}{\rho}\varepsilon\left(\frac{\partial\phi}{\partial x}\right), \qquad (4.23)$$

$$\frac{\partial u_y}{\partial t}=\nu\left(\frac{\partial^2 u_y}{\partial x^2}+\frac{\partial^2 u_y}{\partial y^2}+\frac{\partial^2 u_y}{\partial z^2}\right)+\frac{pC}{\rho}\varepsilon\left(\frac{\partial\phi}{\partial y}\right), \qquad (4.24)$$

$$\frac{\partial u_z}{\partial t}=\nu\left(\frac{\partial^2 u_z}{\partial x^2}+\frac{\partial^2 u_z}{\partial y^2}+\frac{\partial^2 u_z}{\partial z^2}\right)+\frac{pC}{\rho}\varepsilon\left(\frac{\partial\phi}{\partial z}\right), \qquad (4.25)$$

where $\nu = \eta/\rho$ is kinematic viscosity and has a unit of $\mathrm{m^2s^{-1}}$. In Equations (4.22) to (4.25), the electric field is replaced by the electric potential using

$$[E] = -\nabla\cdot\phi, \qquad (4.26)$$

and the electric potential ϕ is governed by the Poisson's equation

$$\nabla^2\phi = \frac{\partial\phi}{\partial x^2}+\frac{\partial\phi}{\partial y^2}+\frac{\partial\phi}{\partial z^2} = -\frac{q}{\varepsilon_0}. \qquad (4.27)$$

Lateral axes are named x and y, respectively, and vertical axis is z in Figure 4.1. Dimensionless variables are obtained by introducing characteristic length and velocity of the lateral axes, L_0 and U_0, and characteristic voltage of electrode, ϕ_0, respectively. The results are $c = {C_i}/{c_s}$, $\tau = {t}/{\tau_0}$, $\bar{u}_x = {u_x}/{U_0}$, $\bar{u}_y = {u_y}/{U_0}$, $\bar{u}_z = {u_z}/{\xi U_0}$ and $\bar{\phi} = {\phi}/{\phi_0}$. Ratio of the vertical to the lateral dimensions is ξ, and solubility of drug in the epithelial fluid is c_s. The dimensionless equations are obtained by plugging those variables into Equations (4.22) to (4.25) and (4.27):

$$\begin{aligned}\frac{\partial c}{\partial \tau} = &\left(\frac{\partial^2 c}{\partial \bar{x}^2} + \frac{\partial^2 c}{\partial \bar{y}^2} + \frac{1}{\xi^2}\frac{\partial^2 c}{\partial \bar{z}^2}\right) - \left\{\left(\bar{u}_x - R\left(\frac{\partial \bar{\phi}}{\partial \bar{x}}\right)\right)\frac{\partial c}{\partial \bar{x}}\right. \\ &\left. + \left(\bar{u}_y - R\left(\frac{\partial \bar{\phi}}{\partial \bar{y}}\right)\right)\frac{\partial c}{\partial \bar{y}} + \frac{1}{\xi}\left(\bar{u}_z - R\frac{1}{\xi}\left(\frac{\partial \bar{\phi}}{\partial \bar{z}}\right)\right)\frac{\partial c}{\partial \bar{z}}\right\} - Kc^2,\end{aligned} \tag{4.28}$$

$$\frac{\partial \bar{u}_x}{\partial \tau} = Sc\left(\frac{\partial^2 \bar{u}_x}{\partial \bar{x}^2} + \frac{\partial^2 \bar{u}_x}{\partial \bar{y}^2} + \frac{1}{\xi^2}\frac{\partial^2 \bar{u}_x}{\partial \bar{z}^2}\right) + Mc\left(\frac{\partial \bar{\phi}}{\partial \bar{x}}\right), \tag{4.29}$$

$$\frac{\partial \bar{u}_y}{\partial \tau} = Sc\left(\frac{\partial^2 \bar{u}_y}{\partial \bar{x}^2} + \frac{\partial^2 \bar{u}_y}{\partial \bar{y}^2} + \frac{1}{\xi^2}\frac{\partial^2 \bar{u}_y}{\partial \bar{z}^2}\right) + Mc\left(\frac{\partial \bar{\phi}}{\partial \bar{y}}\right), \tag{4.30}$$

$$\frac{\partial \bar{u}_z}{\partial \tau} = Sc\left(\frac{\partial^2 \bar{u}_z}{\partial \bar{x}^2} + \frac{\partial^2 \bar{u}_z}{\partial \bar{y}^2} + \frac{1}{\xi^2}\frac{\partial^2 \bar{u}_z}{\partial \bar{z}^2}\right) + Mc\frac{1}{\xi}\left(\frac{\partial \bar{\phi}}{\partial \bar{z}}\right), \tag{4.31}$$

and

$$\frac{\partial \bar{\phi}}{\partial \bar{x}^2} + \frac{\partial \bar{\phi}}{\partial \bar{y}^2} + \frac{1}{\xi^2}\frac{\partial \bar{\phi}}{\partial \bar{z}^2} = -Pc. \tag{4.32}$$

By letting characteristic time $\tau_0 = \frac{L_0^2}{D}$ and velocity $U_0 = \frac{D}{L_0} = \frac{L_0}{\tau_0}$, ratio of electromotive motion to convective mass transport of drug molecule is represented by $R = \frac{p\mu\phi_0}{U_0}$, electromotive motion to diffusion by $K = R\frac{L_0^2 c_s p}{\phi_0}$, momentum diffusivity to the mass diffusivity by $Sc = \frac{\nu}{D}$ (the Schmidt number), electromotive motion to convective flow by $M = R\frac{c_s L_0^2}{\rho\mu D}$ and finally, $P = \frac{pL_0^2}{\varepsilon\phi_0}$. The choice of the characteristic velocity yields the Sherwood number of 1, i.e., $\frac{U_0 L_0}{D} = 1$.

Dissolution of microneedle causes change in drug concentration at its surface such that

$$\left(\frac{\partial c}{\partial \bar{x}}\right)\bigg|_{\bar{x}=L(\tau)} = N\left(\rho_M - c|_{\bar{x}=L(\tau)}\right), \tag{4.33}$$

where dimensionless parameter is defined as $N = \frac{k_D L_0}{D}$, and normalized density of drug in microneedle is $\rho_M = \frac{\rho_s}{c_s}$. Equation (4.33) holds only in the presence of microneedle. Once microneedle has disappeared, Equation (4.33) should be replaced by symmetric condition such as

$$\left(\frac{\partial c}{\partial \bar{x}}\right)\bigg|_{\bar{x}=L(\tau)} = 0. \tag{4.34}$$

In Equations (4.33) and (4.34), $L(\tau)$ means distance between surfaces of microneedle and electrode, which is governed by

$$\frac{dL}{d\tau} = Q\left(1 - c|_{\bar{x}=L(\tau)}\right). \tag{4.35}$$

Equation (4.35) also holds only in the presence of microneedle, i.e., $L(\infty) \rightarrow 1$. The dimensionless dissolution rate constant is defined by $Q = \frac{L_0 k_D}{D\rho_M}$. At the boundary between the epidermis and the body, the perfect sink condition is assumed such that

$$c\big|_{\bar{z}=1}. \tag{4.36}$$

Other boundary conditions necessary for simulations will be set up adequately upon definition of geometry to be analyzed. In general, increase in dimension of simulation may yield higher accuracy of analysis. However, complexity of simulation and demand on computational resources increase as well. Therefore, many simulation-involved analyses on drug delivery systems or other studies have been carried out in reduced (i.e., one- or two-) dimensions. In the rest of this section, results of one-, two- and three-dimensional simulations of the given problem have been presented. As stated above, computational resources and wall-clock time of simulation increases with the dimension. Nevertheless, the results of the case studies are compared. In addition, effective analytical strategies (i.e., accuracy and computer resources) are discussed.

4.3.2 Simulations of One-Dimensional Transport

The drug delivery domain in the one-dimensional study is defined by a line segment of unit length, see Figure 4.8. The origin of the coordinate lies at surface of an electrode. The center of the microneedle is located at x=1. Since the microneedles and the electrodes are placed alternately in an array, another electrode is at x=2. However, the domain from x=1 to x=2 will not be analyzed because of symmetry. The equations to be solved are reduced forms of Equations (4.28), (4.29) and (4.32) by setting obtained derivative terms

with respect to y equal to zero and by combining the boundary condition at the end of the epidermis, Equation (4.36), and Equation (4.33) or (4.34):

$$\frac{\partial c}{\partial \tau} = \left(\frac{\partial^2 c}{\partial \bar{x}^2}\right) - \left\{\bar{u}_x - R\left(\frac{\partial \bar{\phi}}{\partial \bar{x}}\right)\right\}\frac{\partial c}{\partial \bar{x}} - Kc^2 - k_{ab}c, \tag{4.37}$$

where k_{ab} is a dimensionless constant related to the drug absorption which should be determined by experiments.

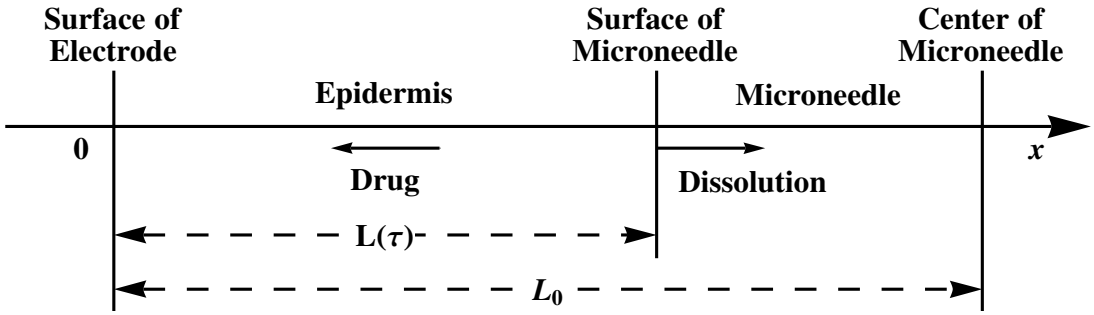

Figure 4.8 Physical configuration used for one-dimensional simulation of the proposed drug delivery system.

Equation (4.37) is subjected to Equation (4.33) until microneedle disappears due to dissolution, i.e., $L(\tau) \to 1$, and then, to Equation (4.34) . Initial and other boundary conditions are as follows. At the surface of the electrode, no flux (or the symmetry boundary condition can also be applied resulting in the same equation) is assumed:

$$\left(\frac{\partial c}{\partial \bar{x}}\right)\bigg|_{\bar{x}=0} = 0. \tag{4.38}$$

And at both ends, epithelial fluid does not escape the domain:

$$\bar{u}\big|_{\bar{x}=0} = \bar{u}\big|_{\bar{x}=L(\tau)} = 0. \tag{4.39}$$

Finally, the initial epidermis is drug-free and the epithelial fluid is not moving:

$$c|_{\tau=0} = 0, \tag{4.40}$$

and

$$\bar{u}_x|_{\tau=0} = 0. \tag{4.41}$$

Computer program to solve the one-dimensional problem has been written in Mathematica® environment. In the solution procedure, $L(\tau)$ is discretized into a number of segments following rule of orthogonal collocation [20]. The rest region from $L(\tau)$ to 1 is out of consideration. The simulation will give the drug concentration profile, velocity of epithelial fluid and electric potential at adjoining points formed by adjacent segments, called collocation points. In the orthogonal collocation method, partial differential equation (PDE), e.g., Equations (4.37), and the ordinary differential equation (ODE) are reduced to a set of ordinary differential equations and a set of algebraic equations, respectively. Although Mathematica® provides built-in powerful integration tools, they are not implemented in this simulation because the following features are not allowed:

Moving Boundary Problem Due to the dissolution, the domain, ranged from 0 to $L(\tau)$, is expanding. This causes the absolute position of the collocation points to be shifted toward the center of the microneedle at every time step in the integration, even though their relative positions remain unchanged. Consequently, the concentration, velocity and electric potential should be updated at new collocation points using a linear interpolation after each step.

Implicit User-Defined Function The discretized governing equations are a set of ODEs for concentration and velocity profiles, and a set of algebraic equations for electric potential. In the integration of ODEs, the solutions to the set of the algebraic equations are used as if they were coefficients. In cases where the algebraic equations are explicit (e.g., $y = f(x)$), it is possible to incorporate them into the built-in function *NDSolve*. However, the algebraic equations for electric potential are implicit (e.g., $f(x,y) = 0$).

To show the electrical enhancement in drug delivery by a self-dissolving microneedle patch, simulations are performed with various values of R, K and M while others are fixed at Sc=0.01, P=0.1, Q=0.1, N=0.1 and k_{ab}=0.1. These numbers do not reflect experimental particle motion through the skin as a result of iontophoresis. For example, there have been reports on the occurence of electroosmotic flow as a significant factor in iontophoretic transdermal drug delivery. However, the contribution of the electromotive flow relative to the bulk fluid flow (i.e, R) has not been documented in this work. These model parameters are selected for the purpose of the simulations. The values of R, K and M, related to the electric field or the electric properties of system, are set equal to each other as 0 (no electric current), 0.1 and 1. Initial radius of the microneedle is 0.2 so that length of the epidermis, i.e., $L(\tau)$, is expanding from 0.8 to 1.0 as time passes. As a result, fractional releases of drug into systemic circulation are estimated and demonstrated in Figure 4.9. According to Figure 4.9, the drug delivery is apparently enhanced by the applied electric field. In this simulation, however, the elapsed times until complete dissolutions of the microneedles are 2.056 in all cases. Even though the decreasing dissolution times are observed with increasing electric field when smaller step size of time in simulation is used, it is not suitable for validation of drug delivery enhancement scenario (electric field will activate both mechanisms of diffusion and dissolution).

To magnify the effect of the electric field on the dissolution time, Two parameters are increased, i.e., Q=N=0.3. They are related directly to the rate of dissolution and its

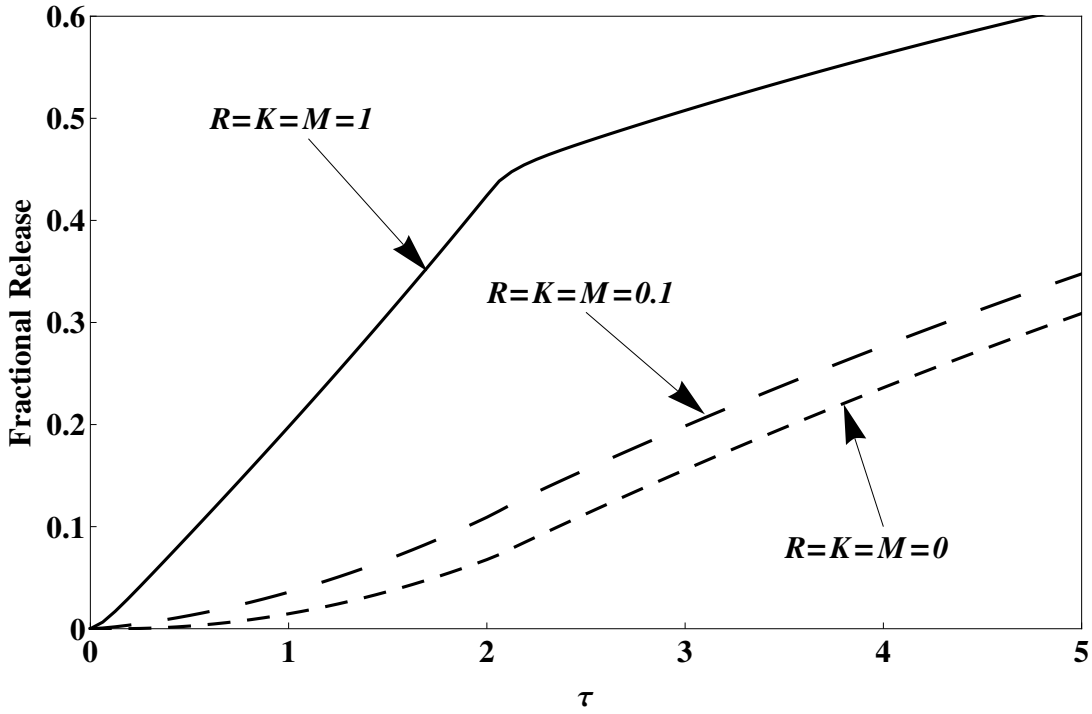

Figure 4.9 Fractional release of drug at various intensities of the electric field calculated through the one-dimensional simulations.

effect on concentration, respectively. Then, the dissolution times are estimated while R=M are varied from 0 to 1. Numerical instability is observed for R and M greater than 1 in this simulation. In the new simulation, K is fixed at 0.1 because K is related to the electrical properties,and is helpful to identify the isolated effect of the intensity of the electric field. Based on Figure 4.10, dissolution time is decreased as increasing electric field, and thus, the drug delivery enhancement scenario is proved in this one-dimensional simulation.

Each set of simulations with different set of parameters can provide characteristic information of the proposed drug delivery system: the first set of simulations is good for showing the enhanced drug delivery in terms of the absorption but not suitable to distinguish the dissolution time, on the other hand, the second set is good for visualizing the effect of an electric field on the dissolution time and not appropriate to show enhanced absorption of drug.

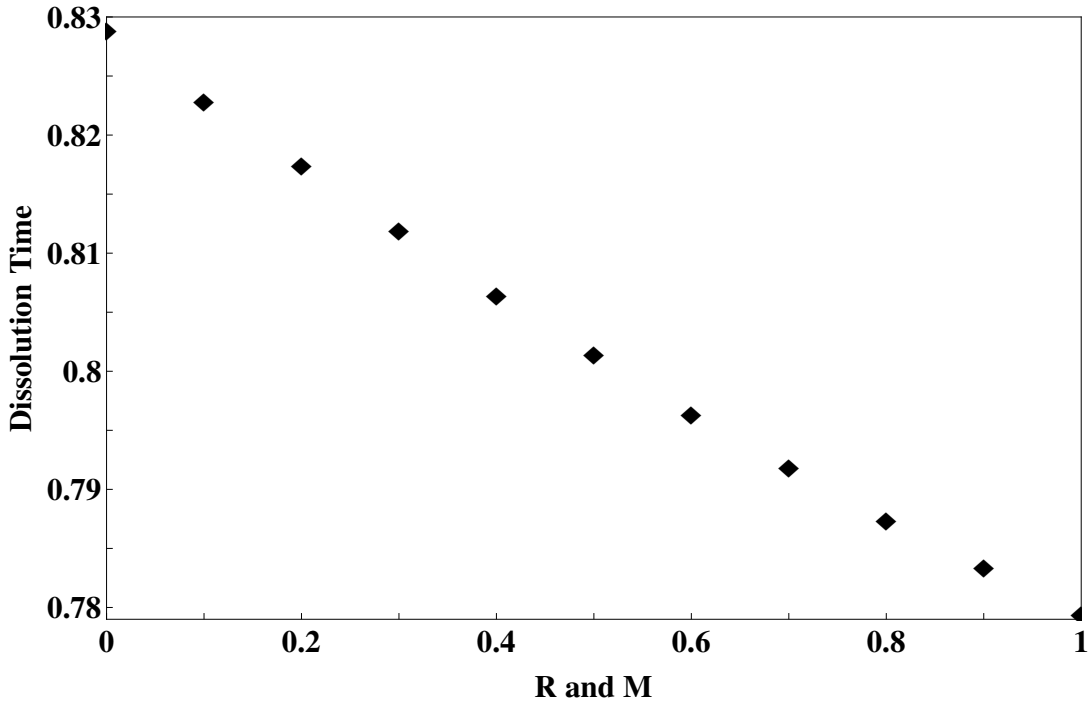

Figure 4.10 Dissolution time with increasing electric field.

4.3.3 Simulations of Two-Dimensional Transport

The domain of two-dimensional simulation consists of the lateral (x; along skin) and vertical (z; to depth of skin) axes, see Figure 4.11. In Figure 4.11, The center of base of conical microneedle is located at (x, z)=(1, 0), and the apex faces to the systemic circulation (triangular area shaded by lines). The base of electrode is placed at the origin (thickest line). The height of microneedle is set as one half. To implement two-dimensional orthogonal collocation technique, the square domain is first divided into 9 layers including the top and bottom boundaries (dotted lines). The length of each line is determined by orthogonal collocation rule [20]. Every line is also divided into 9 collocation points using the same rule (filled circles). The differential equations to be solved in this work are derived from Equations (4.28), (4.29), (4.30) and (4.32) by setting the derivatives with respect to y as 0. Discrete forms of those equations are set of 147 ODEs (=(7 internal collocation points)$^2\times$(1 for concentration and 2 velocities)) plus 49 algebraic equations for the electric potential.

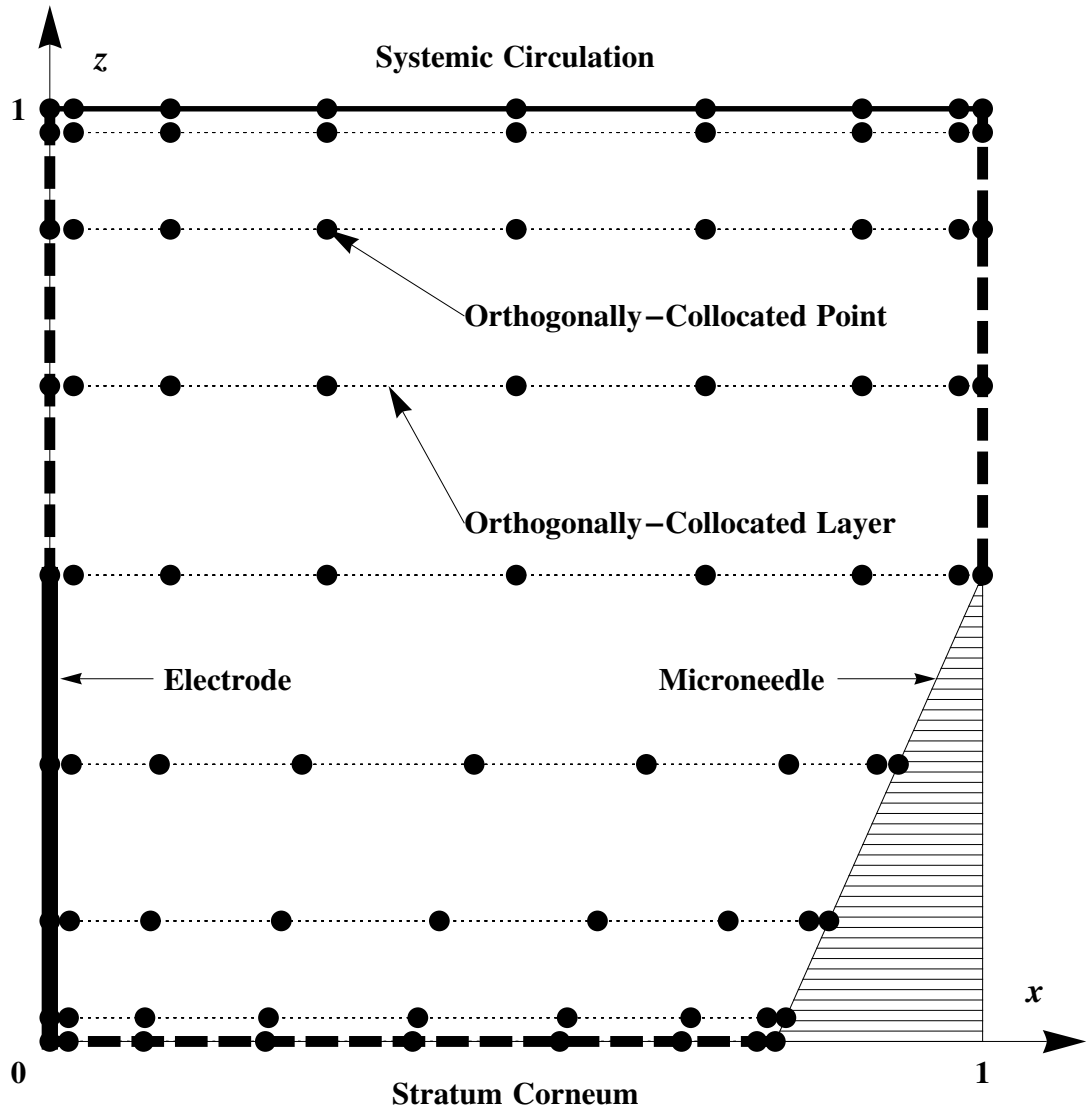

Figure 4.11 Dimensionless domain for two-dimensional simulations.

In Figure 4.11, the top and bottom boundaries are set electrically insulated, and, for boundaries denoted by the thick-dashed-vertical lines, electric potential as well as concentration and velocities are symmetric. The perfect sink condition is used at the top where the absorption of drug occurred while no flux exists at the stratum corneum (the bottom line). No fluid-motion assumption is made at the top and bottom lines. At the electrode, the electric potential is set to 1, and at the surface of microneedle, its value is 0.

According to the orthogonal-collocation discretization, there are 9 equations for $L(\tau)$ such that

$$L_d(0) = 1 - \left(\frac{1}{2} - d\right)\tan\theta, \tag{4.42}$$

where d is the depth of line and θ is the half angle of apex. After $L(\tau)$ reaches 1, Equation (4.42) no longer applies.

Two-dimensional simulations have been performed for τ=0 to 4 with the same values of the parameters used in the one-dimensional study. In addition, the ratio of the vertical to the lateral dimensions of the domain, ξ, is set equal to 0.9, and $\theta = \pi/6$. Concentrations of drug at the selected times are plotted in Figures 4.12 through 4.15. For comparisons, each figure contains two parts: the upper ones, or parts (a), show the concentrations in the epidermis without electric field, while the lower ones, or parts (b), are the case where electric field is applied, i.e., R=K=M=1. In those figures, the dissolving microneedles are shown at the rightmost corners of surfaces (the corners look as if they were cut by a knife). At τ=0.2 (Figure 4.12), the concentration increases in the beginning. At τ=1 (Figure 4.13), it seems to reach the maximum. At τ=2 (Figure 4.14), the concentration decreases and the microneedle has considerably shrunk. At τ=2.5 (Figure 4.15), the dissolutions of the microneedles are almost completed and most drugs are already absorbed to the systemic circulation. The noticeable observation is that the highest concentration, the darkest portion of the surface, as well as the overall concentrations in the part (a) in Figure 4.12 are greater than those in the part (b) of the same figure. This trend is also observed in the other figures, Figures 4.13 to 4.13. It implies that the electric field lessens the drug concentration near the microneedle and that the drug delivery has been enhanced by the electric field in the sense that more drug has escaped from the epidermis, i.e., absorbed into the systemic circulation.

Electrical enhancement of transdermal delivery through self-dissolving microneedle patch is quantitatively presented in Figure 4.16. In Figure 4.16, the significant enhancement is observed only at the beginning of the therapy (τ<1.5). A zoom-in plot is added as

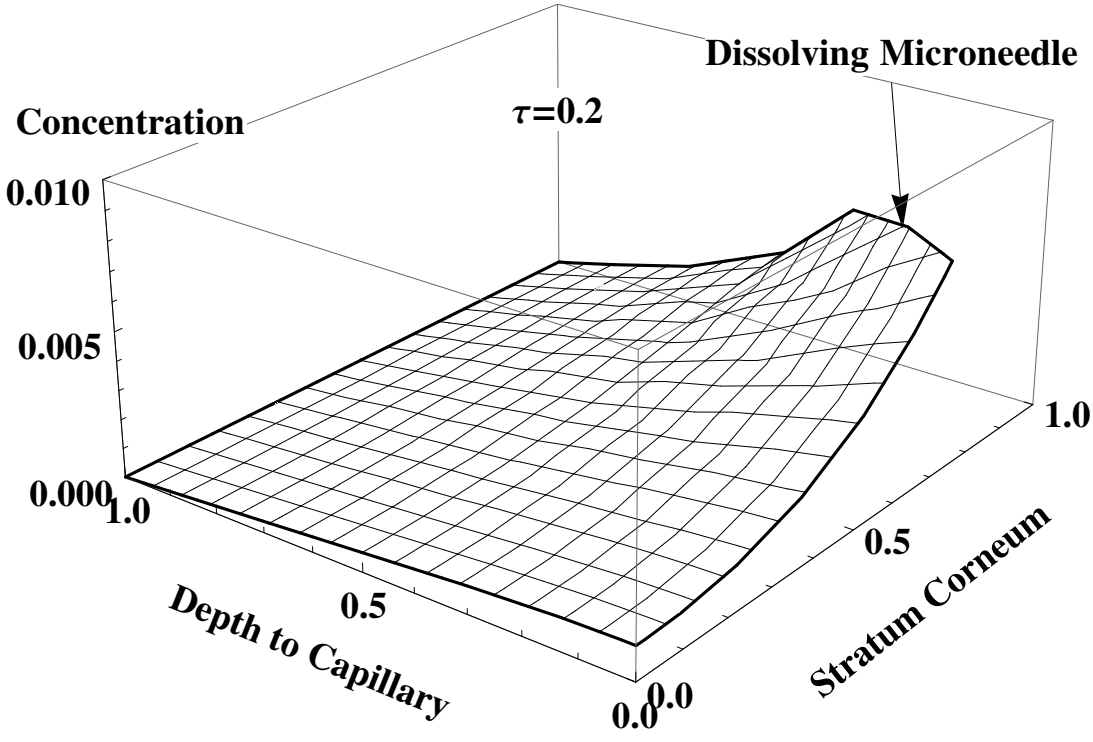

(a)

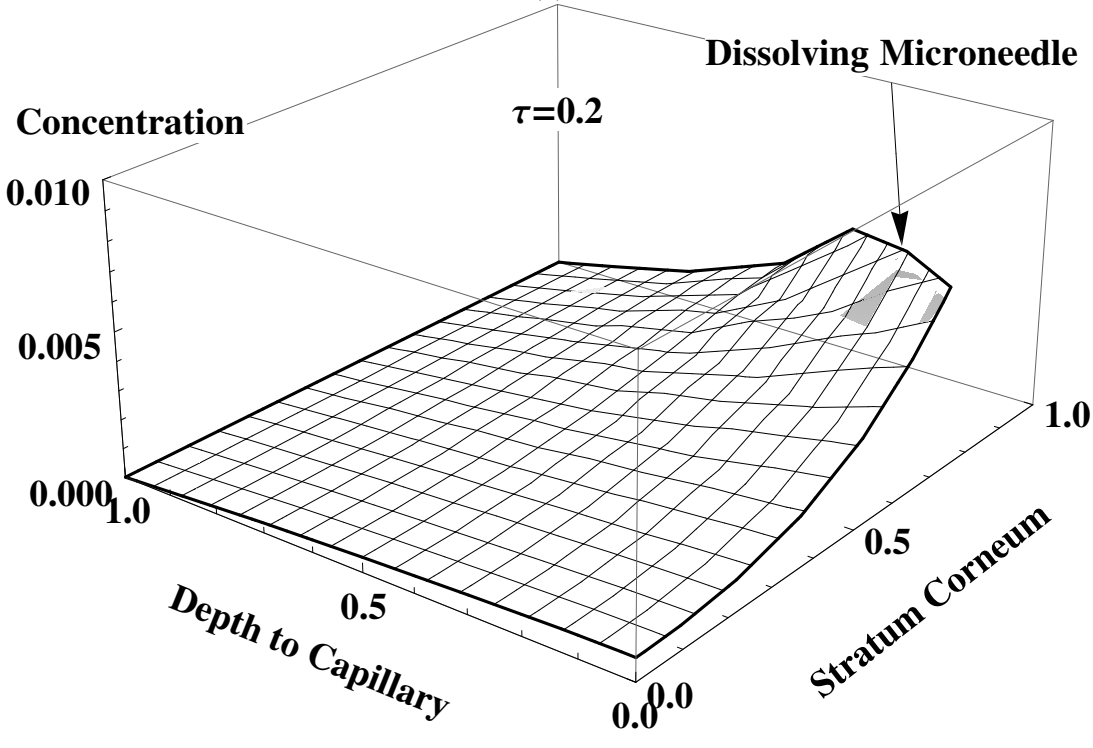

(b)

Figure 4.12 Concentration surfaces at τ=0.2: (a) R=K=M=0, (b) R=K=M=1.

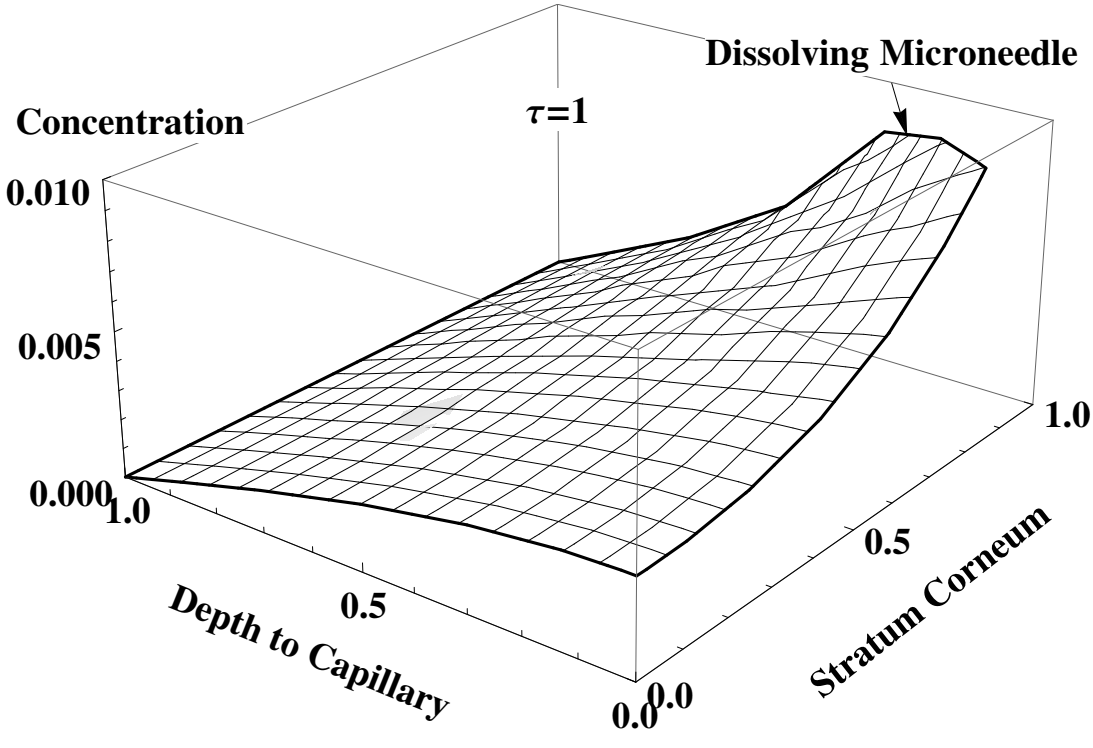

(a)

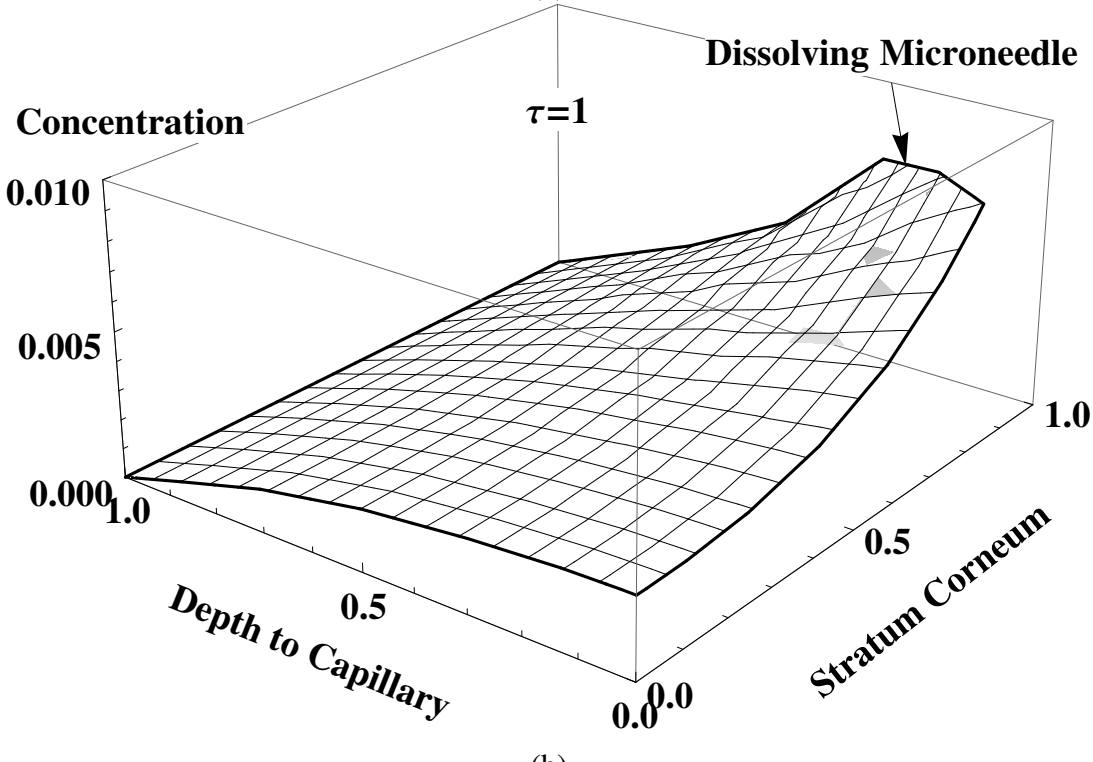

(b)

Figure 4.13 Concentration surfaces at τ=1: (a) R=K=M=0, (b) R=K=M=1.

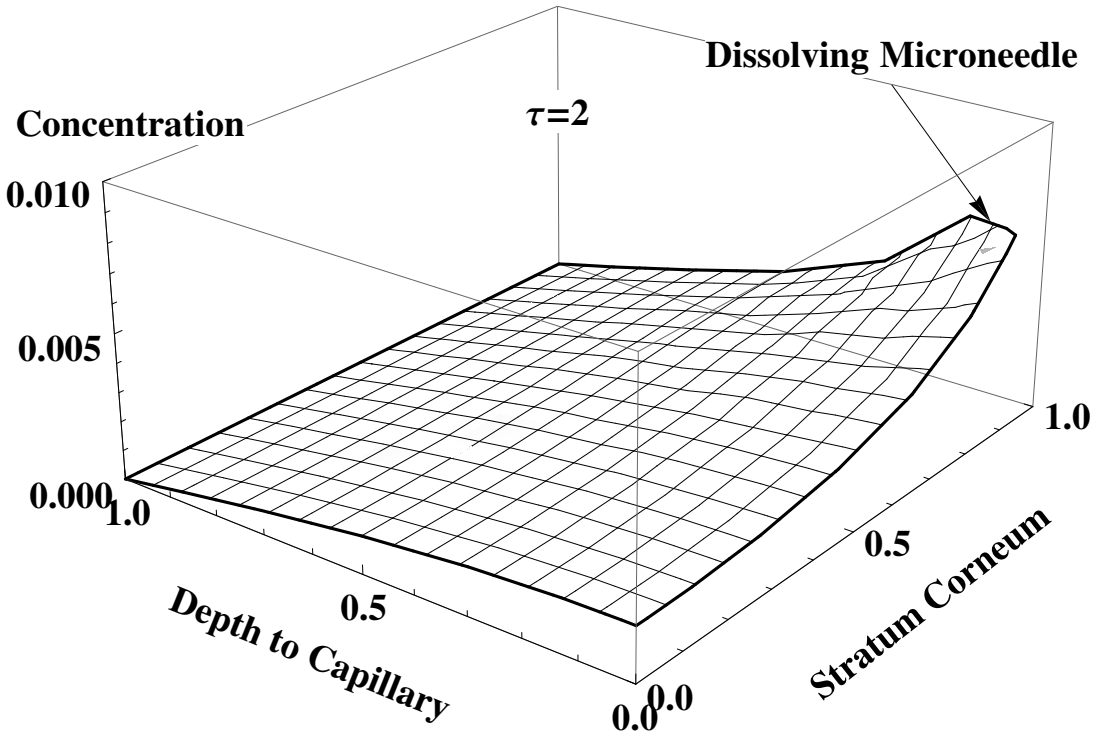

(a)

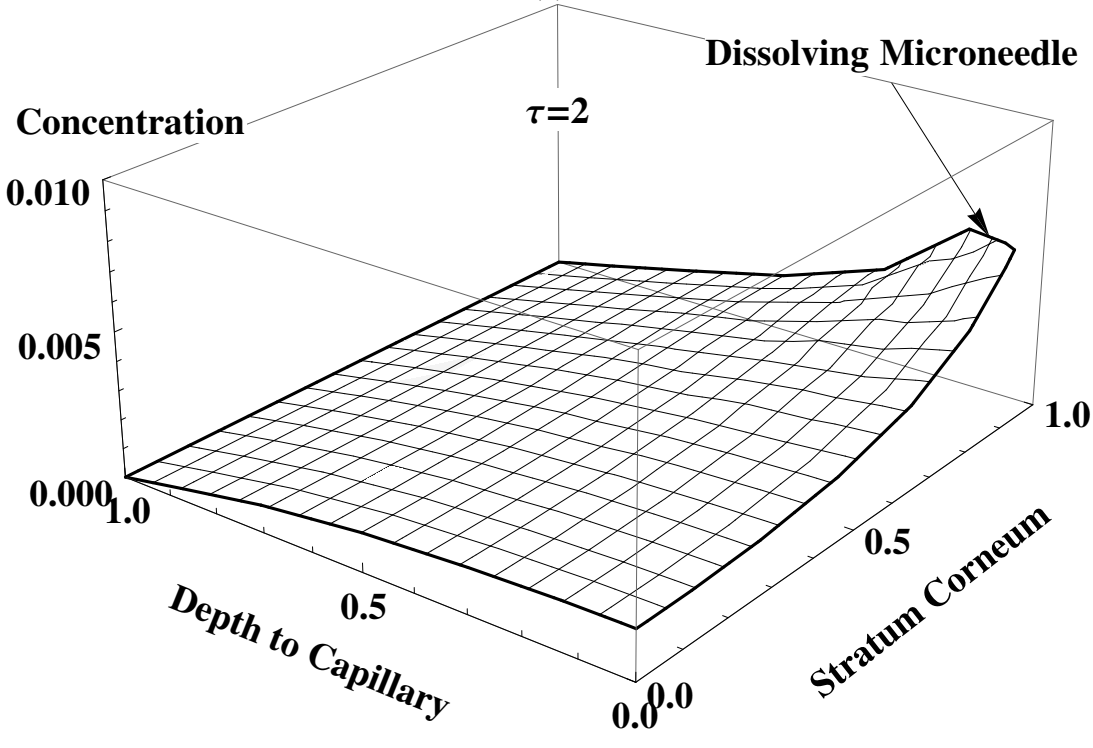

(b)

Figure 4.14 Concentration surfaces at τ=2: (a) R=K=M=0, (b) R=K=M=1.

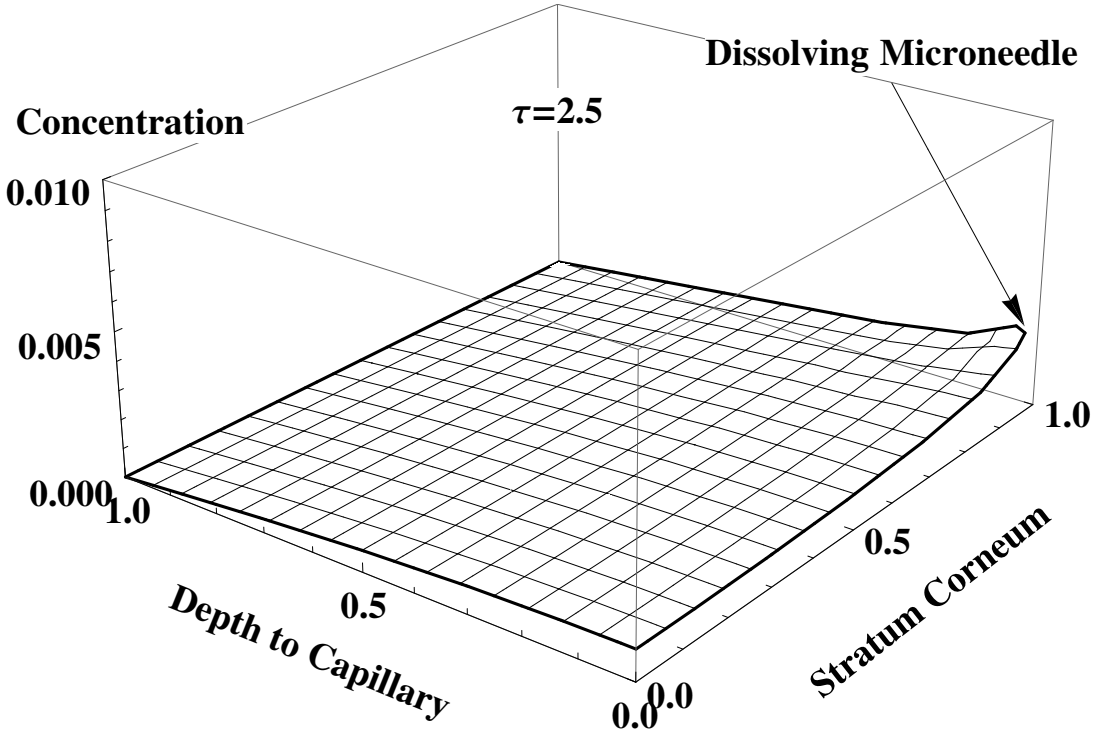

(a)

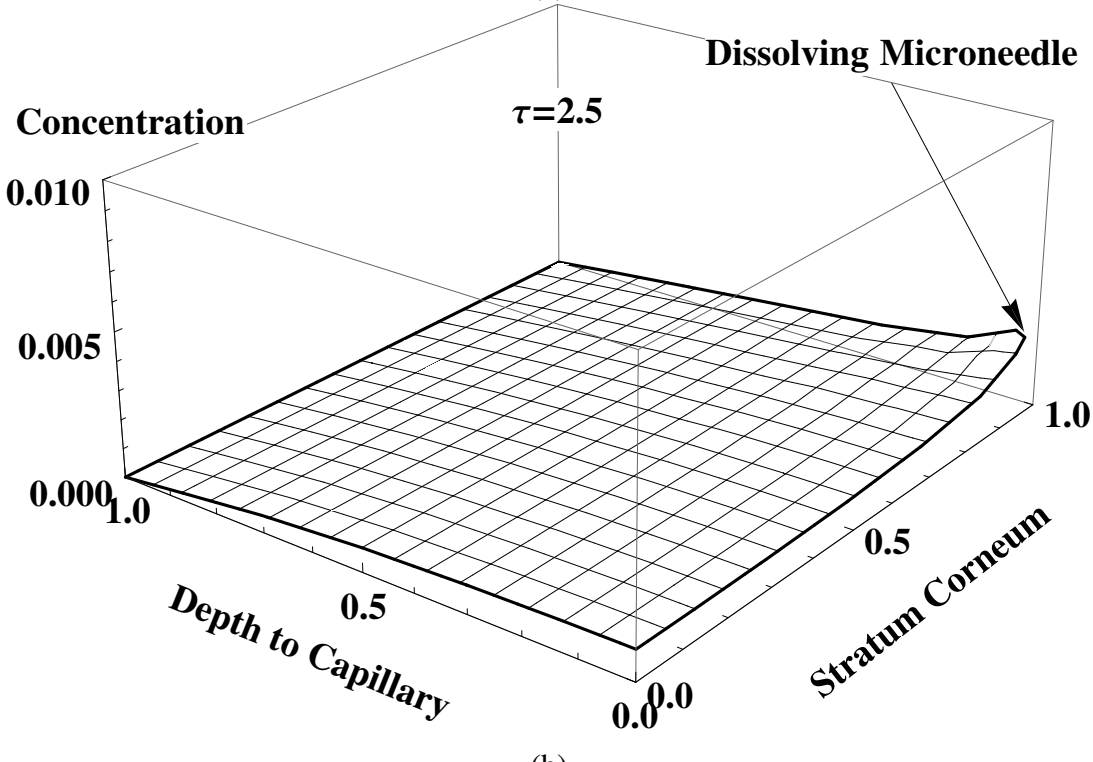

(b)

Figure 4.15 Concentration surfaces at τ=2.5: (a) R=K=M=0, (b) R=K=M=1.

a sub-axis of Figure 4.16. As discussed in the one-dimensional study, the electric field not only activates the spread of drug along skin (along the secondary direction of drug delivery) but also holds the drug within the epidermis (against the primary direction), see Figure 4.1. This is the reason why the fractional releases get closer and closer to one another as time passes. From Figure 4.16, it is recommended that the power supply be switched off before τ=1.2 when the extent of the enhancement is still large. Otherwise, the benefit from the use of the electric field will be lost. As a result, the additional expenses due to preparing and formulating the electrodes and other peripheral devices will be wasted.

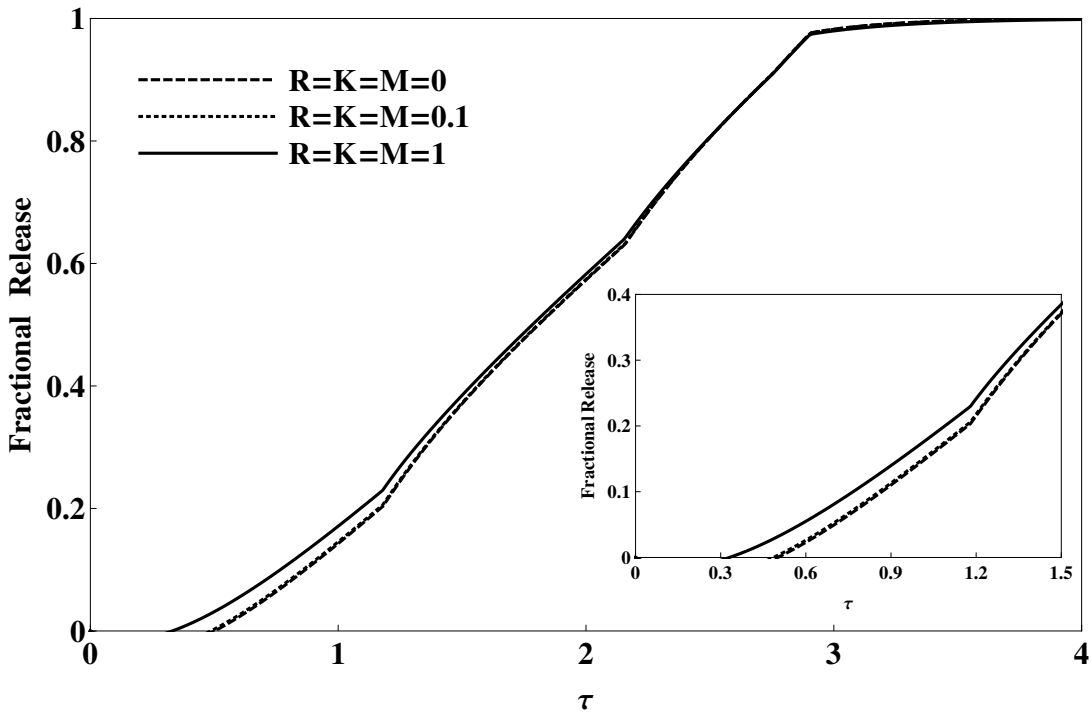

Figure 4.16 Fractional releases through self-dissolving microneedle patch at various intensities of electric field in two-dimensional study.

The dissolution time in the two-dimensional study is 2.91 for all three cases. Indeed, the results of the estimations of dissolution times show that dissolution rate visibly increased only with stronger electric field (not shown). However, in order to visualize the extremely small differences, much smaller size of time step in the fourth order Runge-Kutta method should be used, which requires additional computational resources and time.

Nevertheless, those small changes in the dissolution time may not be worth investigating because it will produce no practical meaning.

4.3.4 Simulations of Three-Dimensional Transport

Domain of three-dimensional simulation is defined as a cube (the length of a side is 1). The base (i.e., x-y plane at z=0) of the cube is placed on the surface of skin (or stratum corneum) and the top face (at z=1) is the boundary between epidermis and body. The centers of bases of conical microneedles are placed at (0,1,0) and (1,0,0) and the electrodes are located at (0,0,0) and (1,1,0). The heights of microneedles and the electrodes are all one half. To define the orthogonal collocation points in the space, the cube is sliced into 9 square planes (including the top and the bottom faces) parallel to the base according to the orthogonal collocation rule [20]. Since three-dimensional configuration of the given domain is very complicated to draw, one square plane at the depth of γ, i.e., (x,y,γ), is representatively shown in Figure 4.17. Based on these descriptions, the plane that is placed lower than the tips of microneedles should contain two one-quarter circles (microneedles; the shaded areas) at the points (1,0,γ) and (0,1,γ). The initial radii of those circles depend on the depth of the plane, γ, such that

$$r = r_b\left(1 - 2\gamma\right), \tag{4.43}$$

where r_b is the radius of the base of microneedle. Equation (4.43) holds only when the depth γ is less than one half, otherwise, r is zero (no microneedle). Although the dimension of the electrode is similar to that of the microneedle, the electrodes are drawn as points at (0,0,γ) and (1,1,γ) in Figure 4.17. The other area in the plane is filled with epithelial fluid.

The area filled with the epithelial fluid is divided into lines, i.e., $L\left(\tau = 0\right)$, the number and the relative positions of which are also same as those of the collocation points.

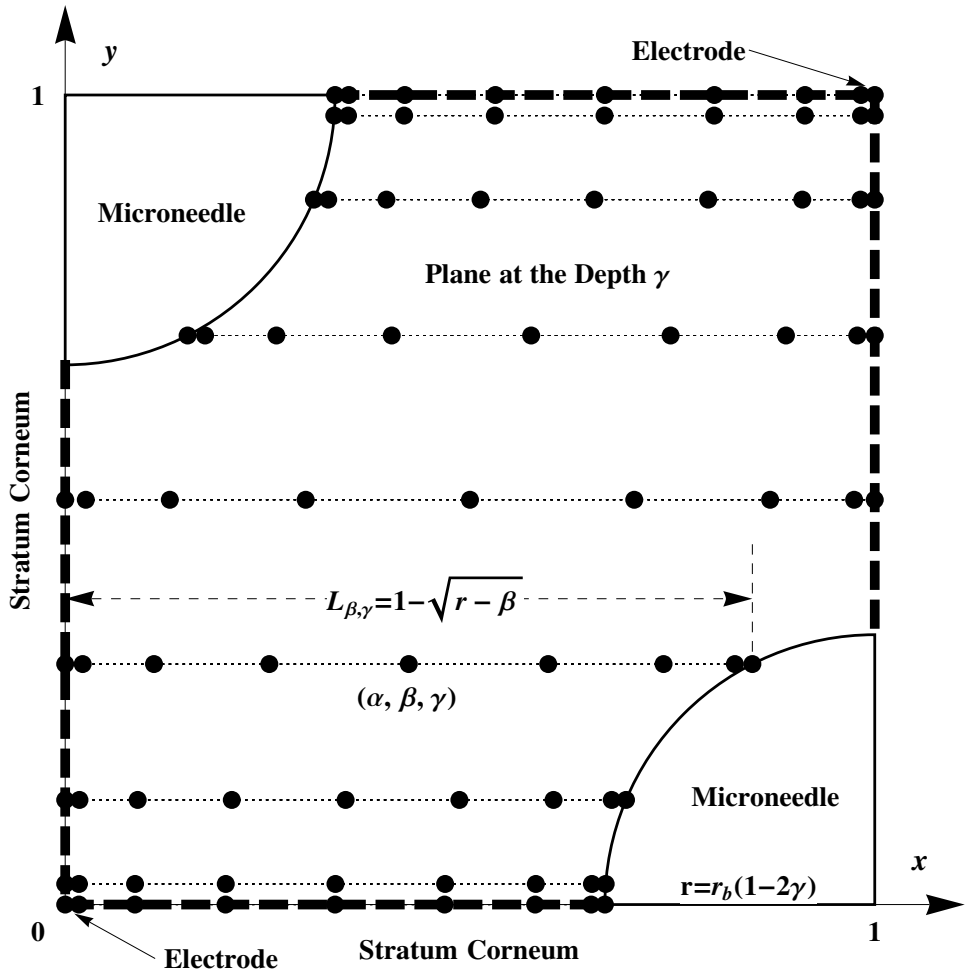

Figure 4.17 Top view of the square plane at the depth of γ in the domain of the three dimensional study.

Then, the collocation points are located on each line. Supposed that a line, $L_{\beta,\gamma}(\tau = 0)$, passes through a point (α,β $\left(< {}^{1}\!/_{2}\right)$,$\gamma$) in the domain and either of its end is placed on the circle, i.e., the surface of the microneedle, the length of the line which is occupied by the epithelial fluid is obtained by

$$L_{\beta,\gamma}(\tau = 0) = 1 - \sqrt{r - \beta}. \tag{4.44}$$

In the case where β is greater than one half, β in Equation (4.44) is replaced by $(1 - \beta)$.

The differential equations to be solved are Equations (4.28) to (4.32) and (4.35)

without any modification. The thick dashed lines in Figure 4.17 denote the side walls of the cubic domain at which the flux of drug, the velocities of the epithelial fluid and the electric current are all zero due to the symmetry condition. At the thin arcs, which mean the surfaces of the microneedles, Equation (4.33) is implemented. The thick dashed lines cover the entire square except the portions of the electrodes. The boundary condition, Equation (4.33), is removed as the microneedles disappear. The top and the bottom planes of the cubic domain represent the boundary between the epidermis and the region where the capillary vessels are found and the stratum corneum, respectively. At the top plate, the flux of the drug, the velocities of the epithelial fluid and the electric current are set to zero. At the bottom plate, a perfect sink condition is assumed. The velocities of the epithelial fluid and the electric current are set to zero.

The three dimensional simulations are performed with the same values of the parameters as used in the one and two dimensional studies. A few illustrations are shown to convey the outcomes of this research. In Figures 4.18 to 4.20, the concentration distributions at τ=0.2 and at three different depths (z=0 at the stratum corneum for Figure 4.18, z=0.297 for Figure 4.19, and z=0.703 for Figure 4.20) are demonstrated. The concentrations at upper layers are too low to lead to meaningful discussions. The upper axes of those figures show the concentrations when no electrically-enhancing action is taken, and the lower ones with R=K=M=1.

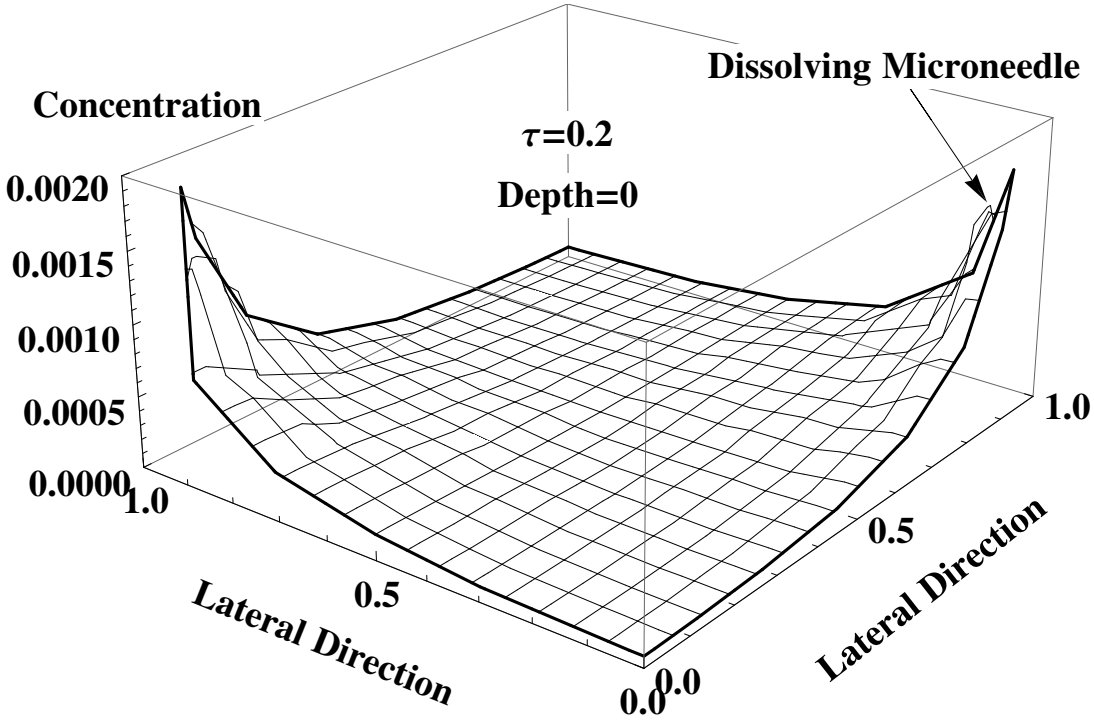

(a)

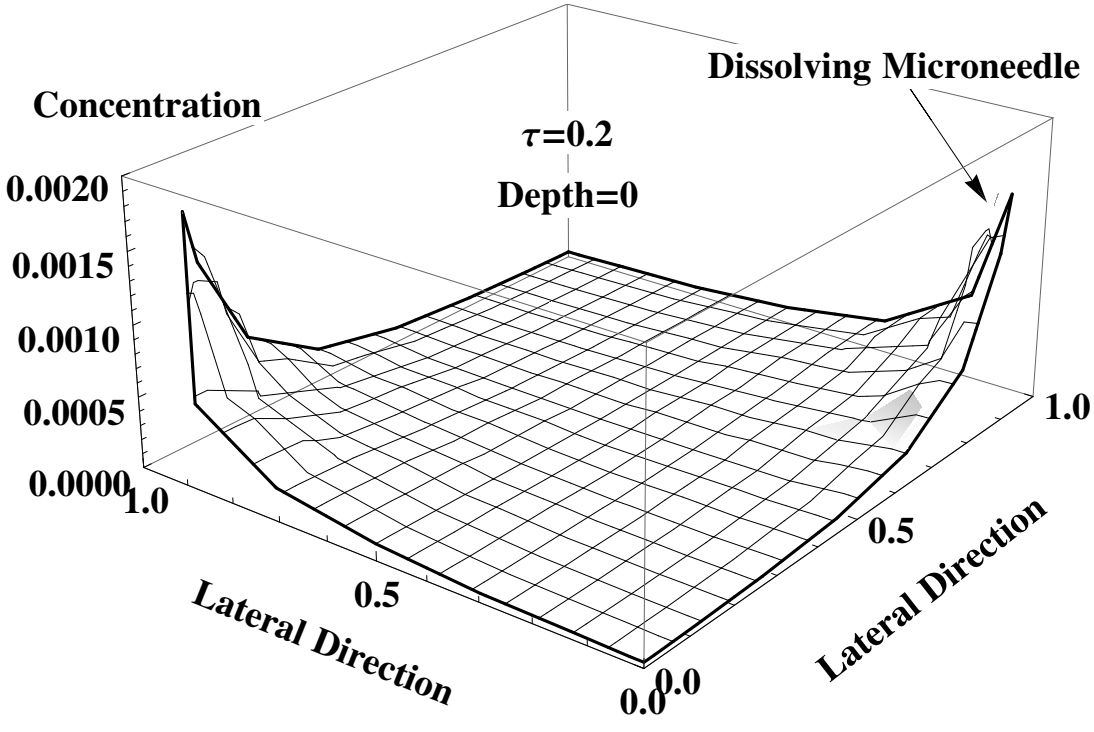

(b)

Figure 4.18 Concentration profile at the depth γ=0 at τ=0.2: (a) R=K=M=0, (b) R=K=M=1.

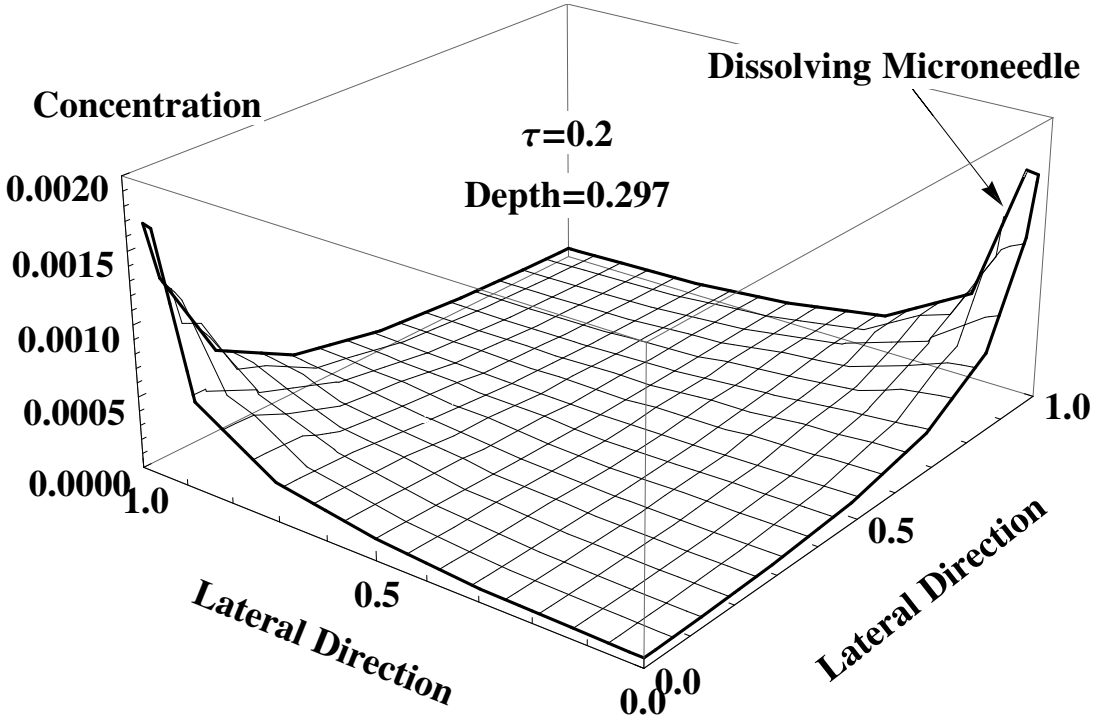

(a)

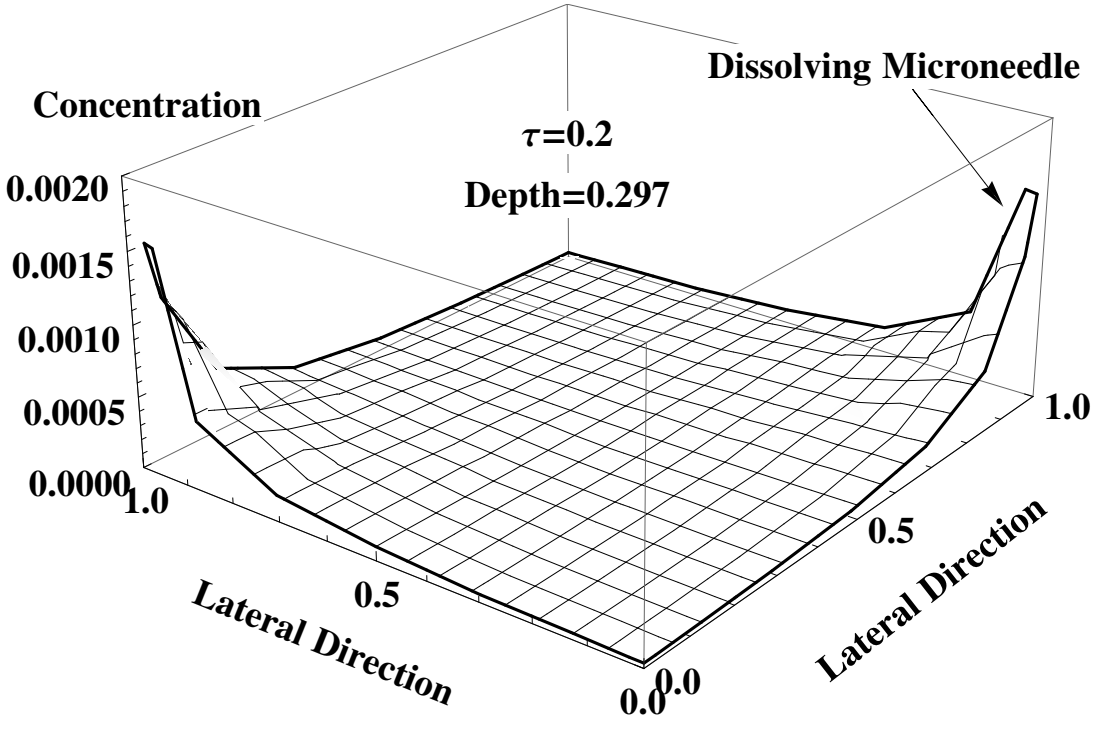

(b)

Figure 4.19 Concentration profile at the depth γ=0.297 at τ=0.2: (a) R=K=M=0, (b) R=K=M=1.

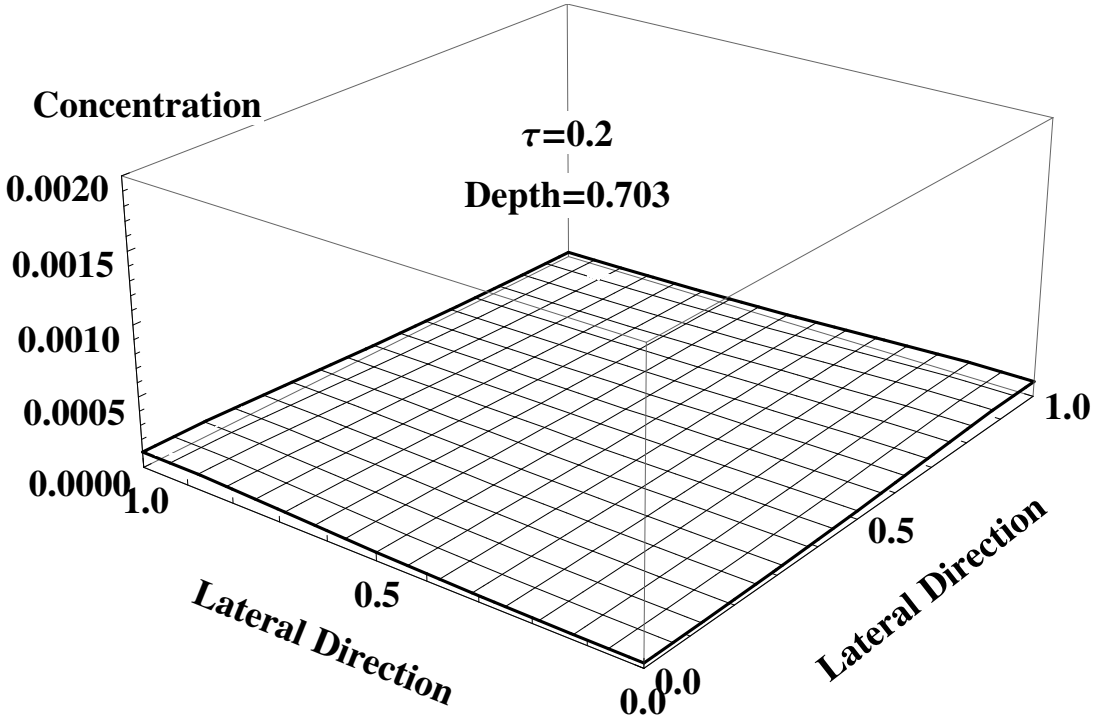

(a)

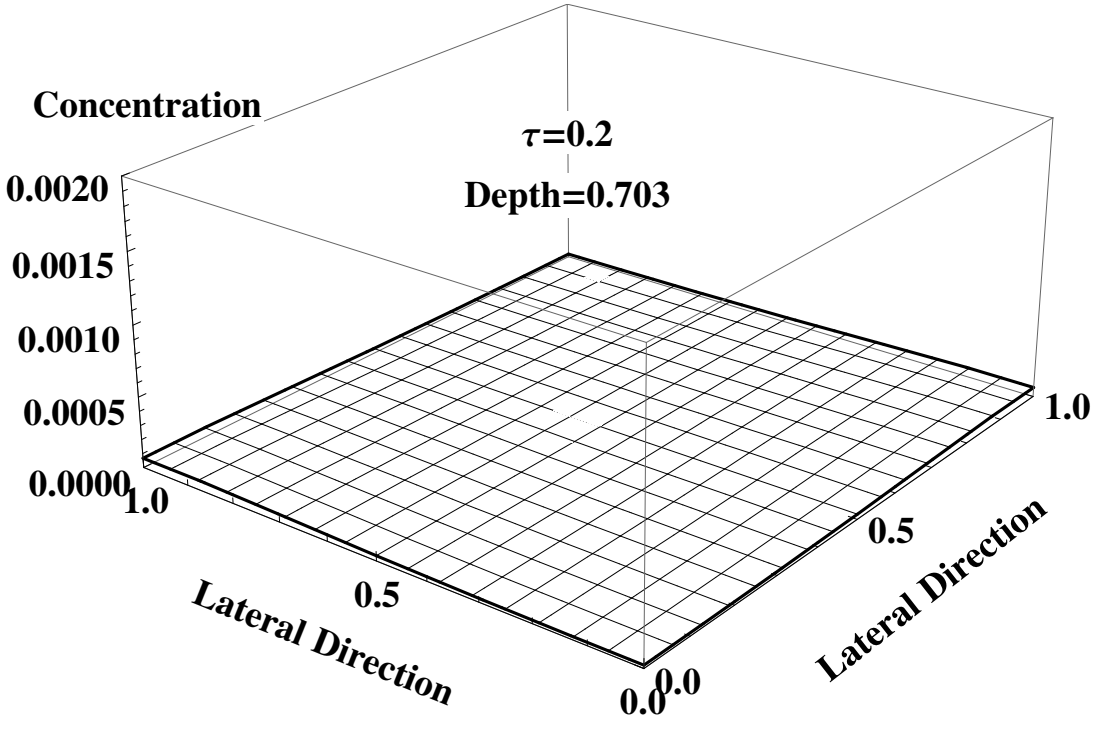

(b)

Figure 4.20 Concentration profile at the depth γ=0.703 and at τ=0.2: (a) R=K=M=0, (b) R=K=M=1.

In Figures 4.18 to 4.20, the centers of the bases of the microneedles are located at (1,0,0) and (0,1,0). Since the initial height of the microneedle is set one half, no microneedle can be found in Figure 4.20. The highest concentration of part (a) in Figure 4.18 is slightly but apparently higher than that of part (b) in the same figure (the leftmost region of the concentration surface of part (a) crossed the line, but that of part (b) does not). This trend is also observed in Figures 4.19 and 4.20, and shows that the applied electric field lowers the drug concentration around the microneedle to activate the dissolution.

In Figure 4.21, the concentrations at the depth of 0.703 after a long time elapses, i.e., τ=1.4 are drawn: part (a) with no electric field, and part (b) with electric field. The main observations are that the drug is more concentrated around the electrodes than where the microneedles are placed, and that the overall concentration in the presence of the electrical enhancement, part (b), is lower than that without it, part (a). These findings provide further evidence of how drug delivery is enhanced by the presence of the electric field.

4.4 Electrically Enhanced Self-Dissolving Microneedle Patch

The aims of this investigation are 1) to propose a new enhanced transdermal delivery system using an array of self-dissolving microneedles and microelectrodes on a patch, 2) to quantitatively and qualitatively investigate the feasibilities of the proposed delivery platform and the enhancement scenario, 3) to build up guidelines to future clinical experiments for obtaining the accurate values of the cited physical properties, and 4) to build up guidelines to product design. Up to the previous section, the first two goals are achieved. The next two objectives are discussed in Sections 4.4.1 and 4.4.2.

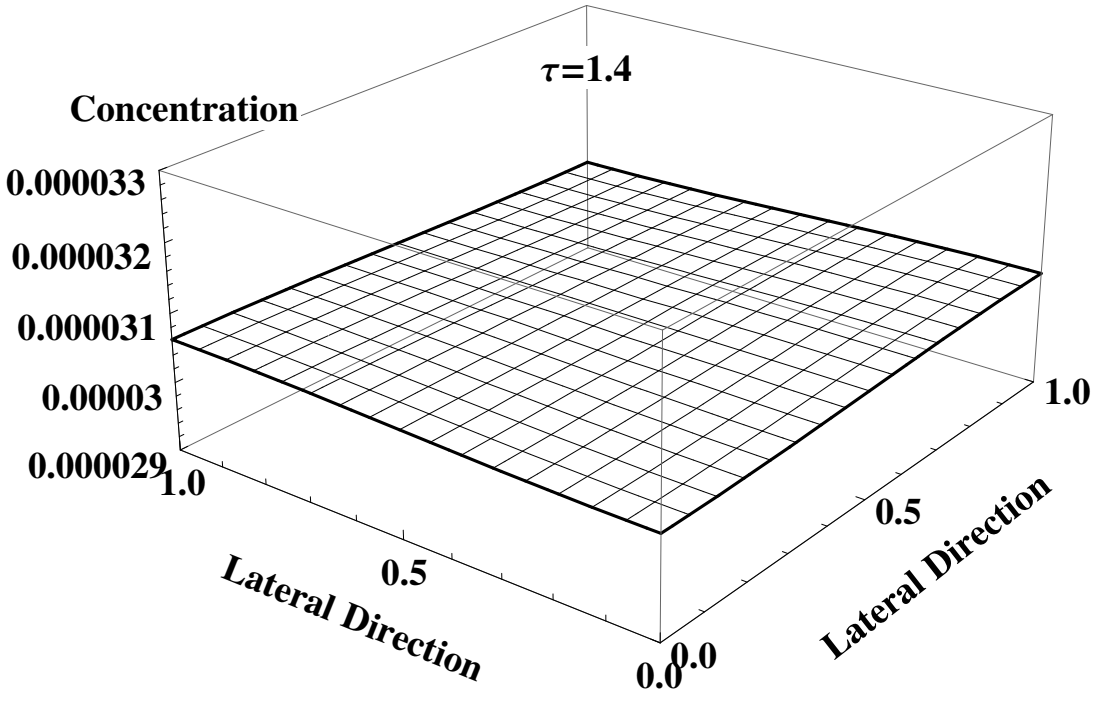

(a)

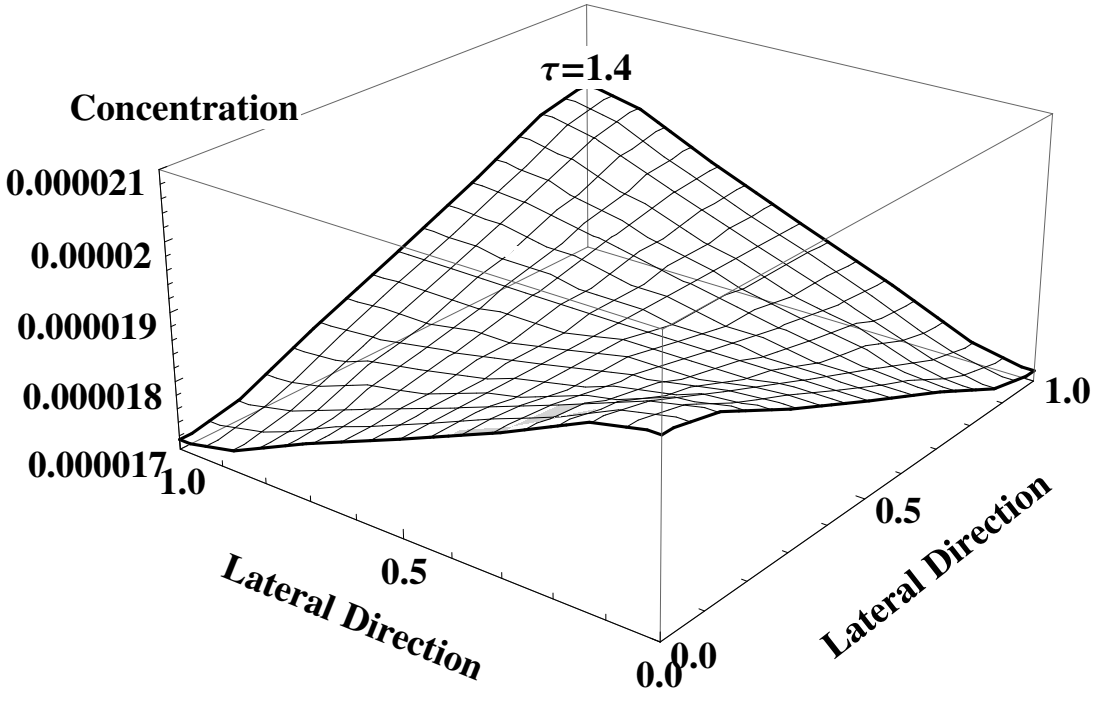

(b)

Figure 4.21 Concentration profile at the depth γ=0.703 and at τ=1.4: (a) R=K=M=0, (b) R=K=M=1.

4.4.1 Experimental Guidelines

The in vivo or in vitro experiments are very important for validating the mathematical model. This study focused on simulations and dimensionless analyses because the physical properties involved in the mathematical models are not available. Results of clinical experiments, particularly designed for the proposed drug delivery platform, are also lacking in the literatures. This section is committed to the use of the mathematical model and the simulation in the generation of the clinical data and in the analysis on the obtained data to estimate the values of the model parameters.

The elaborate fabrication method of an array of soluble microneedles is available in the literature [11]. One of the formulation methods of the patch discussed in this research is as follows. Electronic circuit is used as a patch substrate. A flexible design is desirable to make sure that the patch attaches tightly to the curvy surface of a skin. On the electronic circuit, an array of hard metal electrodes is placed in a way that the distance between the adjacent (not diagonally) electrodes is twice that between the adjacent soluble microneedle and the electrode on the complete array of the patch. The electrodes are interconnected through the flexible circuit. Bores that will firmly hold the microneedles in place are made by a micro-drilling tool. An array of soluble microneedles is fabricated following the procedures described in the previous researches [11]. An individual microneedle is taken from the array, and it is nailed firmly (the sharp tip upward) to one of the bores prepared on the flexible circuit substrate. In the end, the circuit is connected to a power supply for a laboratory purpose, the serial connection of one or more dry batteries (providing 1.5 V per each) may be recommended.

In clinical tests, the prepared self-dissolving microneedle and electrode patches are placed on the skins of subjects. The blood samples are periodically taken from the subject. The time intervals between samples are set by the experienced clinical scientists. The serum concentrations of drug are measured from the samples and, hence, graphs of the serum concentration vs. treatment time are prepared and ready to be analyzed.

From the resulting graph, conventional pharmacokinetic analyses can be implemented to estimate the values of the maximum serum concentration, $C_{\max}$, the time to reach the maximum concentration, $T_{\max}$, and the area under the curve, AUC. Those pharmacokinetic parameters are taken into account when a product is designed. After this investigation, additional task is suggested to be done. In other word, the estimations of the all parameters involved in the model should be conducted by fitting the model-predicted serum concentration profile to the clinical data using the nonlinear regression or at least some trial-and-error procedures if a high performance computer is not available. For example, the regression yields a set of seven independent equations such that $R = \frac{p\mu\phi_0}{U_0}$, $K = R\frac{L_0^2 c_s p}{\phi_0}$, $M = R\frac{c_s L_0^2}{\rho\mu D}$, $Sc = \frac{\nu}{D}$, $P = \frac{pL_0^2}{\varepsilon\phi_0}$, $N = \frac{k_D L_0}{D}$ and $\tau_0 = \frac{L_0^2}{D}$. The parameter, $Q = \frac{L_0 k_D}{D\rho_M}$, are automatically determined with N and ρ_M. There are seven independent constants (ρ, μ, p, D, ε, ν and k_D). The properties such as ϕ_0, L_0, ρ_s and $\rho_M = \frac{\rho_s}{c_s}$ can be determined by the fabrication method of the patch by the researchers. The system of seven algebraic equations are solved to yield

$$\rho = \left(\frac{K\tau_0}{MR}\right)\frac{{\phi_0}^2}{L_0^2 U_0}, \tag{4.45}$$

$$\mu = \left(\frac{R^2}{K}\right)\frac{c_s L_0^2 u_0}{\phi_0^2}, \tag{4.46}$$

$$p = \left(\frac{K}{R}\right)\frac{\phi_0^2}{c_s L_0^2}, \tag{4.47}$$

$$D = \frac{L_0^2}{\tau_0}, \tag{4.48}$$

$$\varepsilon = \left(\frac{K}{PR}\right) {c_s}^{-1}, \tag{4.49}$$

$$\nu = ScD, \tag{4.50}$$

and

$$k_D = \left(\frac{N}{\tau_0}\right) L_0. \tag{4.51}$$

These values can be used to predict the transdermal drug delivery through the proposed platform with the different designs which are not yet explored by the clinical tests.

The in vivo validation of the drug delivery enhancement scenario can be conducted by applying two patches simultaneously in one subject. One patch has the circuit connected to the battery, and the other does not. Then, when a certain time has elapsed, the two patches are simultaneously removed from the subject's skin, and the shapes of the remaining microneedles are recorded for further comparison. To avoid any side effect due to the multiple dosages, the size of the array in one patch may be reduced.

4.4.2 Product Design Guidelines

The parameters obtained from Equations. (4.45) to (4.51) can be used in the manufacturing step of the product. As in the results of the three simulation studies, the predictions with various designs can provide preliminary information on the design of the electrode-mounted self-dissolving microneedle patch. Specifications such as the time to turn off the device, the distance between microneedles, the dimensions of the conical microneedle, the

size of the array, the electric potential of the electrode (it is related to the choice of the battery), can be estimated.

4.5 Conclusions

The new transdermal drug delivery system using a self-dissolving microneedle enhanced by an applied electric field is proposed in this study. The drug delivery platform is inspired by the previous soluble microneedle therapy system and iontophoresis. For example, the shape of the electrode is similar to that of the microneedle. The electrodes and the microneedles are placed alternately in an array on the flexible patch substrate. At the beginning of the treatment, the electrodes and the microneedles are inserted into the epidermis bypassing the stratum corneum, and, at the sane time, the electric current is applied. The drug delivery is enhanced by the electric field which first attracts the drug molecules and results in lower concentration around the microneedle. Consequently, the dissolution rate of the microneedle will increase since the driving force of the dissolution (the difference between the surrounding concentration and the solubility) is kept high. The delivery platform needs to be validated using clinical test results. The rest of this research is dedicated to test the concept with simple lab experiments, conduct simulations using the model and suggest experimental guidelines for future clinical test.

The preliminary studies are conducted. The active diffusion of Indigo Carmine by the electric field is first tested. Then the in vitro releases of benzocaine from lozenges with/without an electric current are compared. The results of two pilot experiments show that 1) the drug moves toward the cathode in a faster speed of the passive diffusion, 2) the dissolution is affected by the electric field, and 3) the release is enhanced under the electric field. In the next investigation, the mathematical model of the dissolution of a conical microneedle in a well-stirred container is set up to show the behaviors of the dissolving microneedle and the concentrations in the epidermis during the treatment. Although the mathematical simulations in the next sections have the same purposes, it is still impor-

tant because more intuitive, concise and even faster analyses are possible with the simpler model.

The mathematical equations describing the motion of drug and epithelial fluid, the electric field and the size of the self-dissolving microneedle have been derived with the relevant boundary conditions. The outcomes of the one dimensional simulation are 1) the fractional release with the electric field is much faster than that without the electric field, 2) the electric field accelerates the dissolution of the microneedle so that the dissolution time decreases with increasing intensity of the electric field.

In two dimensional simulation, the concentration profiles are visualized to make readers understand the detailed events that take place in the epidermis. A lower concentration under the electric field is observed around the microneedle compared to the case when no electric field is applied. The fractional releases with/without the electric field are also compared. The results show that, at the beginning of the treatment, the release seems to be activated by the electric field, but, after a long time, the two release profiles are getting closer. This is because the attraction of drug by the applied electric field accelerates the dissolution but also prevents the drug from escaping the epidermis. This observation as well as the time of dissolution in the one dimensional simulation lead to the conclusion that the electric field should be removed after a certain time, e.g., it is about τ=1.2 based on the analysis of the two dimensional simulation.

The results of the three dimensional simulation give another insight into the mechanisms of the drug delivery. In Figures 4.18 to 4.20, the behaviors of the concentration profiles with/without the electric field are similar as expected from the previous simpler simulations such that the lower concentration is observed when the electric field is applied. The more significant aspect is shown in Figure 4.21 where the concentrations around the electrode are higher than other places after a long time has lapsed, e.g., τ=1.4. This means the drug is attracted by the electric field, and also implies that the continued electric field may prevent the drug from being absorbed to the systemic circulation. Without the electric

field, part (a) in Figure 4.21, such behavior is not found. Based on the findings from the mathematical models and the simulations, guidelines for the clinical experiments and the product design are made. The guidelines include the fabrication method of an array of the self-dissolving microneedles and the electrodes on the patch substrate, properties that must be measured, and how to estimate the unknown physical properties from the obtained data.

CHAPTER 5

CONCLUSIONS

The main purpose of this research is to provide a platform that will help improve research on drug delivery. To achieve this goal, close collaborations with other researchers are necessary along with the development of mathematical models of various drug delivery systems. Several examples are provided in this work to show the advantages of theoretical studies. Methods of incorporating the findings in experimental investigations are also outlined.

In the first project, a method to obtain the optimal intravenous dosage regimen is discussed. The hybrid use of the already-invented dosage forms such as a bolus injection and a constant rate infusion can minimize the time it takes to achieve a desired therapeutic effect of a drug with the guaranteed safety. The investigation used a two-compartment pharmacokinetic model to develop the optimal dosage regimens of the drug theophylline.

In the second project, the design problem of the transdermal drug delivery patch assisted by an external heating device is studied. The heating pad has been already used in many oriental countries to encourage the therapeutic effect of the drug. However, the controlled release of drug from the patch by the heating pad has never been discussed, even though it is very important for preventing accidental overdose. The mathematical model allows the control and thus the optimal design of the corticosterone delivery system by introducing the design factors: the mass of the heating pad (MS), the overall heat transfer coefficient (OH), the initial reaction rate (IR) and the initial corticosterone concentration (IC). The investigation reveals the optimal values of those factors as well as the relative importance (the priorities in the design that maximizes the therapeutic effect when limited resource is provided): IC>MS>IR>OH.

The last research deals with a proposed drug delivery system. In that prototype, self-dissolving microneedles are used to bypass the stratum corneum, and an electric field is simultaneously applied to the epidermis to enhance diffusion and dissolution. This is an

advanced form of the hybrid system of the soluble microneedle plus iontophoresis in the sense that the electrodes are also inserted into the epidermis as solid microneedles. The work should analyze the problem in the absence of clinical test data and known electro-hydrodynamic properties. Therefore, dimensionless analyses, based on the results of the one-, two- and three-dimensional simulations, are only used to decipher the drug delivery in the platform. The key outcomes of the research are that the applied electric field activates drug delivery by encouraging the diffusion of drug in the epithelial fluid and, consequently, accelerating the dissolution. At some time, the electric field needs to be removed in order to allow the drug to be absorbed into the systemic circulation. Based on these results, guidelines for the future experiments and the products are suggested.

The three research projects have successfully provided materials to show the advantages of the mathematical models and the computer simulations in the design and control of drug delivery systems. This work can be used, in conjunction with experimental data, by researchers around the world to further the development of efficient drug delivery devices and improved administration protocols.

REFERENCES

[1] M. Fernandes, L. Simon and N.W. Loney, Mathematical modeling of transdermal drug-delivery systems: analysis and applications, J. Membrane Sci. 256 (2005) 184-192.

[2] A.J. Lee, J.R. King and S. Hibberd, Mathematical modeling of the release of drug from porous, nonswelling transdermal drug-delivery devices, Math. Med. Biol. 15 (1998) 135-163.

[3] K.S. Kim and L. Simon, Modeling and design of transdermal drug delivery patches containing an external heating device, J. Pharm. Sci., in review.

[4] Y. Nir, A. Paz, E. Sabo and I. Potasman, Fear of injections in young adults: prevalence and associations, Am. J. Trop. Med. Hyg. 68 (2003) 341-344.

[5] K.S Kim. and L. Simon, Optimal intravenous bolus-infusion drug-dosage regimen based on two-compartment pharmacokinetic models, Comput. Chem. Eng. 33 (2009) 1212-1219.

[6] S. Meylan, A.M. Dufty and J. Clobert, The effect of transdermal corticosterone application on plasma corticosterone levels in pregnant Lacerta vivipara, Comp. Biochem. Phys. A 134 (2003) 497-503.

[7] D. Lee, N. Ashcraft, E. Verploegen, E. Pashkovski and D.A. Weitz, Permeability of model stratum corneum lipid membrane measured using quartz crystal microbalance, Langmuir 25 (2009) 5762-5766.

[8] T.S. Shomaker, J. Zhang, and M.A. Ashburn, A pilot study assessing the impact of heat on the transdermal delivery of testosterone, J. Clin. Pharmacol. 41 (2001) 677-682.

[9] M.A. Ashburn, L.L. Ogden, J. Zhang, G. Love and S.V. Basta, The pharmacokinetics of transdermal fentanyl delivered with and without controlled heat, J. Pain 4 (2003) 291-297.

[10] M.R. Prausnitz, Microneedles for transdermal drug delivery, Adv. Drug Deliver. Rev. 56 (2004) 581-587.

[11] J.W. Lee, J.H. Park and M.R. Prausnitz, Dissolving microneedles for transdermal drug delivery, Biomaterials 29 (2008) 2113-2124.

[12] V. Vemulapalli, Y. Yang, P.M. Friden and A.K. Banga, Synergistic effect of iontophoresis and soluble microneedles for transdermal delivery of methotrexate, J. Pharm. Pharmacol. 60 (2008) 27-33.

[13] M.Mueller, A. de la Pena and H. Derendorf, Issues in pharmacokinetics and pharmacodynamics of anti-infective agents: kill curves versus MIC, Antimicrob. Agents Ch. 48 (2004) 369-377.

[14] T.N.Tozer and M. Rowland, Introduction to Pharmacokinetics and Pharmacodynamics, Lippincott Williams & Wilkins, Maryland, 2006.

[15] M. Wheeler, P.K. Birmingham, R.A. Lugo, C.L. Heffner and C.J. Coté, The Pharmacokinetics of the Intravenous Formulation of Fentanyl Citrate Administered Orally in Children Undergoing General Anesthesia, Anesth. Analg. 99 (2004) 1347-1351.

[16] R.K. Portenoy, D. Taylor, J. Messina and L. Tremmel, A randomized, placebo-controlled study of fentanyl buccal tablet for breakthrough pain in opioid-treated patients with cancer, Clin. J. Pain 22 (2006) 805-811.

[17] P.A.Mitenko and R.I. Ogilvie, Pharmacokinetics of intravenous theophylline, Clin. Pharmacol. Ther. 14 (1973) 509-513.

[18] J.G. Wagner, A safe method for rapidly achieving plasma concentration plateaus, Clin. Pharmacol. Ther. 16 (1975) 691-700.

[19] L.A. Wheeler and L.B. Sheiner, A general method for optimal drug dose computation, J. Pharmacokinet. Biop. 4 (1976) 487-497.

[20] B.A. Finlayson, Nonlinear analysis in chemical engineering, McGraw-Hill, New York, 1980.

[21] A. Goyal, S. Mandapuram, B. Michniak and L. Simon, Application of orthogonal collocation and regression techniques for recovering parameters of a two-pathway transdermal drug-delivery model, Comput. Chem. Eng. 31 (2007) 107-120.

[22] D.D. Tang-Liu, R.L. Williams and S. Riegelman, Nonlinear theophylline elimination, Clin. Pharmacol. Ther. 31 (1982) 358-369.

[23] H. Kanazawa, R. Atsumia, Y. Matsushimaa and J. Kizub, Determination of theophylline and its metabolites in biological samples by liquid chromatography?mass spectrometry, J. Chromatogr. A 870 (2000) 87-96.

[24] S.H. Strogatz, Nonlinear Dynamics and Chaos, Perseus Book Publishing, Massachusetts, 1994.

[25] M. Weinerger and L. Hendeles, Theophylline in asthma, New Engl. J. Med. 334 (1996) 1380-1388.

[26] A. Vale, Theophylline, Medicine 35 (2007) 657.

[27] T. Ishizaki and M. Kubo, Incidence of apparent Michaelis-Menten kinetic behavior of theophylline and its parameters (Vmax and Km) among asthmatic children and adults, Ther. Drug Monit. 9 (1987) 11-20.

[28] P.K. Wilkinson, A.J. Sedman, E. Sakmar, R.H. Earhart, D.J. Weidler and J.G. Wagner, Blood ethanol concentrations during and following constant-rate intravenous infusion of alcohol, Clin. Pharmacol. Ther. 19 (1976) 213-223.

[29] M.D.Levitt and D.G. Levitt, Use of a two-compartment model to assess the pharmacokinetics of human ethanol metabolism, Alcohol. Clin. Exp. Res. 22 (1998) 1680-1688.

[30] R.H. Guy, J. Hadgraft and D.A.W. Bucks, Transdermal drug delivery and cutaneous metabolism, Xenobiotica 17 (1987) 325-343.

[31] A. Saadeddin, F. Torres-Molina, J. Carcel-Trullols, A. Araico and J.-E. Peris, Pharmacokinectics of the time-dependent elimination of all-trans-retinoic acid in rats, AAPS PharmSci 6 (2004) 1-9.

[32] J.A. Orsini, P.J. Moate, K. Kuersten, L.R. Soma and R.C. Boston, Pharmacokinetics of fentanyl delivered transdermally in healthy adult horses variability among horses and its clinical implications, J. Vet. Pharmacol. Ther. 29 (2006) 539-546.

[33] I.B. Pathan and C.M. Setty, Chemical penetration enhancers transdermal drug delivery systems, Trop. J. Pharm. Res. 8 (2009) 173-179.

[34] L.P. Gangarosa Sr., A. Ozawa, M. Ohkido, Y. Shimomura and J.M. Hill, Iontophoresis for enhancing penetration of dermatologic and antiviral drugs, J. Dermatol. 22 (1995) 865-875.

[35] J. Hirvonen, Y.N. Kalia and R.H. Guy, Transdermal delivery of peptides by iontophoresis, Nat. Biotechnol. 14 (1996) 1710-1713.

[36] T. Terahara, S. Mitragotri, J. Kost and R. Langer, Dependence of low-frequency sonophoresis on ultrasound parameters; distance of the horn and intensity, Int. J. Pharm. 235 (2002) 35-42.

[37] G. Merino, Y.N. Kalia, M.B. Delgado-Charro, R.O. Potts, H. Richard and R.H. Guy, Frequency and thermal effects on the enhancement of transdermal transport by sonophoresis, J. Control. Release 88 (2003) 85-94.

[38] H.Y. Zhang and S.H. Yeo, Design and fabrication of a sonophoresis device with a flat flextensional transducer for transdermal drug delivery, Sensor Actuat. A-Phys. 115 (2004) 133-139.

[39] E.H. Leach, R.A. Peters and R.J. Rossiter, Experimental thermal burns, especially the moderate temperature burn, Q. J. Exp. Physiol. 32 (1943) 67-86.

[40] L. Simon, Analysis of heat-aided membrane-controlled drug release from a process control perspective, Int. J. Heat Mass Tran. 50 (2007) 2425-2433.

[41] L. Simon, Timely drug delivery from controlled-release devices: dynamic analysis and novel design concepts, Math. Biosci. 217 (2009) 151-158.

[42] R.H. Perry and D.W. Green, Perry's Chemical Engineers' Handbook, 8th ed., McGraw-Hill, New York, 2008.

[43] K. Tojo, Y.W. Chien, Y. Sun and M. Ghannam, Membrane transport of drug under nonisothermal conditions, J. Chem. Eng. Jpn. 20 (1987) 626-629.

[44] Q. Fan, K.K. Sirkar and B. Michniak, Iontophoretic transdermal drug delivery system using a conducting polymeric membrane, J. Membrane Sci. 321 (2008) 240-249.

[45] W.M. Saltzman, Drug Delivery: Engineering Principles for Drug Therapy, Oxford University Press, New York, 2001.

[46] F. Bernardo and P.M. Saraiva, A theoretical model for transdermal drug delivery from emulsions and its dependence upon formulation, J. Pharm. Sci. 97 (2008) 3781-3809.

[47] S. Meylan, J. Belliure, J. Clobert and M. De Fraipont, Stress and body condition as prenatal and postnatal determinants of dispersal in the common lizard (Lacerta vivipara), Horm. Behav. 42 (2002) 319-326.

[48] S. Meylan, A.M. Dufty and J. Clobert, The effect of transdermal corticosterone application on plasma corticosterone levels in pregnant Lacerta vivipara, Comp. Biochem. Phys. A 134 (2003) 497-503.

[49] S.E. La Fleur, S.F. Akana, S.L. Manalo and M.F. Dallman, Interaction between corticosterone and insulin in obesity: Regulation of lard intake and fat stores, Endocrinology 145 (2004) 2174-2185.

[50] S. Pattanayak and T. Bhowmick, Thermal characteristics of poly(ethylene vinyl acetate) from 80 to 300 K, Cryogenics 30 (1990) 795-798.

[51] S.A. Kumar, S. Thomas and M.G. Kumaran, Transport of aromatic hydrocarbons through poly(ethylene-co-vinyl acetate) membranes, Polymer 38 (1997) 4629-4640.

[52] K. Kretsos, M.A. Miller, G. Zamora-Estrada and G.B. Kasting, Partitioning, diffusivity and clearance of skin permeants in mammalian dermis, Int. J. Pharm. 346 (2008) 64-79.

[53] S. Mitragotri, In situ determination of partition and diffusion coefficients in the lipid bilayers of stratum corneum, Pharm. Res. 17 (2000) 1026-1029.

[54] I. Dincer and S. Dost, An analytical model for moisture diffusion in solid objects during drying, Dry. Technol. 13 (1995) 425-435.

[55] J. Zhang, W. Hull and L. Rigby, Controlled heat induced rapid delivery of pharmaceuticals from skin depot, U.S. Patent No. 6756053, 2004.

[56] L. Simon and A. Goyal, Dynamics and control of percutaneous drug absorption in the presence of epidermal turnover, J. Pharm. Sci. 98 (2009) 187-204.

[57] M.E. Johnson, S. Mitragotri, A. Patel, D. Blankschtein and R. Langer, Synergistic effects of chemical enhancers and therapeutic ultrasound on transdermal drug delivery, J. Pharm. Sci. 85 (1996) 670-679.

[58] R.B. Bird, W.E. Stewart and E.N. Lightfoot, Transport Phenomena 2nd ed., John Wiley & Sons, Inc., New York, 2006.

[59] S. Prodduturi, G. Smith, A. Wokovich, W. Doub, B. Westenberger and L. Buhse, Reservoir based fentanyl transdermal drug delivery systems: effect of patch age on drug release and skin permeation, Pharm. Res. 26 (2009) 1344-1352.

[60] Y. Ito, E. Hagiwara, A. Saeki, N. Sugioka and K. Takada, Feasibility of microneedles for percutaneous absorption of insulin, Eur. J. Pharm. Sci. 29 (2006) 82-88.

[61] S. Henry, D.V. Mcallister, M.G. Allen and M.R. Prausnitz, Microfabricated microneedles: a novel approach to transdermal drug delivery, J. Pharm. Sci. 87 (1998) 922-925.

[62] K. Hansen and B. Haldin, A solid microstructured transdermal system for systemic delivery of salt & proteins, Drug Deliver. Technol. 8 (2008) 38-42.

[63] S.L. Banks, R.R. Pinninti, H.S. Gill, P.A. Crooks, M.R. Prausnitz and A.L. Stinchcomb, Flux across microneedle-treated skin is increased by increasing charge of Naltrexone and Naltrexol in vitro, Pharm. Res. 25 (2008) 1677-1685.

[64] E.V. Mukerjee, S.D. Collins, R.R. Isseroff and R.L. Smith, Microneedle array for transdermal biological fluid extraction and in situ analysis, J. Sensor Actuat. A 114 (2004) 267-275.

[65] S.Y. Kwon, Dissolvable microneedle patch for biopharmaceuticals delivery and vaccination, Drug Delivery Report Winter 2007/2008 (2008) 56-57.

[66] R. Vanbever, N. Lecouturier and V. Preat, Transdermal delivery of metoprolol by electroporation, Pharm. Res. 11 (1994) 1657-1662.

[67] H.S. Minkowitz, Fentanyl iontophoretic transdermal system: a review, Tech. Region. Anesth. Pain manag. 11 (2007) 3-8.

[68] K. Fellinger and J. Schmidt, Klinik and Therapies des Chromischen Gelenkreumatismus, Maudrich Vienna, Austria (1954) 549-552.

[69] S. Mitragotri and J. Kost, Low-frequency sonophoresis, Adv. Drug Deliver. Rev. 56 (2004) 589-601.

[70] I. Lavon and J. Kost, Ultrasound and transdermal drug delivery, Drug Delivery Today 9 (2004) 670-676.

[71] P. Khanna, J.A. Strom, J.I. Malone and S. Bhansali, Microneedle-Based Automated Therapy for Diabetes Mellitus, J. Diabetes Sci. Technol. 2 (2008) 1122-1129.

[72] H. Kimura, Y. Ogura, M. Hashizoe, H. Nishiwaki, Y. Honda and Y. Ikada, A new vitreal drug delivery system using an implantable biodegradable polymeric device, Invest. Ophth. Vis. Sci. 35 (1994) 2815-2819.

[73] M. Grassi and G. Grassi, Mathematical modeling and controlled drug delivery: matrix systems, Curr. Drug Deliver. 2 (2005) 97-116.

[74] H.E. Bodde and J.G.H. Joosten, A mathematical model for drug release from a two-phase system to a perfect sink, Int. J. Pharm. 26 (1985) 57-76.

[75] D.L. Bernik, D. Zubiri, M.E. Monge and R.M. Negri, New kinetic model of drug release from swollen gels under non-sink conditions, Colloid. Surface. A 273 (2006) 165-173.

[76] A.M. Abu-Khalaf and M.A. Soliman, Drug release from spherical particles under nonsink conditions. I. Theoretical evaluation, Drug Dev. Ind. Pharm. 22 (1996) 465-469.

[77] R. Luttge, E.J.W. Berenschot, M.J. deBoer, D.M. Altpeter, E.X. Vrouwe, A. Berg and M. Elwenspoek, Integrated lithographic Molding for microneedle-based devices, J. Microelectromech. S. 16 (2007) 872-884.

[78] K. Hansen and B. Haldin, A solid microstructured transdermal system for systemic delivery of salt & proteins, Drug Deliver. Technol. 8 (2008) 38-42.

[79] J. Jiang, H.S. Gill, D. Ghate, B.E. McCarey, S.R. Patel, H.F. Edelhauser and M.R. Prausnitz, Coated microneedles for drug delivery to the eye, Invest. Ophth. Vis. Sci. 48 (2007) 4038-4043.

[80] H.S. Gill and M.R. Prausnitz, Coated microneedles for transdermal delivery, J. Control. Release 117 (2007) 227-237.

[81] H.S. Gill and M.R. Prausnitz, Coating formulations for microneedles, Pharm. Res. 24 (2007) 1369-1380.

[82] H.J.G.E. Gardeniers, R. Luttge, E.J.W. Berenschot, M.J. deBoer, S.Y. Yeshurun, M. Hefetz, R. vanąŕt Oever and A. van den Berg, Micromachined hollow microneedles for transdermal liquid transport, J. Microelectromech. S. 12 (2003) 855-862.

[83] B. Stoeber and D. Liepmann, Arrays of hollow out-of-plane microneedles for drug delivery, J. Microelectromech. S. 14 (2005) 472-479.

[84] S.P. Davis, W. Martanto, M.G. Allen and M.R. Prausnitz, Hollow metal microneedles for insulin delivery to diabetic rats, IEEE T. Bio-Med Eng. 52 (2005) 909-915.

[85] W. Martanto, J.S. Moore, O. Kashlan, R. Kamath, P.M. Wang, J.M. O'Neal and M.R. Prausnitz, Microinfusion using hollow microneedles, Pharm. Res. 23 (2006) 104-113.

[86] E.V. Mukerjee, Collins S.D., Isseroff R.R. and Smith R.L., Microneedle array for transdermal biological fluid extraction and in situ analysis, J. Sensor. Actuat. A 114 (2004) 267-275.

[87] M.R. Prausnitz and R. Langer, Transdermal drug delivery, Nat. Biotechnol. 26 (2008) 1261-1268.

[88] J.A. Subramony, A. Sharma and J.B. Phipps, Microprocessor controlled transdermal drug delivery, Int. J. Pharm. 317 (2006) 1-6.

[89] L.T. Cherney, Electrohydrodynamics of electrified liquid menisci and emitted jets, J. Aerosol Sci. 30 (1999) 851-862.

[90] A. Castellanos, Electrohydrodynamics, Springer-Verlag, NY, 1998.

[91] A.R.F. Elhefnawya and A.F. El-Bassiouny, Nonlinear stability and chaos in electrohydrodynamics, Chaos, Solitons & Fractals 23 (2005) 289-312.

[92] H. Kim, S.G. Bankoff and M.J. Miksis, The effect of an electrostatic field on film flow down an inclined plane, Phys. Fluids A-Fluid 4 (1992) 2117-2130.

[93] S.G. Bankoff, M.L. Miksis, H. Kim and R. Gwinner, Design considerations for the rotating electrostatic liquid-film radiator, Nucl. Eng. Des. 149 (1994) 441-47.

[94] H. Kim, Characteristics of solitary waves on a running film down an inclined plane under an electrostatic field, Korean J. Chem. Eng. 20 (2003) 803-811.

[95] K.S. Kim and H. Kim, Hydraulic-jump behavior of a thin film flowing down an inclined plane under an electrostatic field, Korean J. Chem. Eng. 25 (2008) 25-33.

[96] S.K. Li, A.-H. Ghanem, K.D. Peck and W.I. Higuchi, Iontophoretic transport across a synthetic membrane and human epidermal membrane: a study of the effects of permeant charge, J. Pharm. Sci. 86 (1997) 680-689.

[97] M.S. Roberts, P.M. Lai and T.G. Anissimov, Epidermal iontophoresis: I. Development of the ionic mobility-pore model, Pharm. Res. 15 (1998) 1569-1578.

[98] P.M. Lai and M.S. Roberts, Epidermal iontophoresis: II. Application of the ionic mobility-pore model to the transport of local anesthetics, Pharm. Res. 15 (1998) 1579-1588.

[99] L. Simon, A.W. Weltner, Y. Wang and B. Michniak, A parametric study of iontophoretic transdermal drug-delivery systems, J. Membrane Sci. 278 (2006) 124-132.

[100] Y.N. Kalia, A. Naik, J. Garrison and R.H. Guy, Iontophoretic drug delivery, Adv. Drug Deliver. Rev. 56 (2004) 619-658.